Functional Analysis of Two Major Sperm Tail Proteins Identifies ODF1 as Being Essential for the Tight Linkage of the Sperm Head to the Tail via SPAG4 and ODF2 as A Component of the β-catenin Destruction Complex

Dissertation

for the award of the degree

"Doctor rerum naturalium" (Dr. rer. nat.)

of the Georg-August-Universität Göttingen

within the doctoral program Biology

of the Georg-August University School of Science (GAUSS)

submitted by

Kefei Yang

from Liaoning, P. R. China

Göttingen, 2014

Thesis committee

Supervisor: Prof. Dr. Sigrid Hoyer-Fender
Department of Developmental Biology,
Johann-Friedrich-Blumenbach-Institute of Zoology and
Anthropology, Georg-August-University of Göttingen

Co-supervisor: Prof. Dr. med. Dr. h. c. Wolfgang Engel
Department of Human Genetics, University Medicine,
Georg-August-University of Göttingen

Extended thesis committee

Prof. Dr. Detlef Doenecke
Department of Molecular Biology, University Medicine,
Georg-August-University of Göttingen

Prof. Dr. Ernst A. Wimmer
Department of Developmental Biology,
Johann-Friedrich-Blumenbach-Institute of Zoology and
Anthropology, Georg-August-University of Göttingen

Prof. Dr. Martin Göpfert
Department of Cellular Neurobiology
Schwann-Schleiden Research Centre

Prof. Dr. Michael Kessel
Department of Developmental Biology
Max Plank Institute for Biophysical Chemistry

Date of the oral examination: 04. 06. 2014

Declaration

I declare that this doctoral thesis titled "Functional Analysis of Two Major Sperm Tail Proteins Identifies ODF1 as Being Essential for the Tight Linkage of the Sperm Head to the Tail via SPAG4 and ODF2 as A Component of the β-catenin Destruction Complex" was a product of my experimental research work carried out in the Department of Developmental Biology, Georg-August University Göttingen, and that it has not been submitted elsewhere for the award of any degree. Works of other people cited herein have been indicated specifically, or acknowledged by means of completed references.

Dedication

To my Family

Acknowledgment

constructs. I also want to thank Marco Andreas Tylkowski, Daniela Hüber, and Jasmin Dröge for taking part of ODF2 research. Special thanks go to bachelor students of our group, Luis Haupt, Zahra Basir Kazerouni, Constanza Tapia, Annie Angelique Nono Megaptche and Melek Umay Tüz, for their wonderful help.

To the past and present colleagues / friends Jianwei Li, Christian Ogaugwu, Bing Zhang, Weronika Sura, Van Ahn Dao, Martin Ehrle, Yonggang Hu, Ingrid Curril, Montserrat Torres Oliva, Yuyin Cai, Qiang Wu, Jordi Tomas Roig, I am very grateful for all the help, suggestions and discussions. Members in Department of Developmental Biology are very much appreciated for their help and assistance, especially Beate Preitz, Birgit Rossi, Helma Gries, Katrin Kanbach, Angelika Löffers and Selen Pfändner.

So much appreciated is Dr. Jianwei Li for correcting results part of this thesis.

Lot of thanks go to my friends Jianwei Li, Christian Ogaugwu, Naihang Guo, Bing Zhang, Qiujun Zhan, Kuan Lu, Lin Luo, Narisu Tao, Tselmeg Uriankhai, Yonggang Hu, Jianhong Wu, Zhiyuan Shi, Xinxin Cai, Yuyin Cai, Qiang Wu for their support and making my stay in Göttingen more exciting.

Last but not least, I want to thank my husband Jianfeng Wang and my parents, without their support, understanding and encouragement this thesis would not have been possible.

Table of Contents

Abstract

In the mammalian sperm tail, the outer dense fibers (ODFs) are accessory fibers accompanying the axonemal tubuli doublets on their outer site. The ODFs are composed of at least 14 polypeptides of which only a few have been identified. Among these components, ODF1 interacts with ODF2, and both of them are major proteins of ODFs. Although ODF1 and ODF2 have similar names, which exclusively characterize their location, the fundamental biological functions of them are entirely different.

ODF1 belongs to small heat shock protein (sHSP) family, based on its overall structural features and especially on its conserved α-crystallin domain that are characteristic of sHSPs. Therefore, ODF1 was also called HSPB10. The expression of mouse *Odf1* is restricted to testis and is first detectable at the round spermatid stage. In addition, immunoelectron microscopy revealed that ODF1 protein is specifically located to the ODFs and connecting piece. To study the role of ODF1 in sperm function, *Odf1*-deficient mice were generated and shown here that ODF1 is essential for male fertility. Homozygous ODF1-deficient male mice are infertile, whereas heterozygous male mice are fertile but show reduced sperm motility. *Odf1*-deficient male mice are infertile due to the detachment of the sperm head. Although headless tails are somehow motile, transmission electron microscopy revealed disturbed organization of the mitochondrial sheath, as well as of the outer dense fibers. These results thus suggest that ODF1, besides being involved in the correct arrangement of mitochondrial sheath and outer dense fibers, is essential for rigid junction of sperm head and tail.

In somatic cells the cytoskeleton is linked to the nucleoskeleton by nuclear membrane proteins with conserved SUN or KASH domains. SPAG4 is a member of the SUN domain protein family and locates to the nuclear membrane. It directly interacts with ODF1 and recruits ODF1 to the nuclear membrane. Furthermore, SPAG4 is restricted to spermatids and enriched at the posterior part of elongating spermatid nuclei. However, location of SPAG4 is not affected by ODF1 deficiency. Therefore, SPAG4

and ODF1 seem to be integral components of the head-tail coupling apparatus, and the tight linkage of head to tail in sperm might be mediated by the nuclear membrane protein SPAG4 and its binding to ODF1 in the connecting piece.

Whereas ODF1 is exclusively expressed in spermatids, ODF2, respectively its splice isoform Cenexin, is not only expressed in male germ cells but also localizes generally to the appendages of the mother centriole in somatic cells. As an important centrosomal component, ODF2 is essential for cilia formation and for embryonic development. Since Wnt pathway components are associated with centrosomes and vice versa centrosomal/basal body components have been implicated in modulating Wnt pathways, the relationship of ODF2 and canonical Wnt pathway was investigated. ODF2 inhibited the canonical Wnt pathway. Moreover, ODF2 over-expression repressed transcription of the endogenous Wnt target gene *c-Myc* and diminished *XWnt8*-induced secondary axis formation in *Xenopus* embryos. ODF2 interacted with components of the β-catenin destruction complex Axin1, Axin2, and β-catenin, and supported β-catenin degradation. Therefore, ODF2 most likely is a component of the β-catenin destruction complex, and this complex might be involved in the regulation of centrosome cohesion via promoting the degradation of β-catenin.

1. Introduction

1.1 Mammalian spermatogenesis and male germ cell specific proteins

The process in which spermatogonia form spermatozoa is known as spermatogenesis. Spermatogenesis occurs within testis. The seminiferous tubules of the testis are the starting point for the progress, where stem cells adjacent to the inner tubule wall divide in a centripetal direction to produce immature sperm and are released into the lumen of tubule (Fig. 1.1). Spermatozoa formed in the testis enter the *caput* (head) epididymis, progress to the *corpus* (body), and finally reach the *cauda* (tail) region, where they are stored. Sperm entering the *caput* epididymis lack the motility-ability to reach an oocyte. During their transit in the epididymis, sperm mature (Jones, 1999). Final maturation of sperm is completed in the female reproductive tract and called capacitation (Chang, 1951; Austin, 1951).

Spermatogenesis can be divided into three phases based upon functional considerations: (1) the proliferative phase (spermatogonia), in which cells undergo rapid successive divisions; (2) the meiotic phase (spermatocytes), in which genetic material is recombined and segregated; (3) the differentiation or spermiogenic phase (spermatids), in which spermatids thransform into cells structurally equipped to reach and fertilize the oocyte (Russell *et al.*, 1990).

There are many germ-cell specific proteins, which are expressed depending on different sperm development stages. Among them, the expression of mouse ODF1 is restricted to testis and is first detectable at the round spermatid stage. In addition, immunoelectron microscopy revealed that ODF1 protein is specifically located to the outer dense fibers (Burmester and Hoyer-Fender, 1996; Morales *et al.*, 1994). ODF1 therefore seems to be functionally involved in spermatid differentiation and formation of sperm tail. Like ODF1, SPAG4 is exclusively transcribed in round spermatids and translated in elongating spermatids (Shao, *et al.*, 1999). The most works of my study are about ODF1 and SPAG4 proteins, therefore both of them will be introduced later on with more details.

3

1.1.1 The proliferative and meiotic phases

Reproductive strategies in males of all species command that the cell numbers are increased early in the progress of spermatogenesis. The spermatogonial cell population may fulfill this need. These relatively immature cells undergo numerous mitoses to build a large population of cells that will subsequently undergo meiosis and differentiation to form sperm. There are three types of spermatogonia: stem cell spermatogonia, proliferative spermatogonia, and differentiating spermatogonia. The first two groups are undifferentiated spermatogonia. The stem cell spermatogonia may serve as a potential source of germ cells that can repopulate the seminiferous tubule after damage of the testis. The proliferative and differentiating spermatogonia show a higher mitotic rate and are more susceptible to agents that affect spermatogenesis (Russell *et al.*, 1990).

After the differentiation phase most of mature spermatogonia divide to form the primary spermatocytes (Fig. 1.1). They are characterized by highly condensed chromosomes giving the nucleus a coarse chromatin pattern and an intermediate position in the seminiferous epithelium. Primary spermatocytes go through the first meiotic division divided into prophase (subdividing into preleptotene, leptotene, zygotene, pachytene and diplotene), metaphase, anaphase and telophase and become secondary spermatocytes. The cells quickly proceed through this stage and complete the second meiotic division. Meiosis is the process by which the diploid number of chromosomes present in the stem cells (spermatogonia) is reduced to the haploid number present in mature spermatozoa. The products of the second meiotic division are called spermatids (Fig. 1.1).

Fig. 1.1: Spermatogenesis. The sperm development occurs in the seminiferous tubules of the testes. The mature spermatogonia divide to form the primary spermatocytes, which go through the first meiotic division and become secondary spermatocytes. After secondary meiotic division, the diploid number of chromosomes present in spermatogonia is reduced to the haploid number present in spermatid. At the end, round spermatids transform into elongated non-motile cells, which are released into the lumen of the seminiferous tubules and subsequently transferred into the epididymis.

1.1.2 Spermiogenesis

This phase is the process in which round spermatids transform into elongated non-motile cells. This process occurs without cell division and is one of the most phenomenal cell transformations in the body.

Shortly after the spermatids are formed, the Golgi apparatus is involved in producing small condensing vacuoles (proacrosomal vesicles) containing dense material (proacrosomal granules). One to four proacrosomal granules coalesce within one large

5

membrane bounded vesicle containing a single granule called acrosomal vesicle. The round acrosomal vesicle becomes then flat on that side that makes contact with the nuclear surface. The Golgi apparatus is positioned nearby and contributes more and more to the developing acrosome (Fig. 1.2). As time passes, the cell starts to take on an elongate shape, and the nucleus elongates progressively. The cytoplasm is stretched out along the flagellum and the Golgi apparatus moves away from the acrosome and migrates to the caudal aspect of the cell (Russell *et al.*, 1990).

In the young spermatids, the centriole pair migrates to the cell surface, and one of the two centrioles forms an axoneme containing microtubules (9+2 arrangement) that causes the spermatid plasma membrane to protrude from the cell. Then the centrioles pair moves from cell surface to the nucleus and the plasma membrane attached to the centriole folds inwards. After contacting the nucleus, the flagellar centriole indents the nucleus to form an implantation fossa (Fawcett *et al.*, 1969). Later on, the flagellum matures and is divided into mid, principal, and end pieces (Fig. 1.3; Fawcett, 1958 and 1975). Mitochondria are recruited from the cytoplasm to form a helical pattern around the mid piece of the flagellum (Fig. 1.3). Outer dense fibers form both in the mid piece and principal piece (Fig. 1.3; Irons and Clermont, 1982). A fibrous sheath is also formed in the principal piece (Fig. 1.3; Irons and Clermont, 1982).

In most species, up to certain stage, the nucleus of the spermatid is globular. Thereafter, the sperm head of each species achieves its characteristic shape (Fawcett, 1958 and 1975; Fawcett *et al.*, 1971). The mouse sperm head has a sickle-shape like that of the rat (Tang *et al*., 1982). In the immature sperm head, a cytoskeletal complex named manchette surrounds the nucleus by a sleeve of microtubules (Wolosewick and Bryan, 1977). Spermatid head changes in size and shape during spermiogenesis and becomes hydrodynamically streamlined to move in the fluid environment of the female reproductive tract. To promote spermatids to become smaller and more streamlined, the chromatin is first reorganized and tightly packaged, and second the cytoplasm is eliminated during spermatid elongation (Sprando and Rusell, 1987). Thereafter, some cytoplasm is eliminated just before sperm release by minute structures (tubulobulbar complexes) (Russell and Clermont, 1976; Russell, 1979;

Russell and Malone, 1980). Finally, cytoplasmic package (residual body) is formed at sperm release and pinched off from the spermatid to reduce one-fourth of the volume of the spermatids original size (Sprando and Rusell, 1987; Fawcett and Phillips, 1969; Russell, 1984). These cytoplasmic fragments are phagocytized and digested by the Sertoli cell (Kerr and de Kretser, 1974). After cytoplasmic elimination, a small amount of cytoplasm (cytoplasmic droplet) remains around the neck of the spermatid.
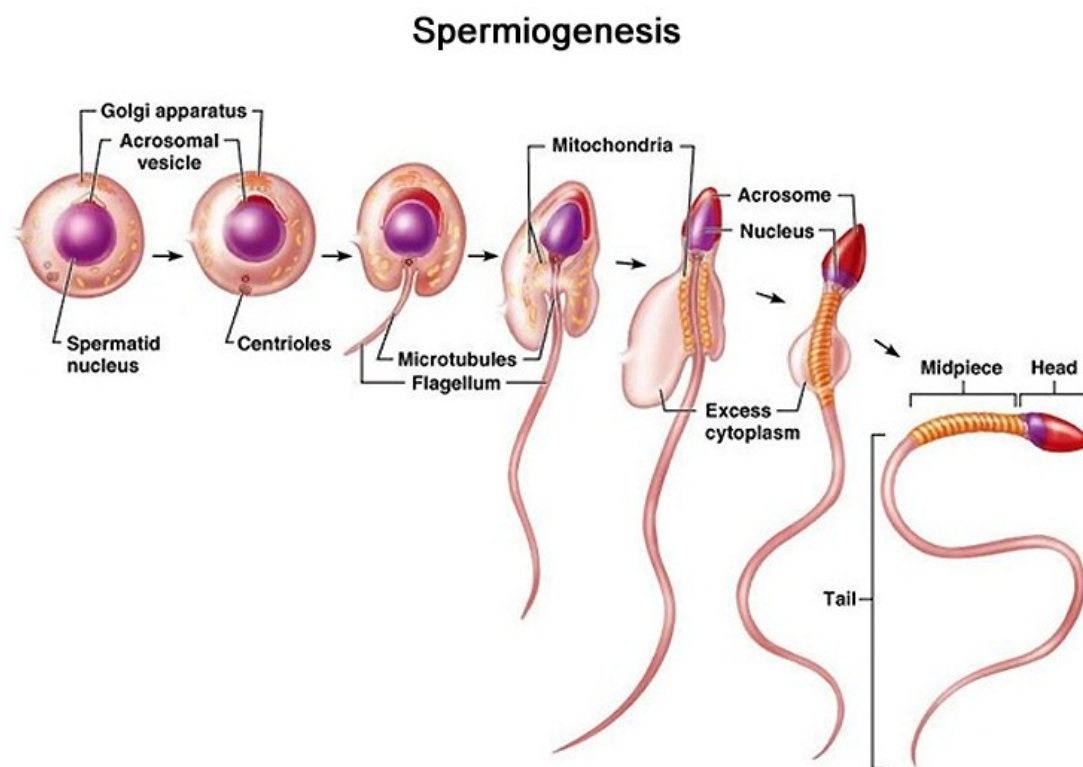
Spermiogenesis

Fig. 1.2: Schematic drawing of spermiogenesis, here shown for human. During spermiogenesis, the spermatid transforms from spherical form to an elongate shape. The centrioles go to the cell surface and one of them forms the axoneme, and afterwards, the flagellum is formed as sperm tail. Mitochondria are arranged to form a helical matrix surrounding the mid piece of the flagellum. The Golgi apparatus is involved in producing proacrosomal vesicles and contributes more and more to the developing acrosome. Some cytoplasm is eliminated and cytoplasmic package is formed, and pinched off from the spermatid. (The picture is from © 2004 Pearson, inc., publishing as Benjamin Cummings).

The end products of spermiogenesis are spermatozoa. Spermatozoa consist of a head and a tail (Fig. 1.3). The head comprises the nucleus and the acrosome attached at its cranial pole. At the caudal end the spermatozoan nucleus is anchored to the tail, which is responsible for sperm motility and movement towards the oocyte. In order to propel the spermatozoan head and to circumvent its disconnection from the sperm tail, sperm head and tail must be tightly linked to each other. Firm coupling is achieved by a sophisticated structure, the connecting piece.
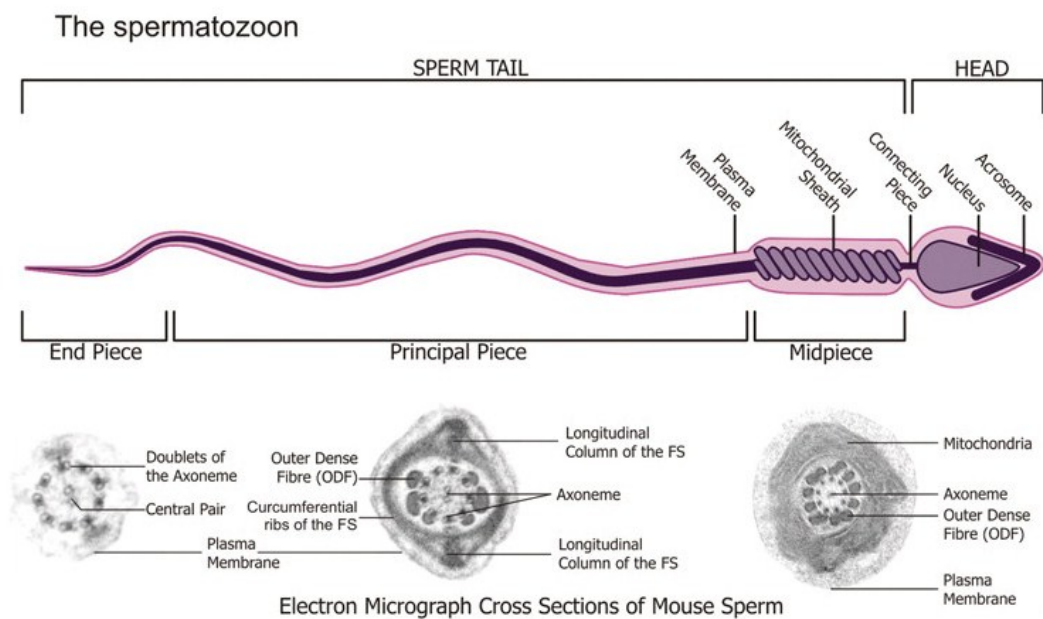
Fig. 1.3: The Spermatozoon. The spermatozoon is constituted of two main regions, the head and the tail. The anterior portion of the head is covered by the acrosomal cap and the head is joined to the tail by the connecting piece. The tail is divided into three regions: the midpiece; principal piece; and the end-piece. The electron micrographs showing cross-sections (not to scale) of each region highlight the main components of the tail structure: the axoneme; outer dense fibers (ODFs); and the mitochondrial sheath (midpiece) and fibrous sheath (FS) (principal piece). The end-piece consists solely of the axoneme and plasma membrane (Borg *et al.*, 2010).

1.1.2.1 Connecting piece of mature spermatozoa

The connecting piece is organized into nine longitudinal segmented columns that fuse cranially to form the capitulum (Fig. 1.4). The capitulum is a dense fibrous plate-like structure that conforms to the shape of the implantation fossa (Toshimori, 1998). The capitulum is the counterpart of the basal plate, a dense structure that lines the outer nuclear membrane at the implantation fossa. The interspace between the two membranes of the nuclear envelope in this region contains a regular array of periodic densities 6 nm wide and 6 nm apart (Fawcett, 1975). Freeze-fracture studies indicate that the membrane of the nuclear envelope at the implantation fossa contains a dense population of large and regularly spaced intramembranous particles surrounding a central particle-free region (Fried and Fawcett, 1974). The narrow region between capitulum and basal plate is traversed with fine filaments, these filaments are presumably responsible for attaching the capitulum of the flagellum to the basal plate of the head (Pedersen, 1972; Stackpole and Devorkin, 1974). Extending posteriorly from the capitulum two major and five minor segmented columns of 1-2 μm in length are usually found (Fig. 1.4). These two major columns split into two columns each and along with the other five columns, fuse to the nine outer dense fibers extending throughout the middle piece and principal piece of the flagellum. However, the segmented columns and the outer dense fibers have different origins, and the continuity between them develops late in spermiogenesis (Fawcett *et al.*, 1969; Zamboni and Stefanini, 1971). The segmented columns of the connecting piece are cross-striated, with a typical periodicity of 6.65 nm between segments. Each segment has nine or ten horizontal bands (Fawcett *et al.*, 1969).

The tight coupling between sperm head and tail is essential for successful fertilization. Impaired formation of intimate connection between head and tail causes increased instability of head-tail junction eventually resulting in acephalic spermatozoa and human male infertility (Chemes *et al.*, 1999; chemes, 2012). Although well characterized ultrastructurally, the molecular components responsible for the formation of the connecting piece and the tight linkage of sperm head to tail are

9

scarcely known.
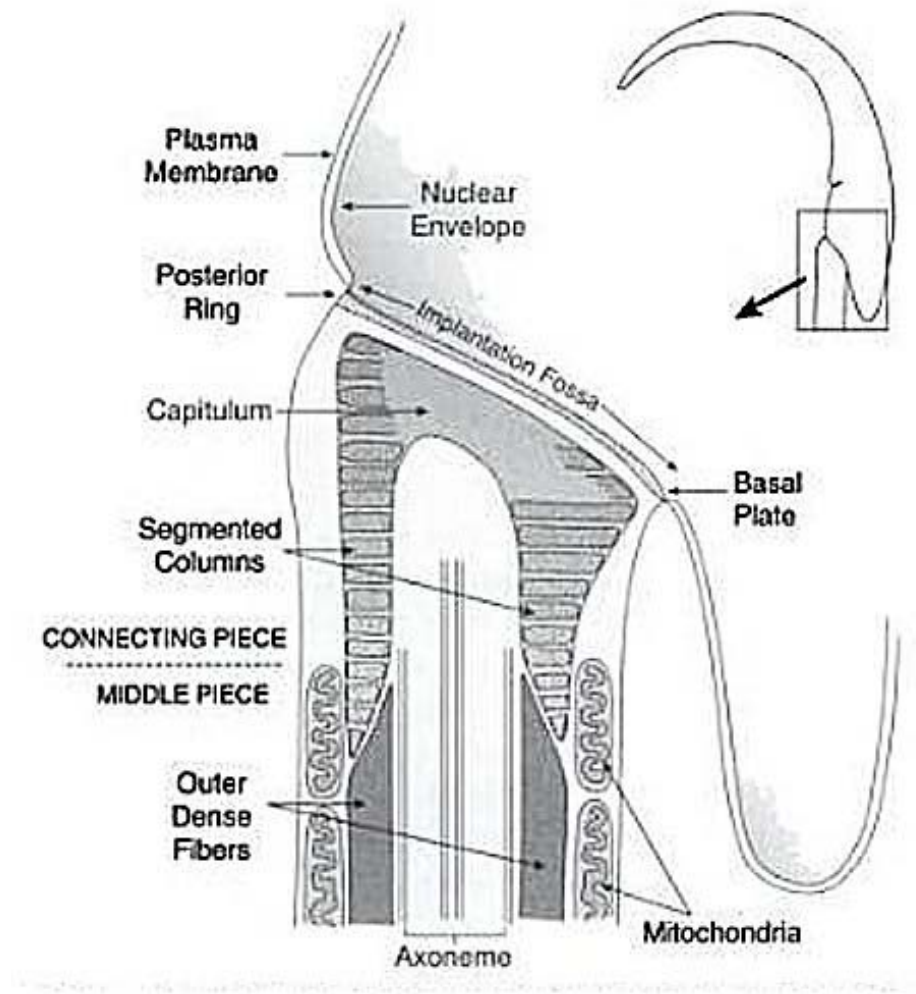
Fig. 1.4: Enlargement of the connecting piece of mouse sperm tail. The capitulum is the counterpart of the basal plate. At their caudal ends the segmented columns pass into the outer dense fibers (ODFs) of the sperm tail (Knobil and Neill's physiology of reproduction, 3. edition, 2006).

1.1.3 The classification of spermatogenesis and spermiogenesis

In seminiferous tubules, the progressing spermatogenesis is grouped into stages. A stage is a defined association of germ cell types at particular phases of development in cross-sectioned tubules, and each cell type of the stage is morphologically integrated with the others in its developmental processes (Russell *et al.*, 1990). By convention,

10

each stage is designated by a Roman numeral (Fig. 1.5). In mice, there are 12 designated stages (Fig. 1.5).

Due to the morphological changes of spermatid during spermiogenesis, spermiogenesis may be divided into various developmental steps. It bases on the form and shape of the acrosome, the spermatid head shape and the degree of chromatin condensation. Steps of spermiogenesis are provided with Arabic number designations (Russell *et al.*, 1990). In mice, there are 16 steps in spermiogenesis (Fig. 1.5).

STAGES OF THE CYCLE
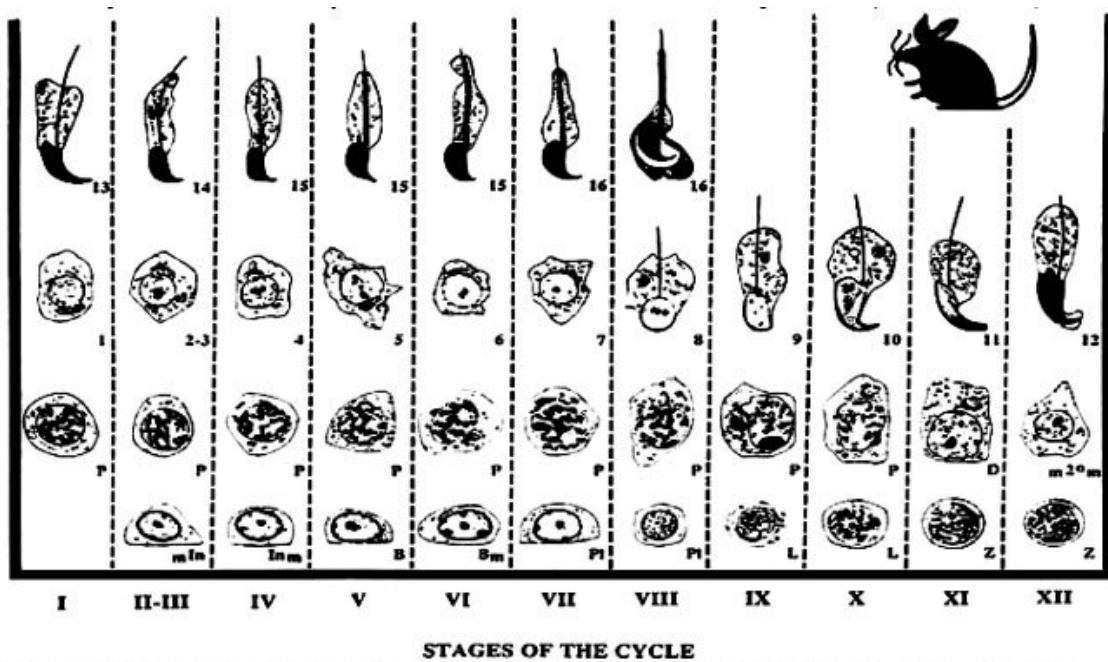
Fig. 1.5 Stages of spermatogenesis and steps of spermiogenesis in mice (Russell *et al.*, 1990).

1.1.4 ODF1 protein

ODF1 is the major protein of mammalian sperm tail outer dense fibers (ODFs), which are cytoskeletal structures specifically found in the sperm tails of vertebrates but not in eukaryotic cilia and flagella in general (Fawcett, 1975). ODFs are accessory fibers accompanying the axonemal tubuli doublets on their outer side and are therefore present ninefold. They are composed of more than a dozen different proteins of which only a few have been identified (Oko, 1988; Petersen *et al.*, 1999; Vera *et al.*, 1984).

11

Although not involved in active motility, ODFs seem to be important for the stability and the elastic recoil of the sperm tail, as well as for support of the flagellar beat (Baltz *et al.*, 1990; Lindemann, 1996). Impaired development of the ODFs has been described as a major cause of tail abnormalities in infertile men, indicating an important function in sperm motility and/or morphology (Haidl *et al.*, 1991).

ODF1 is the most recent protein assigned to small heat shock proteins (sHSPs), based on its overall structural features and especially on its conserved α-crystallin domain that is characteristic of sHSPs (Fontaine *et al.*, 2003). Therefore, ODF1 was also called HSPB10 (Fontaine *et al.*, 2003). Heat shock proteins play an essential role as molecular chaperones by preventing the aggregation of misfolded proteins and have strong cytoprotective effects. A structurally divergent group within the molecular chaperone family is constituted by sHSPs. The super-family of sHSPs comprises 10 proteins with molecular masses ranging from 12 to 43 kDa. Their most pronounced structural feature is the conserved α-crystallin domain of 80 to 100 amino acids. sHSPs interact with a lot of essential cellular structures. Hence, sHSPs seem to be implicated in a wide variety of human diseases (Hishiya *et al.*, 2008; Lanneau *et al.*, 2008; Sun *et al.*, 2005).

The *Odf1* gene, which is a single copy gene located in mice to chromosome 15 region B2-C, as well as its encoded protein, are highly conserved in evolution (Gastmann *et al.*, 1993; Oko, 1988), indicating an important function in sperm motility and/or morphology.

ODF1 has a molecular mass of about 27 kDa with high content of cysteine (between 13% and 17%) and proline (up to 10%), capably forming disulfides (Burfeind and Hoyer-Fender, 1991; Burfeind *et al.*, 1993; Gastmann *et al.*, 1993; Hoyer-Fender *et al.*, 1995; Morales *et al.*, 1994; Van der Hoorn *et al.*, 1990). The high cysteine content of ODF1 may provide free sulphydryl groups for the retention of zinc ions that are enriched in the sperm tail (Calvin *et al.*, 1975). Cysteine and proline are mainly found in the C-terminal end of ODF1 as a repetitive tripeptide motif of C-X-P. Although variability of C-X-P repeat frequencies has been reported, it did not affect male fertility in humans (Hofferbert *et al.*, 1993).

ODF1 is a self-interacting protein but its self-association is weak (Shao and Van der Hoorn, 1996). Moreover, several binding partners were also identified over years, including ODF2. Interaction between ODF1 and ODF2 was proven in a yeast two-hybrid assay and was shown to depend on their leucine-zipper motif (Shao *et al.*, 1997). The scaffold of the ODFs may thus be structured by the two main ODF proteins, ODF1 and ODF2 (Petersen *et al.*, 1999). Other ODF1 interacting proteins are SPAG4, KLC3 (kinesin light chain 3), OIP1 (ODF1-interacting protein), and SPAG5 (Bhullar *et al.*, 2003; Fitzgerald *et al.*, 2006; Shao *et al.*, 1999; Zarsky *et al.*, 2003). SPAG4 is located in the transient manchette and associated with the axoneme in elongating spermatids and epididymal sperm. It binds to ODF1, but not to ODF2 (Shao *et al.*, 1999). SPAG5 is found in rat elongated spermatids and epididymal sperm. SPAG5 associates with ODFs, but not with the axonemal microtubules (Fitzgerald *et al.*, 2006). OIP1 is a member of the RING finger family that are often E3 ubiquitin protein ligases. OIP1 binds to the conserved C-X-P motif in the C-terminal end of ODF1 (Zarsky *et al.*, 2003), and ODF1-OIP1 interaction is enhanced by Cdk5/p35-mediated ODF1 phosphorylation (Rosales *et al.*, 2008). In addition to being components of the ODFs, ODF1, ODF2, and ODF1 interacting protein SPAG4 have all been located to the manchette, a transient microtubular structure that seems to be important for the shaping of the sperm nucleus and the development of the sperm tail (Kierszenbaum *et al.*, 2002).

1.1.5 SPAG4 protein

SPAG4 is a member of the SUN domain proteins and locates to the nuclear membrane. Its expression is restricted to spermatids and it is enriched at the posterior part of elongating spermatids (Yang, *et al*., in preparation).

SUN proteins were discovered by molecular analysis of *Caenorhabditis elegans unc-84* that affected nuclear migration (Horvitz and Sulston, 1980; Sulston and Horvitz, 1981). Sequence comparison revealed conservation of the C-terminal region

of UNC-84 with the C-termini of *Schizosaccharomyces pombe* Sad-1 and two human proteins, SUN1 and SUN2 (Malone *et al.*, 1999). This region that consists of ~175 amino acids was hence named SUN domain (for <u>s</u>ad-1 and <u>un</u>c-84). SUN domain proteins have at least one transmembrane domain that localizes to the nuclear membrane. Altogether, SUN domain proteins are most likely located in the inner nuclear membrane with their SUN domains in the perinuclear space whereas their N-terminal regions extend into the nucleoplasm (Malone *et al.*, 1999; Dreger *et al.*, 2001; Schirmer *et al.*, 2003; Hodzic *et al.*, 2004; Liu *et al.*, 2007). Due to the presence of short coiled-coil regions SUN domain proteins are able to form dimers or multimers (Crisp *et al.*, 2006; Haque *et al.*, 2006; Lu *et al.*, 2008; Malone *et al.*, 1999). The N-terminal nucleoplasmic regions of SUN1 and SUN2 interact with A- and B-type lamins whereas the conserved SUN domain itself interacts with the conserved KASH domain found in the outer nuclear membrane proteins Klarsicht, ANC-1, SYNE-1/Nesprin, and MSP-300 (hence termed KASH for <u>K</u>larsicht/<u>A</u>nc-1/<u>S</u>yne-1 <u>h</u>omology) (Hodzic *et al.*, 2004; Padmakumar *et al.*, 2005; Haque *et al.*, 2006; McGhee *et al.*, 2006; Tzur *et al.*, 2006; Crisp *et al.*, 2006).

KASH and SUN domain proteins thus bridge the nuclear envelope to function as a linker of the nucleoskeleton to the cytoskeleton complexes (Crisp *et al.*, 2006; Haque *et al.*, 2006; McGhee *et al.*, 2006; Razafsky and Hodzic, 2009; Starr and Fridolfsson, 2010). In mammals, so far, at least five SUN domain proteins are present of which SUN1 and SUN2 are widely expressed whereas SUN3/SUNC1, SUN4/SPAG4, and SUN5/SPAG4L are largely restricted to testis. It has been reported that SPAG4 locates in the manchette and the axoneme, binds to ODF1, and is switched on in neoplastic tissues (Shao *et al.*, 1999; Kennedy *et al.*, 2004).

1.2 Centrosome, primary cilium and basal body

The centrosome is located at the cell center close to the cell nucleus. It is the major microtubule-organizing center (MTOC) of the eukaryotic cell and generates the

mitotic spindle during mitosis. The centrosome consists of the mother centriole, which is characterized by the presence of distal and subdistal appendages, and the daughter centriole (Fig. 1.6 A). Centrioles are mainly built from α / β tubulin dimers and are surrounded by pericentriolar material (PCM) (Kellogg *et al.*, 1994; Stearns and Winey, 1997; Zimmermann *et al.*, 1999; Bornens, 2002). In animal cells, centrosomes duplicate once per cell cycle, strictly dictated by cell cycle control mechanism. In S phase, the new centrioles start to form from the original mother and daughter centrioles. These procentrioles elongate through S to G2 phases and then the original daughter centriole acquires appendage proteins in late G2 / early M phase to become a new mother centriole (Fig. 1.6 B).

In eukaryotic cells, primary cilia are anchored to the cell by the basal bodies, which develop from the mother centriole of the centrosome (Wheatley *et al.*, 1996). As essential sensory organelles they project from the surface of cells (Huangfu *et al.*, 2003; Pazour and Witman, 2003; Corbit *et al.*, 2005; Haycraft *et al.*, 2005; Huangfu and Anderson, 2005; May *et al.*, 2005; Pan *et al.*, 2005; Schneider *et al.*, 2005; Michaud and Yoder, 2006). They are generally immotile having nine peripheral doublet microtubules. Primary cilia are found singly on cells whereas motile cilia with additional two central microtubules occur in groups. Primary cilia exist on most epithelial and stromal cells throughout the mammalian body. So far, it has been found that primary cilia are involved in several signaling pathways essential for growth and differentiation, including the Hedgehog (Hh), Wnt, and PDGF pathways (Eggenschwiler and Anderson, 2007; Berbari *et al.*, 2009).

The basal body is converted from the mother centriole. When the cell leaves mitosis and enters G0 phase, the mother centriole associates with ciliary vesicles that cap its distal end (Sorokin, 1962), migrates to the cell surface and subsequently docks at the plasma membrane. In the transition zone, the axonemal doublets of the primary cilium are shifted from triplet microtubules in the basal body, and the outer doublet microtubules are connected to the ciliary membrane with Y-shaped bridges, the transition fibers. Transition fibers and basal feet originate from distal and subdistal appendages of the mother centriole, respectively (Fig. 1.6 C). Transition fibers (distal

appendages) function to anchor the basal body to the membrane in the transition zone (Anderson, 1972). In addition, transition fibers (distal appendages) might also be important for the docking of intraflagellar transport (IFT) proteins to promote ciliogenesis (Deane *et al.*, 2001). Striated rootlets extend from the proximal end of the basal body into the cytoplasm supporting the cilium (Tachi *et al.*, 1974).
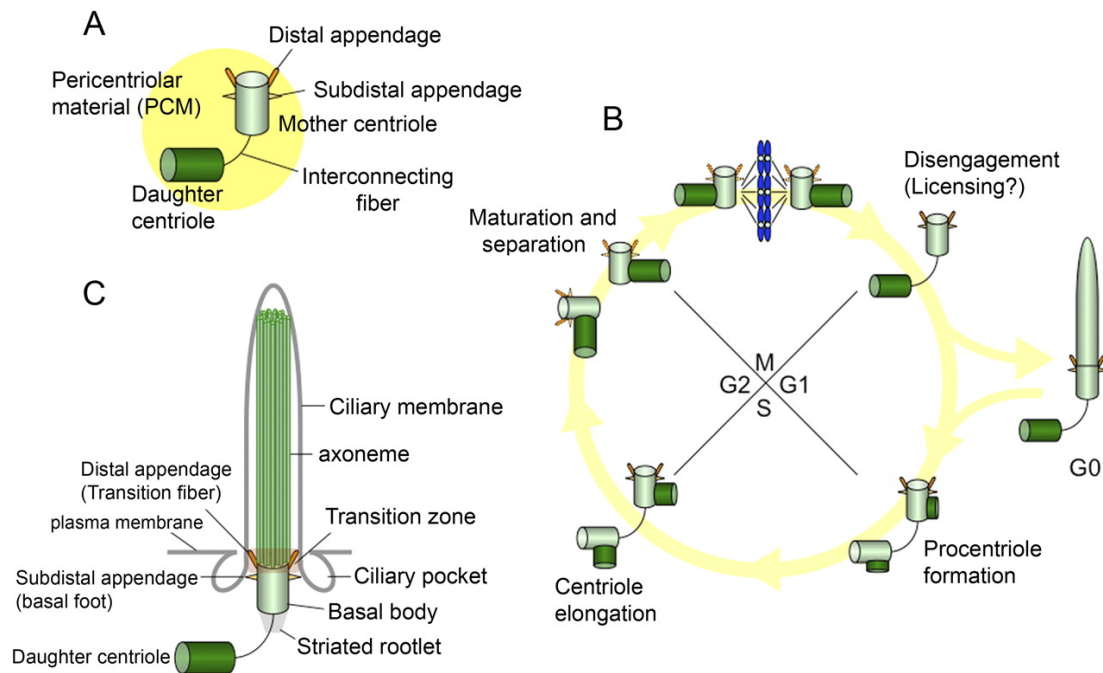
Fig. 1.6: Centrosome, primary cilium and cell cycle. (A), the structure of centrosome. **(B),** the centrosome duplication during cell cycle. When the cell leaves G0 phase, the primary cilium disappears and the basal body becomes the centrosome generating the mitotic spindle with major impacts on chromosome segregation and cytokinesis. **(C),** the structure of primary cilium. In G0 phase the centrosome goes to the cell surface and the mother centriole becomes the basal body. The primary cilium is formed from the basal body (review of Kobayashi and Dynlacht, 2011).

1.2.1 ODF2 protein

Originally, ODF2 was found in the mammalian sperm tail and is the major component of the outer dense fibers (ODFs) (Brohmann *et al.*, 1997; Shao *et al.*, 1997; Turner *et*

al., 1997; Hoyer-Fender *et al*., 1998; Schalles *et al*., 1998; Petersen *et al*., 1999). Comparing to ODF1, which is another important protein of the outer dense fibers and restricted to spermatids, ODF2 generally localizes also to the appendages of the mother centriole in somatic cells (Nakagawa *et al.*, 2001; Hoyer-Fender *et al.*, 2003; Donkor *et al.*, 2004). More precisely, Cenexin is confirmed as an isoform of ODF2 which is constantly expressed in all tissues whereas ODF2 was upregulated in testes (Hüber and Hoyer-Fender, 2007). Both proteins differ by a peptide of 42 amino acids at the N-terminal region which is present in Cenexin and absent in ODF2. This cenexin insertion is encoded by exon 3b and starts with codons for the amino acids MKDR. In the C-terminal region two leucine zipper motifs are present which are responsible for interaction with ODF1 (Shao *et al*., 1997). According to a secondary structure prediction (Lupas *et al*., 1991), ODF2 has a coiled-coil structure on its C-terminal end. The contribution of this coiled-coil structure most probably relies on promoting self-association and the formation of higher-order structures. Alternative splicing of ODF2/Cenexin transcripts encodes isoforms with masses between 70 and 100 kDa. At the C-terminal end human and rat Cenexin isoforms have an extension of ~150 amino acids that is not present in ODF2 isoforms (Soung *et al*., 2006; Rivkin *et al*., 2008).

1.3 Wnt signaling pathways

Wnt signaling pathways play crucial roles in cell proliferation, cell fate specification and morphogenesis in early embryos. They consist of proteins which can pass the signals from the cellular outside via cell surface receptors to the cellular inside. Three Wnt signaling pathways have been characterized: the canonical Wnt / β-catenin pathway, the planar cell polarity pathway (PCP pathway) and the calcium pathway. The PCP pathway is one of the non-canonical pathways (β-catenin-independent pathways), controlling cell polarity in the plane of epithelial tissues in *Drosophila* (Lawrence *et al.*, 2007; Seifert and Mlodzik, 2007). The other non-canonical pathway,

the calcium pathway, can help to regulate calcium release from the endoplasmic reticulum (ER) in order to control intracellular calcium levels and this pathway is dependent on G-proteins (Kohn and Moon, 2005; Slusarski and Pelegri 2007).

The canonical Wnt pathway is a β-catenin dependent Wnt pathway therefore also called β-catenin pathway. In this pathway, β-catenin as a transcriptional co-activator plays a key role in transmitting extracellular signals for the activation of target genes. In the absence of Wnt, β-catenin is constitutively phosphorylated by a destruction complex consisting of Axin, Dvl, APC and GSK3β (glycogen synthase kinase 3β). The phosphorylated β-catenin is subsequently ubiquitinated by the E3 ligase *β*-TrCP (*β*- transducin repeat-containing protein) and degraded in the proteasome. This degradation results in a low cellular β-catenin level (Fig. 1.7 A). In contrast, in the presence of Wnt, Wnt ligand binds to its receptor Fz (Frizzled) and co-receptor LRP6. Then the activated Frizzled receptors recruit the cytoplasmic protein Dishevelled (Dvl) to the receptor complex via direct binding and subsequently multimerizes and induces formation of LRP-associated Wnt signalsomes (Bilic *et al.*, 2007). The intra cellular region of LRP6 is phosphorylated by GSK3β or CK1 (casein kinase 1). The phosphorylated LRP6 and activated Dvl recruit Axin to the cell membrane, resulting in the dissociation of β-catenin from the destruction complex (Schwarz-Romond *et al.*, 2007). Therefore β-catenin accumulates in the cytoplasm and enters into the nucleus to bind to TCF (T-cell factor) / LEF (lymphoid enhancer factor), thereby activating the Wnt transcriptional process (Fig. 1.7 B) (reviews of MacDonald, Tamai and He, 2009 and Tolwinski and Wieschaus, 2004).
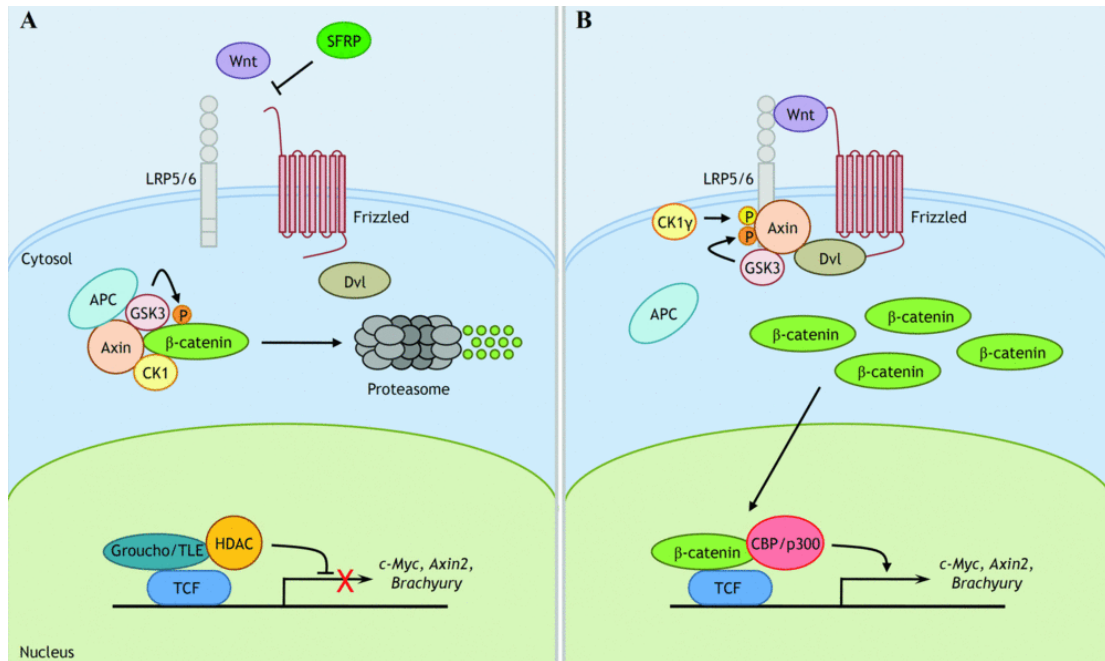
Fig. 1.7: Wnt/β-catenin signalling pathway. (A), in the absence of Wnt ligands. β-catenin is phosphorylated by the destruction complex (APC, Axin, and GSK3β) and subsequently marked for degradation by the ubiquitin-E3 ligase β-TrCP. **(B)**, in the presence of Wnt ligands. Wnt binds to Fz and LRP6, then LRP5/6 is phosphorylated by GSK3β and CK1γ, after which Axin is recruited to the phospho-LRP5/6 tail. These processes induce dissociation of the β-catenin destruction complex and subsequent accumulation of cytosolic β-catenin. Accumulated β-catenin enters into the nucleus and interacts with TCF / LEF1 for activation of Wnt-responsive genes. SFRP, secreted Fz-related protein (review of Kim, Kim and Jho, 2013).

1.3.1 β-catenin protein

β-catenin (Armadillo in *Drosophila*) is a member of the Armadillo family of proteins, which have multiple copies of the so-called armadillo repeat domain (~42 amino acids) composed of three alpha helices (Peifer *et al.*, 1994). In the canonical Wnt pathway, as the key protein β-catenin is responsible for transduction of the signal to the nucleus and thereby the Wnt transcriptional process is activated (Fig. 1.8). Without a Wnt signal, the levels of cytoplasmic free β-catenin are kept low and the majority of β-catenin is located at the cytoplasmic side of the membrane as a component of

cadherin-based cell-cell connections. β-catenin, together with α-catenin and γ-catenin / plakoglobin, link E-cadherin, the key molecule of the Ca^{2+}-dependent cell adhesion, to cytoskeletal structures (Ozawa *et al.*, 1989). Besides these signaling and structural functions, β-catenin was found surprisingly in the centrosome and contributes to centrosomal cohesion and separation at the onset of mitotic spindle formation (Fig. 1.8) (Huang *et al.*, 2007).
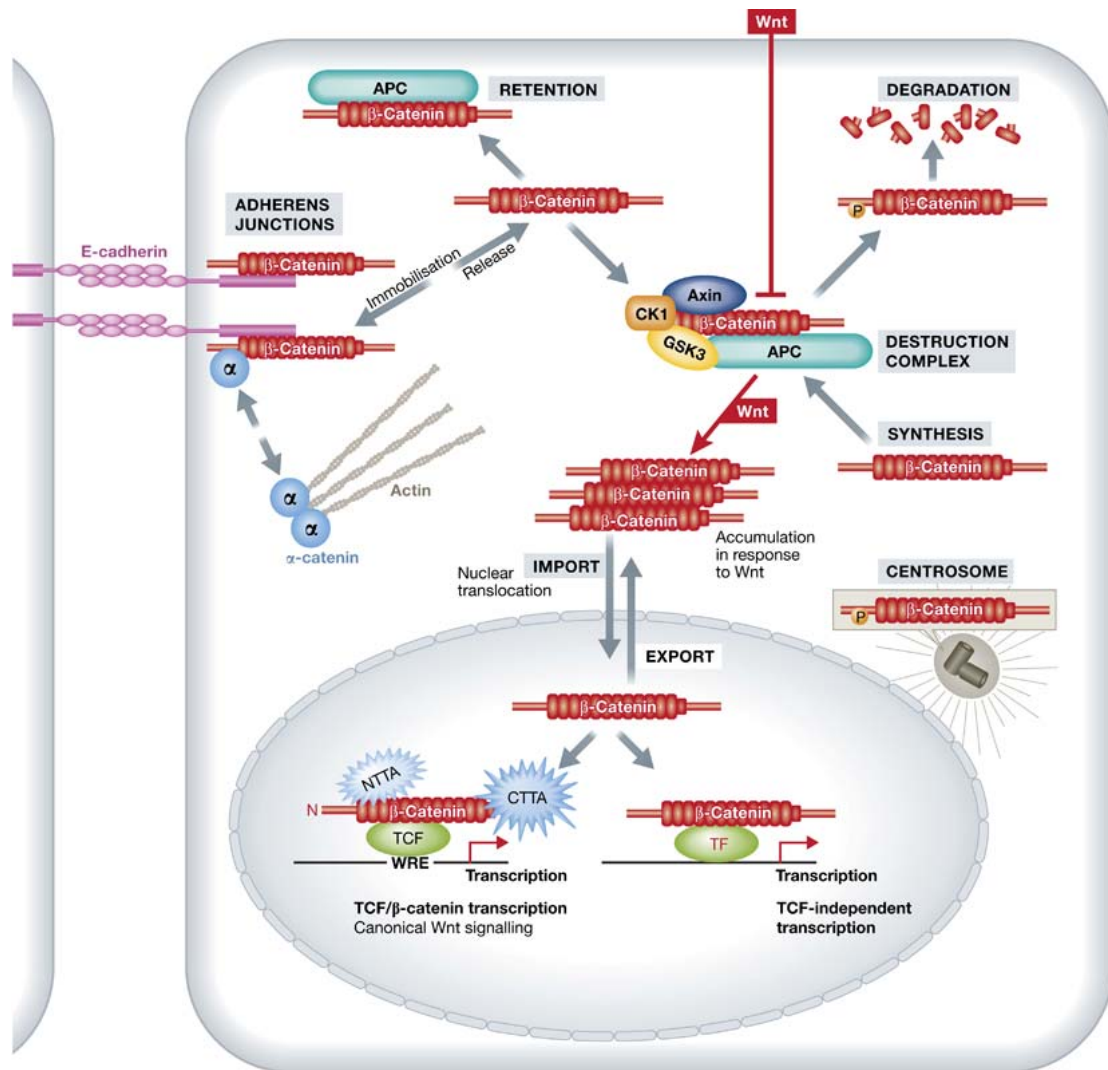
Fig. 1.8: The faces of β-catenin within the cell. So far, β-catenin has three main functions in the cell: **(1)** β-catenin is responsible for transduction of the signal to the nucleus in the case of Wnt-on and thereby the Wnt transcriptional process is activated whereas without Wnt signal the most cytoplasmic β-catenin is phosphorylated by destruction complex and subsequently marked for

degradation by the ubiquitin-E3 ligase β-TrCP. **(2)** β-catenin is located at the cytoplasmic side of the membrane and links E-cadherin to cytoskeletal structures. **(3)** β-catenin contributes to centrosomal cohesion and separation at the onset of mitotic spindle formation (review of Valenta, Hausmann and Basler, 2012).

1.4 Goals of the thesis

The outer dense fibers (ODFs) are prominent sperm tail-specific cytoskeletal structures. They seem to be important for the stability and the elastic recoil of the sperm tail as well as for support of the flagellar beat (Baltz *et al*., 1990; Lindemann, 1996). Impaired development of the outer dense fibers has been described as a major cause of tail abnormalities in infertile men (Haidl *et al*., 1991) indicating an important function in sperm motility and/or morphology. The ODFs are composed of at least 14 polypeptides of which only a few have been identified. So far, the functions of the most proteins of the ODFs are unknown. In this study, I was focusing on functional analyses of two components of ODFs: ODF1 and ODF2. ODF1 specifically expressed in spermatids, ODF2 ubiquitously expressed.

1. To study ODF1 function in formation of the sperm tail cytoskeleton and its impact for stability and motility *Odf1-knock out* mice were generated, subsequently, the phenotypes of these mice were analysed.

2. To find out the function of ODF2 at the appendages of the mother centriole in somatic cells the influence of ODF2 on canonical Wnt pathway key protein β-catenin was analysed.

2. Material and methods

2.1 Material

2.1.1 Biological material

2.1.1.1 Bacterial stains

Eschericia coli strain DH5α was used for subcloning and keeping of plasmid DNA.

2.1.1.2 Cell lines

For analysis the following cell lines were used:

ES: mouse embryonic stem cells

SSC: mouse spermatogonial stem cells

F9: mouse teratocarcinoma cells

NIH3T3: mouse embryonic fibroblast cell line

HEK293: human embryonic kidney cell line

MCF7: human breast adenocarcinoma cell line

MDA-MB-231: human breast adenocarcinoma cell line

2.1.2 Vectors

Vector	Resource	Generated constructs	Reference
pBluescript	Stratagene	*Odf1*	Schweizer
pPNT-M1	Tybulewicz *et al.*, 1991	*Odf1*	Schweizer
pGEMT	Promega	*Odf1*	Schweizer
pECFP-N1	Clontech	*Odf1*	Hoyer-Fender
pcDNA3.1/*myc*-His (-) C	Invitrogen[TM] Life technologies	*Spag4*	Hoyer-Fender
pcDNA3.1HA/*myc*-His (-) C	Invitrogen[TM] Life technologies	*Spag4; Spag4-N; Spag4-C; EYFP-Spag4*	Hoyer-Fender

pEGFP-N1	Clontech	*13.8NC-GFP; 13.8NCΔGFP; 13.8; N-terminal; human Odf2; cenexin; cenexin insertion; ODF2NC; ODF2N2C; ODF2NC1; ODF2NC2; pEGFP-1; ninein*	Hoyer-Fender
phRL-SV40	Promega		
pGL3	Promega	*Fopflash (OF)*	Vogelstein
pGL3	Promega	*Topflash (OT)*	Vogelstein
pCI-neo	Promega	*β-catenin*	Vogelstein
pIRES-EGFP	Clontech	*shODF2*	Haupt
pCS2	Invitrogen™ Life technologies	*Odf2, Xwnt-8, GFP*	Henningsfeld
pQM-NTag/B	Abcam		
FPCAV2 (modified from pQM-NTag/B)	Hoyer-Fender	*α-tubulin; γ-tubulin; ε-tubulin*	Hoyer-Fender

Tab. 2.1: Vectors.

2.1.3 Oligonucleotides

Name	Target gene	Species	Sequence
Odf1SPst	*Odf1*	mouse	CTGCAGCTCAGAGTCTTGTCTGTG
Odf1SHindIII	*Odf1*	mouse	AAGCTTAGACTGTTCTCCACAG
Odf1-I	*Odf1*	mouse	ATCAACTCTGCCTGAGAC
Neomy	*Odf1*	mouse	CCTTCTATCGCCTCCTTGACG
Odf1-5´ko	*Odf1*	mouse	AGGAAGAAGGGACTAGAG
Odf1-N	*Odf1*	mouse	GAGCTCAAGCTTTGGCCGCACTGAGTTGTC
MSYCP35`Kpn1	*SYCP3*	mouse	GACGGTACCATGCTTCGAGGGTGTGGG
MSYCP3r	*SYCP3*	mouse	TTGACACAATCGTGGAGAGAA
Stra8 for	*Stra8*	mouse	TCACAGCCTCAAAGTGGCAGG
Stra8 rev	*Stra8*	mouse	GCAACAGAGTGGAGGAGGAGT
Hanp1-H1T2-for	*HANP1/H1T2*	mouse	GCTGGCTACTTCAGGGTCT
Hanp1-H1T2-rev	*HANP1/H1T2*	mouse	TGTATGCTGGGAGCGTTG
MMISf	*MIS*	mouse	TTGGTGCTAACCGTGGACTT
MMISr	*MIS*	mouse	GCAGAGCACGAACCAAGCGA
mIns13f	*Ins13*	mouse	TACTGATGCTCCTGGCTCTGG
mIns13r	*Ins13*	mouse	TTAGACTGTTTGGGACACAGG
138NCEcoRI	*Odf2*	mouse	GGAATTCATGTCCGCCTCATCCTCAGGC
DH1rev	*Odf2*	mouse	CAGCTTCCCGATGGTATCCTTCAAG
Odf1-C	*Odf1*	mouse	CCGCGGTACCCAAGATCATCTTCCTACA
SPAG4 C KpnI	*Spag4*	mouse	GGTACCGATGGGGGTCCCCCTGTGAC

23

Spag4 650 for	*Spag4*	mouse	TGCAGGGAAATCTGCTCC
SPAG4 N XbaI	*Spag4*	mouse	TCTAGAATGCGGCGGAGCCCCCGC
SPAG4N2XbaI	*Spag4*	mouse	TCTAGAGAACCTACGGAGATGCTGAC
SPAG4C2KpnI	*Spag4*	mouse	GGTACCTTAGAGTCAGCATCTCCGTAGGTTC
EYFP-C XbaI	*eYfp*	mouse	TCTAGACTTGTACAGCTCGTCCATGC
EYFP–N SpeI	*eYfp*	mouse	ACTAGTATGGTGAGCAAGGGCGAGG
GAPDHfor	*Gapdh*	mouse	CACCACCAACTGCTTAGCC
GAPDHrev	*Gapdh*	mouse	CGGATACATTGGGGGTAGG
hHPRT1_2f_390	*HPRT*	human	TTTGCTGACCTGCTGGAT
hHPRT1_2r_631	*HPRT*	human	GGATTATACTGCCTGACCAAG
hCmyc_2f_344	*C-Myc*	human	TTGCCGCATCCACGAAAC
hCmyc_2r_615	*C-Myc*	human	GTCGAGGTCATAGTTCCTGTTGGT

Tab. 2.2: Oligonucleotides.

2.1.4 Enzymes

Enzyme type	Enzyme	Resource
Restrication enzyme	XbaI	Fermentas
	EcoRI	
	NotI	
	XhoI	
	PstI	
	HindIII	
	KpnI	
DNA-polymerase	Mango Taq DNA polymerase	Bioline
	Taq polymerase	Fermentas
DNase	RQ1 DNase	Roche
DNA ligase	T4 DNA ligase	Fermentas
Proteinase kinase	Proteinase K	Sigma-Aldrich
Protease inhibitor	protease inhibitor cocktail (100x)	Thermo Scientific
Hyaluronidase	Hyaluronidase	Supplied by human genetic institute (Göttingen)

Tab. 2.3: Enzymes.

2.1.5 Antibodies

2.1.5.1 Primary antibodies

Target protein	Antibody name	Host	Resource
α-tubulin	anti-α-tubulin mouse monoclonal antibody (DM1A)	mouse	Calbiochem
SPAG4	anti-SPAG4 antibody (sc-85927)	rabbit	Santa Cruz Biotechnology
ODF1	Anti-ODF1	rabbit	The Abs were affinity purified as described by Brohmann *et al.* (1997) using an antiserum against total ODF proteins and bacterially expressed mouse ODF1 fused to MBP (maltose binding protein*; pOdf1-MBP*).
GFP	Anti-GFP	rabbit	Invitrogen
Myc-tag	Anti-myc polyclonal	rabbit	Millipore
HA-tag	HA.C5	mouse	Abcam
γ-tubulin	GTU-88	mouse	Sigma
β-catenin	Rabbit polyclonal to beta Catenin (ab6302)	rabbit	Abcam
Axin1	Axin1 (C76H11) Rabbit mAb	rabbit	Cell Signaling Technology
Axin2	Axin2 (76G6) Rabbit mAb	rabbit	Cell Signaling Technology
Phospho-Tau	p-Tau (Ser 404)	rabbit	Santa Cruz Biotechnology

Tab. 2.4: Primary antibodies.

2.1.5.2 Secondary antibodies

Target protein	Antibody name	Host	Resource
mouse IgG	Anti mouse-HRP 4759	goat	Carl Roth
	MFP 590	goat	Molecular Probes
Rabbit IgG	Anti rabbit IgG HRP	goat	Sigma Biosciences
	Alexa 488	goat	Molecular Probes

Tab. 2.5: Secondary antibodies.

2.1.6 Culture media for *E. coli* cultures

Name	Ingredients
LB medium (Luria Bertani medium)	10 g tryptone 5 g yeast extract 10 g NaCl pH 7,5 diluted in milliq H_2O
LB agar plate	1,5% (w/v) agar in LB medium
Ampicillin medium	100 μg/ml ampicillin in LB medium
Kanamycin medium	50 μg/ml kanamycin in LB medium

Tab. 2.6: Culture media for *E. coli* cultures.

2.1.7 Culture media for eukaryotic cell culture

Cell line	Ingredients
NIH3T3 HEK293	Gibco DMEM + Glutamax-I 1x 500 ml (contains 4,5 g/l D-glucose and sodium pyruvate) penicillin-streptomycin 1% FBS 10%
MCF7	Gibco DMEM + Glutamax-I 1x 500 ml (contains 4,5 g/l D-glucose and sodium pyruvate) penicillin-streptomycin 1% FBS 10% NEAA 500 μl insulin 2 mg
MDA-MB-231	RPMI medium 1640 + Glutamax-I 1x 500 ml 25 mM HEPES Penicillin-Streptomycin 1% FBS 10%

Tab. 2.7: Culture media for eukaryotic cell culture.

Besides insulin all media and supplements were ordered from Gibco Life Technologies. Insulin was ordered from Sigma-Aldrich.

Freezing medium: Complete medium with additional 10% FBS and 10% DMSO (Sigma-Aldrich).

Serum starvation medium is complete medium but only with 0.5% FBS.

2.1.8 Buffers and solutions

Name	Ingredients
Acid-ethanol	250 μl of 37% HCl in 70 ml of 70% ethanol
Ammoniac-H_2O	100 μl of 30-33% ammoniac in 80 ml H_2O
Bouin's solution	15 v of 1.2% picric acid
	5 v of 37% PFA
	1 v glacial acetic acid
Buffer A	15 mM $MgSO_4$
	0.1 mM EDTA
	25 mM DTT
	1 mM ATP
	200 μM coenzyme A
	200 μM D-luciferin
	200 mM Tris
	final pH 8.0
Buffer B	10 mM sodium acetate
	15 mM EDTA
	500 mM NaCl
	50 μM APMBT
	4 μM benzyl-coelenterazine
	500 mM Na_2SO_4
	25 mM Na_4PPi
	final pH 5.0
Denaturation buffer (8x)	250 mM Tris-HCl (pH 6.8)
	8% (w/v) SDS
	40% (w/v) 2-β-Mercaptoethanol
	0.004% (w/v) bromophenol blue
	40% (w/v) glycerol
DNA loading buffer (6x)	0.09% (w/v) xylene cyanol FF
	60 mM EDTA
	0.09% (w/v) bromophenol blue
	60% (w/v) glycine
Ethidium bromide	10 mg/ml ethidium bromide
	Working solution 5 μg/ml
IVF Cook medium	Supplied by human genetic institute (Göttingen)
KHM buffer	110 mM KOAc
	20 mM Hepes (pH 7.4)
	2 mM $MgCl_2$
Laemmli electrophoreses buffer (10x)	0.25 M Tris
	2 M (w/v) glycine
	1% (w/v) SDS
Lysis buffer for Co-IP	150 mM NaCl

	2 mM EDTA
	1% Triton X-100
	1x of protease inhibitor cocktail (100x)
	in PBS (pH 7.2)
Lysis buffer for *in situ* proteinase K digestion	0.4% (w/v) SDS
	2% Triton X-100
	400 mM NaCl
	50 mM Tris-HCl (pH 7.4)
	1 mM DTT
	1x of protease inhibitor cocktail (100x)
Lysis buffer for reporter gene assay	0.25% Triton X-100
	in 150 mM Hepes (pH 8.0)
5% Milk buffer	5% (w/v) skimmed milk powder (slightly soluble) in TBST
MBS	88 mM NaCl
	1 mM KCl
	2.4 mM NaHCO$_3$
	15 mM Hepes (pH7.6)
	0.3 mM Ca(NO$_3$)$_2$
	0.41 mM CaCl$_2$
	0.82 mM MgSO$_4$
	50 μg/ml gentamycin
PBT	1% (w/v) BSA
	0.5% Tween 20
	in PBS (pH 7.5)
PBS	145 mM NaCl
	7 mM Na$_2$HPO$_4$
	3 mM NaH$_2$PO$_4$
SSC (20x)	3 M NaCl
	0.3 M trisodium citrate
	final pH 7.0
SSPE (20x)	3.6 M NaCl
	0.2M NaH$_2$PO$_4$
	0.02M Na$_2$EDTA
	final pH 7.7
Stripping solution	1.5% (w/v) glycine
	0.1% (w/v) SDS
	1% Tween 20
	Final pH 2.2
TAE buffer (50x)	242 g/l Tris
	57.1 ml/l glacial acetic acid
	100 ml of 0.5 M EDTA
	final pH 8.0

TBST	20 mM Tris-HCl (pH 7.5)
	300 mM NaCl
	0.2% triton X-100
Transfer buffer	1 M Tris
	20 M glycine
	0.4 mM $MgCl_2$
	0.04% (w/v) SDS
	8% methanol
Tyrode's medium	8 g/l NaCl
	200 mg/l KCl
	200 mg/l $CaCl_2$
	100 mg/l $MgCl_2$
	50 mg/l NaH_2PO_4
	1 g/l $NaHCO_3$
	1 g/l glucose
	final pH 6.5

Tab. 2.8: Buffers and solutions. If no other indications, solutions and buffers were not high concentrated and prepared in milliq H_2O.

2.1.9 Chemicals

Name	Producer
Agarose	Carl Roth
Ammoniac (30-33%)	Roth
Ampicillin	AppliChem
APMBT	AppliChem
APS	Sigma-Aldrich
ATP	Bioline
Benzyl-coelenterazine	Synchem
Bromophenol blue	Sigma-Aldrich
BSA	AppliChem
$CaCl_2$	Merck
Calcium ionophore A23187	Sigma-Aldrich
$Ca(NO_3)_2$	Sigma-Aldrich
Coenzyme A	AppliChem
Coomassie brilliant blue R250	Sigma-Aldrich
DAPI	Sigma-Aldrich
50x Denhardt's solution	Invitrogen[TM] of Life Technologies
D-luciferin	Carl Roth
DTT	Sigma-Aldrich
EDTA	Carl Roth
Eosin G-solution 0.5% diluted	Carl Roth

Ethanol	VWR Chemicals
Ethidium bromide	Carl Roth
Ficoll	Supplied by Henningfeld's group
G418	PAA Laboratories GmbH
Gentamycin	Supplied by Henningfeld's group
Glacial acetic acid	Carl Roth
Glucose	Supplied by human genetic institute (Göttingen)
Glycerol	Roth
Glycine	Roth
HCG	Supplied by human genetic institute (Göttingen)
HCl (37%)	Roth
Hematoxylin solution (Gill II)	Carl Roth
HEPES	Roth
Kanamycine	Sigma-Aldrich
KCl	Merck
KOAc	Roth
2-β-Mercaptoethanol	Sigma-Aldrich
Methanol	VWR Chemicals
$MgCl_2$	AppliChem
$MgSO_4$	AppliChem
NaCl	AppliChem
Na_2EDTA	Roth
$NaHCO_3$	Merck
NaH_2PO_4	Merck
Na_2HPO_4	Roth
Na_4PPi	AppliChem
Na_2SO_4	Merck
Nocodazol	Sigma-Aldrich
Nonidet P40	Fluka Chemie AG
Paraffin	Merck
Picric acid	Sigma-Aldrich
PFA	Sigma-Aldrich
PL-FITC	PL biochemicals
PMSF	Sigma-Aldrich
PMSG	Supplied by human genetic institute (Göttingen)
Renaissance Enhanced Luminol Western Blot Chemiluminescence Reagent Plus	NEN Life Science Products
RNA Secure™ Resuspension solution	Ambion
Rotiphorese® gel 40 (29:1)	Roth
Salmon sperm DNA	Sigma-Aldrich
SDS	Roth
skimmed milk powder (slightly soluble)	SUCOFIN®
Sodium acetat	AppliChem

TEMED	Merck
Tris	Roth
Trisodium citrate	Roth
Triton X-100	Sigma-Aldrich
Tween 20	Merck
Xylene cyanol FF	Sigma-Aldrich
Xylol	Roth

Tab. 2.9: Chenicals.

2.1.10 Kits

Name	Producer
EndoFree® Plasmid Purification	Qiagen GmbH
ExoIII/S1 deletion kit	MBI Fermentas
in vitro fertilization medium	Medi-Cult
iQ^{TM} SYBR® Green Supermix	Bio-Rad
Mini prep kit NucleoSpin® plasmid	Macherey-Nagel GmbH&CoKG
peqGOLD RNAPure	PEQLAB
peqGOLD TriFast reagent	PEQLAB
protein G agarose	Thermo Scientific
QIAEX® II Gel Extraction kit (150)	Qiagen GmbH
RevertAid H Minus First Strand cDNA synthesis kit	Fermentas
Transfectin	Bio-Rad
Viagen DirectPCR-Tail	Viagen Biotech
X-tremeGENE HP DNA Transfection Reagent	Roche

Tab. 2.10: Kits.

2.2 Methods

2.2.1 General methods

2.2.1.1 Microbiological methods

2.2.1.1.1 Culture of *E. coli*

E. coli were cultured over night at 37 °C at 220 rpm.

2.2.1.1.2 Storage of *E.coli* cultures

200 μl glycerine was added to 800 μl over night bacterial culture and gently mixed. The mixtures were stored at -80 °C.

2.2.1.1.3 Production of competent bacteria

1 ml over night bacterial culture was added to 100 ml LB medium and incubated at 37 °C until OD_{600} up to 0.35 to 0.4. After incubation the bacterial culture was centrifuged for 20 min at 4 °C at 3000 x g. The pellet was resuspended with 500 μl precooled 50 mM $CaCl_2$. Subsequently the suspension was added into 20 ml 50 mM $CaCl_2$ and vibrated for 30 min at 4 °C. The suspension was then centrifuged for 20 min at 4 °C at 3000 x g. The pellet was repeatedly resuspended with 500 μl precooled 50 mM $CaCl_2$ and added into 5 ml 50 mM $CaCl_2$. 200 μl of the solution was aliquoted into Eppendorf reaction tube, immediately frozen in liquid nitrogen and stored at -80 °C.

2.2.1.1.4 Transformation

Transformation via heat shock into competent *E. coli* strains (DH5α) was performed as described by D. Hanahan (Hanahan, 1983).

Bacteria cells were defrosted on ice and 50 µl of cells was added to the DNA. The cells-DNA-mixture was incubated for 30 min on ice and then heated for 90 sec at 42 °C. After heat shock the cells were cooled for 2 min on ice. 300 µl LB medium without antibiotic was added to the cells and incubated for 1 h at 37 °C. The solution was added onto LB agar plate containing selective antibiotics and incubated over night at 37 °C.

2.2.1.2 Molecular biological methods

2.2.1.2.1 DNA preparation

Small amount of plasmid DNA was prepared with mini prep kit NucleoSpin® plasmid as indicated in the provided instruction manual. DNA for transfection was prepared with EndoFree® Plasmid Purification as indicated in the provided instruction manual. These protocols are based on the alkaline lysis from H.C. Birnboim and J. Doly (Birboim and Doly, 1979).

2.2.1.2.2 DNA purification

DNA was isolated from agarose gel and purified with QIAEX® II Gel Extraction kit as indicated in the provided instruction manual.

2.2.1.2.3 Measurement of DNA and RNA concentrations

1 µl of the nucleic acid mixture was measured by OD_{260} with a photospectrometer (Nanodrop, PeqLab). The dilute reagent was used as blank reference.

2.2.1.2.4 Enzymatic modification of DNA by restriction enzymes

1 µg DNA was digested by 1-1.5 U restriction enzyme in provided buffer. The enzyme volume should not be larger than 10% of total reaction volume.

2.2.1.2.5 Ligation

Ligations were performed with a 3:1 molar ratio insert/vector. 100 ng of the vector was mixed with the insert DNA fragment. 1 µl T4 DNA ligase with provided ligase buffer was added to the DNA mixture. Ligation was performed for 2 h at room temperature or over night at 4 °C.

2.2.1.3 Protein biochemical methods

2.2.1.3.1 Protein extraction and denaturation

Mammalian cells were trypsinized and centrifuged for 3 min at 1000 x g. The cells were washed with PBS and $1x10^6$ cells resuspended in 32 µl PBS. 4 µl 8x denaturation buffer was added to the suspension. The mixture was boiled for 10 min at 95°C.

2.2.1.3.2 SDS-PAGE

Proteins were separated with sodium dodecyl sulfate polyacrylamide gel electrophoresis (SDS-PAGE) (Laemmli, 1970). After denaturation of proteins the samples were loaded to the gel and separated in stacking gel in a SDS gel electrophoresis system (Bio-Rad) for 30 min at 100 V. In resolving gel the samples ran for 1 h at 150 V.

2.2.1.3.3 Transfer of proteins to Hybond ECL membrane

For antibody detection of specific proteins the proteins were transferred onto a Hybond ECL membrane (Amersham Biosiences) (Towbin *et al.*, 1979). The membrane was activated by methanol of transfer buffer. The gel together with membrane was clamped into Whatman papers and sponges. The blotting sandwich was placed in the blot chamber (Bio-Rad) and blotted in transfer buffer for 1 h at 100 V.

2.2.1.3.4 Immunologically protein detection

The membrane containing transferred proteins was blocked by 5% milk buffer for 1 h at room temperature. The primary antibodies were added to the membrane and incubated in 5% milk buffer over night at 4 °C. On next day the membrane was washed with TBST 3 times for 10 min each at room temperature. Incubation of membrane with horseradish peroxidase conjugated secondary antibodies occurred for 1 h at room temperature. After 3 times TBST washing ECL solutions (Pierce) were added to the membrane according to instruction manual. Chemoluminescence was detected by Amersham Hyperfilm[TM] ECL (GE Healthcare).

2.2.1.3.5 Co-IP (Co-immunoprecipitation)

5×10^6 untransfected cells or 24 h post-transfection cells were harvested by trypsination and resuspended in 1 ml lysis buffer by vortexing and passing 10 times through a 21 gauge needle. The cell lysate was then incubated on ice for 20 min followed by sonication 2 times for 45 sec each. After centrifugation at 15,000 x g for 15 min, the supernatant was recovered and splitted into two equal parts. The pellet (described as p) as well as 50 µl of supernatant (described as s) was stored for future Western blot analyses. Furthermore, the supernatant was subjected to immunoprecipitation. One part was incubated with the fishing antibody for 1 h at

room temperature whereas the second part was used as control without antibody incubation. Subsequently, pre-washed protein G agarose beads were added to both probes and mixtures rotated over night at 4 °C. Beads of proteins-antibodies-mixture were collected by centrifugation, and a 50 µl aliquot of the supernatant after centrifugation was taken as depletion control (described as dc). The Beads of proteins-antibodies-mixture were washed 4 times with 1 ml of lysis buffer each. 50 µl last wash buffer was collected (described as lw). Both aliquots were added with 50 µl 2 x denaturation buffer, respectively. After washing beads bound proteins were added with 50 µl 1 x denaturation buffer (described as b). The beads of control probe were collected by centrifugation and added with 50 µl 1 x denaturation buffer (described as bc). The fractions p and s were added with 50 µl 1 x and 2 x denaturation buffer, respectively. All fractions added with denaturation buffer were boiled for 10 min at 95 °C and ready for Western blot analyses.

2.2.1.4 Cell biological methods

2.2.1.4.1 Propagation of eukaryotic cells and subculture

All applied eukaryotic cells were cultured in suitable medium (see 2.1.7) at 37 °C and 5 % CO_2.

The old medium was aspirated and the cells were washed with PBS. 0.25% trypsin was added to the cells and incubated for 3 min at 37 °C. After incubation trypsin was inactivated by adding fresh complete medium containing 10 % FBS. Cells were resuspended with fresh medium and an aliquot of the suspension was transferred into a new flask. Then 10 ml fresh medium was added to the transferred cells in the new flask.

2.2.1.4.2 Defrosting and freezing of eukaryotic cells

For defrosting the cells were removed from liquid nitrogen and quickly put into the pre-warmed water bath for 3 min at 37 °C. Then the 1.5 ml cell-suspension was diluted with fresh medium and centrifuged for 3 min at 800 x g. The supernatant was discarded and the cell pellet resuspended with fresh medium. The suspension was resuspended and centrifuged for 3 min at 800 x g again. 10 ml medium was added to the cell pellet and resuspended, and removed into a new flask.

For freezing the cells were trypsinized and centrifuged for 3 min at 800 x g. Then cells were washed with PBS and resuspended with 3 ml freezing medium. The suspension was splitted into two equal parts and stored in labeled freezing tubes. Cells were firstly incubated for 2 h at -20 °C and subsequently over night at -80 °C. Finally the cells were stored in liquid nitrogen.

2.2.1.4.3 Assembly of transient transfection of cells

Plasmid DNA was transfected into NIH3T3, MCF7 and MDA-MB-231 with Transfectin and into HEK293 with XtremeGeneHP as indicated in the provided instruction manuals. The cells were incubated for 24 to 48 h at 37 °C and 5 % CO_2. After incubation the exogenous proteins were over-expressed and ready for future investigation.

2.2.1.4.4 Assembly of stably transfected cells

Each cell line of NIH3T3, HEK293, MCF7 and MDA-MB-231 was transfected with *Odf2*(*13.8NC)-GFP* and empty vector *pEGFP-N1*, respectively. 48 h post-transfection cells were selected under G418 control. After 8 weeks the stably transfected cells were assembled.

Cell line	G418 concentration in medium
NIH3T3	400 μg/ml
HEK293	400 μg/ml
MCF7	500 μg/ml
MDA-MB-231	600 μg/ml

Tab. 2.11: G418 concentrations of different cell culture media.

2.2.1.4.5 Immunocytology

Untransfected or 24 h post-transfection cells cultured on coverslips were washed 3 times with PBS for 5 min each and fixed in 3.7 % PFA in PBS for 20 min at 4 °C. Then the cells were permeabilized for 10 min with 0.3 % Triton X-100 in PBS at room temperature and blocked for 1 h with PBT. Primary antibodies were added to cells and incubated for 1 h at 37 °C. Cells were washed with PBS for 3 times 5 min each. Then the secondary antibodies were added to cells and incubated for 45 min at 37 °C. The DNA was counterstained with DAPI. After 3 times PBS washing DAKO mounting medium (DAKO) was added to cells and cells were sealed between coverslip and object slide by nail polish. Images were taken by confocal microscopy (LSM 510, Zeiss) and processed using Adobe Photoshop 7.0.

2.2.2 Specific methods of *Odf1*-deficient mice investigation

2.2.2.1 Generation of targeting vector

All mouse experiments were reviewed and approved by the local ethics commission. Licensing for animal experiments was obtained by the Institute of Human Genetics. A genomic *Odf1* cosmid clone (121 J 1787Q3; 129/Ola) was obtained from the Resource Centre of the German Human Genome Project at the Max-Planck-Institute for Molecular Genetics (Berlin, Germany) and mapped for restriction enzyme recognition sites. To assemble the targeting vector, an XbaI fragment containing ~4 kb of the 5` region, including the promoter region, as well as exon 1, was subcloned

into pGEMT, and exoIII deletions, starting from the 3´ region, were performed. A fragment of ~3 kb consisting of the upstream genomic region of the *Odf1* gene was first subcloned via XbaI / EcoRI into pBluescript, followed by NotI / XhoI cloning into pPNT-M1. The ~3.8-kb PstI intron fragment was first subcloned into pBluescript, followed by XbaI / EcoRI directional cloning into pPNT-M1. The resulting targeting vector (Fig. 3.1A) was sequenced to verify the correct orientations of both fragments. The targeting construct was linearized at the unique NotI site before electroporation.

2.2.2.2 Generation of the 3` external probe and Southern blot hybridization

The 3` external hybridization probe was generated by PCR amplification using the primer pair Odf1SPst and Odf1SHindIII out of a genomic *Odf1* clone and cloned into pGEMT.

For Southern blot hybridization, genomic DNA was extracted from ES cells, digested with HindIII, electrophoretically separated on agarose gels, and transferred onto Hybond N membranes (Amersham, Freiburg, Germany) by capillary blotting. The 3´ external probe was labeled with $[^{32}P]$dATP by the random hexanucleotide primer method (AP Feinberg and B. Vogelstein, 1983), and hybridized over night in 5x SSPE, 5x Denhardt's solution, 0.1% SDS, and 100 μg of denatured salmon sperm DNA / ml (E. Southern, 1975) at 65°C. Filters were washed 2 times at room temperature in 2x SSC, then in 1x SSC containing 0.1% SDS, and finally in 0.1x SSC containing 0.1% SDS at hybridization temperature.

2.2.2.3 ES cell culture and generation

ES cell line R1 (provided by A. Nagy, Toronto, Ontario, Canada) was cultured as described by A. Joyner (A. Joyner, 1993). Trypsinized and resuspended ES cells were mixed with 50 mg of linearized target vector and electroporated at 250 V and 500 μF using a Bio-Rad gene pulser apparatus (Bio-Rad). Cells were plated in nonselective

medium containing leukemia inhibitory factor in the presence of G418-resistant embryonic mouse fibroblasts. Selection for homologous recombined ES cells was carried out with medium containing 350 µg/ml G418 and 2 µmol/l ganciclovir. After 10 days of selection, individual drug-resistant clones were picked into 24-well trays. Three days later, individual recombinant ES clones were replicated into 24-well trays for freezing and for isolation of genomic DNA. A total of 10 to 15 compacted recombinant ES cells were microinjected into 3.5-day-old embryos of the C57BL/6 mouse strain (A. Joyner, 1993). The chimeric male mice generated were mated with C57BL/6 females to produce offspring.

Heterozygous *Odf1*-deficient mice generated by mating of chimeric male mice with C57BL/6 females were backcrossed with mice from inbred strain 129Sv to reduce C57BL/6 background genes. Heterozygous offspring were backcrossed with 129Sv mice up to generation N7 that is then supposed to be isogenic.

2.2.2.4 Genotyping

Genomic DNA from tail tip biopsy was extracted with Viagen DirectPCR-Tail and proteinase K digestion as indicated in the provided instruction manual. Genotyping was performed with the following primer pairs: Odf1-I and Neomy for detection of the neomycin cassette in the recombined allele, Odf1-5`ko and Odf1-I for differentiation between the wild-type allele of ~1.5 kb and the recombined allele of ~2.4 kb, and Odf1-I and Odf1-N for detection of the wild-type allele. A first PCR was performed with the primer pair Odf1-I / Neomy for detection of the recombined allele and a second PCR with the primer pair Odf1-I / Odf1-N for detection of the wild-type allele and to differentiate between heterozygous and homozygous mice. Both PCR amplifications were performed with an initial denaturation step at 95°C for 3 min, followed by 35 cycles at 95°C for 30 sec, annealing at 49°c for 30 sec, and elongation at 72°C for 1 min, and a final extension step at 72°C for 8 min. Mango Taq DNA polymerase was used for these two PCRs.

2.2.2.5 Fertility test

The fertility of the *Odf1*-deficient males on a mixed background (C57BL/6 x 129/Sv) was investigated by mating with wildtype females. Mating tests were performed with 11 homozygous male mice (*Odf1*$^{-/-}$) for at least 3 months. As a control group, six of their male littermates with a heterozygous genotype (*Odf1*$^{+/-}$) were mated with wild-type females. Females were checked for the presence of vaginal plugs and/or pregnancy. Pregnant females were removed to holding cages to give birth. The numbers and size of litters sired by each group of males were determined.

The insemination capacity of the heterozygous *Odf1*-deficient males on isogenic background (129/Sv; generation N7) was also investigated by mating with wild-type females. Females were checked for the presence of a vaginal plug. Liquid was isolated from uteri and inspected for the presence of sperm.

2.2.2.6 Reverse transcriptase PCR on genes of *Odf1*-deficient mice

Total RNA was extracted from testes of wild-type, heterozygous, and homozygous *Odf1 knock out* mice, respectively, using peqGOLD RNAPure and digested with RQ1 DNase. RNA was reverse transcribed using RevertAid H Minus First Strand cDNA synthesis kit and oligo(dT)$_{18}$ primer, followed by PCR. The corresponding PCR parameters of each primer pair (annealing temperature, elongation time, and size of amplified fragments) are shown in table 2.12. PCR amplification was performed with an initial denaturation step at 95°C for 3 min, followed by 36 cycles at 95°C for 30 sec, annealing for 30 sec, and elongation at 72°C, and a final extension step at 72°C for 8 min. PCR amplification of *Odf1* was applied with Mango Taq DNA polymerase and all the rest PCRs were performed with Taq polymerase.

Target gene	Primer	Annealing Temprature (°C)	Elongation time	Product size (bp)
SYCP3	MSYCP35`Kpn1	52	1 min	900
	MSYCP3r			
Stra8	Stra8 for	56	30 s	444
	Stra8 rev			
HANP1/H1T2	Hanp1-H1T2-for	50	1 min	800
	Hanp1-H1T2-rev			
MIS	MMISf	56	30 s	315
	MMISr			
Ins13	mIns13f	56	30 s	543
	mIns13r			
Odf2	138NCEcoRI	59	1 min	822/677
	DH1rev			
Odf1	Odf1-N	52	1 min	800
	Odf1-C			

Tab. 2.12: Primers application of RT-PCR in *Odf1 knock out* mice.

2.2.2.7 Histology and immunocytology of mouse tissues

Testes were alternatively fixed in 4% PFA in PBS or in Bouin's solution and embedded in paraffin. Then, 4-µm sections were cut and placed onto Superfrost® slides (Thermo Scientific). Drying of probes was performed by incubation for over night at 55 °C. The probes were deparaffinized with xylol two times for 3 min each and last time for 5 min and then rehydrated in ethanol with decreasing concentration from 100%, 90%, 80%, and down to 70% for 2 min, each. After washing with milliq H_2O, the probes were stained with hematoxylin for 1-2 min and then immediately put into milliq H_2O for short washing, and afterward washed with flowing tap water for 5-15 min. Furthermore, the probes were quickly put into acid-ethanol and removed from the solution, this step was repeated for 3-4 times. Subsequently, the probes were quickly put into ammoniac water and removed from the solution, this step was also repeated for 3-4 times. Then the probes were shortly washed with tap water. Then they were stained with eosin for 1 min. After washing with water the probes were dehydrated in ethanol with increasing concentration from 70%, 80%, 90% and up to

100% for 1 min, each. The probes were put into xylol for 10 min. After all, the sections were embedded with Eukitt quick-hardening mounting medium (FLUKA).

For immunocytology, epididymides were minced in PBS, and the cell suspension was transferred onto Superfrost plus slides by centrifugation at 1,000x g for 5 min. The cells were fixed in 3.7% PFA in PBS, blocked in PBT for 30 min, and incubated with anti-α-tubulin antibody for 1 h. The primary antibody was detected by Cy3-labeled anti-mouse IgG, the DNA was counterstained with DAPI, and the acrosome was decorated with PL-FITC. Images were taken by confocal microscopy (LSM 510, Zeiss) and processed using Adobe Photoshop 7.0.

2.2.2.8 Electron microscopy

Testes and epididymides were fixed in 1% glutaraldehyde in 0.2M phosphate buffer, postfixed with 2% osmium tetroxide, and embedded in epoxy (Epon) resin. Selected areas were sectioned and examined by transmission electron microscopy.

2.2.2.9 Sperm analysis

Heterozygous and homozygous *Odf1*-deficient male mice of the mixed background, wild-type males of C57BL/6 strain, as well as heterozygous *Odf1*-deficient male mice of the isogenic background (generation N7), and wildtype males of 129/Sv strain, were used for sperm analyses. Epididymides were collected and dissected in Tyrode's medium. Sperm number in corpus and cauda epididymis was determined using the Neubauer cell chamber.

For acrosome reaction, spermatozoa were capacitated for 1.5 h in Tyrode's medium and then incubated for 5 min at 37 °C and 5% CO_2 with Tyrode's medium plus 20 μM calcium ionophore. For the determination of the percentage of sperm that had undergone an acrosome reaction, sperm were fixed and stained with Coomassie brilliant blue as described by C. Thaler (C. Thaler, 1995). At least 200 spermatozoa

from each male were examined for the presence or absence of the characteristic dark blue crescent.

2.2.2.10 *In vitro* fertilization (IVF) with heterozygous *Odf1*-deficient males on isogenic background (129/Sv; generation N7)

Adult female mice were superovulated by intraperitoneal injections of 5U PMSG. 48 h later 5U HCG was injected intraperitoneally. Oocytes from superovulated females were isolated 15-17 h after HCG injection. Isolated oocytes were freed from cumulus cells and zona pellucida by incubation in hyaluronidase (300 μg/μl) for 10 min at 37 °C followed by incubation in Tyrode's solution (pH 2.7) for 10-20 sec. Oocytes were then transferred into IVF Cook medium previously equilibrated over night at 37 °C and 5% CO_2. *In vitro* fertilization took place in equilibrated Cook medium containing isolated epididymal spermatozoa for 6 h at 37 °C and 5% CO_2. Oocytes were then washed in pre-equilibrated Cook medium and incubated over night at 37 °C and 5% CO_2. Degenerated oocytes and embryos were counted 24 h after IVF.

2.2.2.11 Sperm motility analysis

Epididymides of three wild-type, heterozygous, and homozygous *Odf1*-deficient males, respectively, were dissected in IVF Cook medium. Spermatozoa were allowed to swim out of the epididymides and incubated for 1.5 h at 37 °C. A total of 13 μl of the sperm suspension was transferred to the incubation chamber, which was set at a temperature of 37 °C. Sperm movement was quantified using the CEROS computer-assisted semen analysis system (version 10; Hamilton Thorne Research, Beverly, MA). Then, 1,000 to 3,000 spermatozoa from each individual were analyzed using the following parameters: negative phase-contrast optics; recording, 60 frames/s; minimum contrast, 60; minimum cell size, 6 pixels; straightness (STR) threshold, $\geq$50%; cutoff of the average path velocity (VAP) and straight line velocity (VSL), 25

and 30 μm/s, respectively; minimum progressive average path velocity (VAP), 75 μm/s; slow cells motile, no (this limit avoids counting sperm moved by others or Brownian motion and low-velocity non-progressive cells); and minimum static contrast, 15 pixels.

For statistical analysis, the frequencies of the six sperm motility parameters VAP, VSL, VCL, ALH, BCF, and STR were examined. Because all analyzed parameters were significantly different from normal distribution (Shapiro-Wilk's W test) and could not be normalized by any transformation, the nonparametric alternative for t test, the Mann-Whitney U test, was used. For statistical testing, sperm motility measurements of each parameter were pooled for mouse type. Statistical analyses were performed by Statistica 9 (StatSoft, Inc., Tulsa, USA).

2.2.3 Specific methods of SPAG4 protein investigation

2.2.3.1 Subcloning of *Spag4* cDNA

The 3` region of *Spag4* was amplified out of mouse testis cDNA using primer pair SPAG4 C KpnI and Spag4 650 for. The PCR product of ~650 bp was isolated and mixed with *Spag4* cDNA clone IRAMp995J1116Q (imaGenes, Germany) which encompasses ~650 bp of the 5` region of full length *Spag4*. A PCR reaction was performed using primer pair SPAG4 C KpnI and SPAG4 N XbaI. The PCR product of ~1.2 kb was eventually subcloned into modified pcDNA3.1/myc-His(-) C digested with KpnI / XbaI. The final clone yielded a protein that was tagged with HA at its N-terminal end and with Myc at its C-terminal end. N-terminal and C-terminal truncated *Spag4* constructs were generated by PCR amplification and finally by subcloning into modified pcDNA3.1HA/*myc*-His(-) C. N-terminally truncated *Spag4-C* was amplified with primer pair SPAG4N2XbaI and SPAG4 C KpnI, and C-terminally truncated *Spag4-N* was generated using primer pair SPAG4 N XbaI and SPAG4C2KpnI. Both constructs were tagged with *HA* at their N-terminal ends. *EYFP-Spag4* was generated by amplification of *EYFP* using primer pair EYFP-C

XbaI and EYFP–N SpeI and ligation to the N-terminal end of *Spag4*. *Odf1* was fused to *ECFP* in *pECFP-N1*. Sequencing always revealed correct reading frames.

2.2.3.2 Reverse transcriptase PCR on *Spag4*

Total RNA was prepared from mouse tissues as well as from different cell lines (ES, SSC, and F9) using peqGOLD TriFast reagent. RNA was first digested with RQ1 DNase. Then cDNA was generated using RevertAid H Minus First Strand cDNA synthesis kit and oligo(dT)$_{18}$ primer. SPAG4 C KpnI and Spag4 650 for primers were used for RT-PCR reaction to amplify *SPAG4*. As control, *GAPDH* (glyceraldehyde-3-phosphate dehydrogenase) was amplified using primers GAPDHfor and GAPDHrev.

2.2.3.3 In situ proteinase K digestion

NIH3T3 cells were transfected with *HA-Spag4-Myc* tagged at the N-terminus with *HA* and at the C-terminus with *Myc*. 24 h post-transfection cells were subjected to *in situ* proteinase K digestion. In brief, cells were washed two times with ice-cold PBS, scraped in PBS and transferred into plastic tubes. Cells were then either incubated in KHM buffer containing 4 μg/ml proteinase K, or in KHM buffer containing 0.5 % Triton X-100 and 4 μg/ml proteinase K for 45 min at room temperature. Thereafter, cells were sedimented by centrifugation and lysed in lysis buffer by passing through a 20-gauge needle. Finally the cells were centrifuged and supernatant as well as pellet was added with denaturation buffer, boiled for 10 min at 95 °C. The denatured probes were ready for future Western blot analyses.

2.2.3.4 Immunocytology on testicular suspensions

Cell suspensions from testes of wild-type or *Odf1*$^{-/-}$ mice were prepared in PBS and

transferred onto superfrost slides. Specimens were fixed in 3.7% PFA in PBS, permeabilized in 0.3% Triton X-100 in PBS for 10 min, and blocked for 1 h in PBS containing 1 % BSA and 0.3 % Triton X-100. Immunocytology was performed with anti-SPAG4 antibody and anti-α-tubulin antibody over night at 4°C.

2.2.3.5 Co-IP with transfected cells and testicular tissue

NIH3T3 or HEK293 cells were either transfected with expression plasmids encoding different regions of *Spag4* or *Odf1*, or with two different full lengths *Spag4* constructs. Coding sequences were fused to diverse tags: *HA-Spag4-C* encoding the C-terminal end of *Spag4* fused to *HA*, *HA-Spag4-N* encoding the N-terminal end of *Spag4* fused to *HA*, full length *Spag4* either fused to *HA / Myc* (*HA-Spag4-Myc*) or to *EYFP* at its N-terminal end (*EYFP-Spag4-Myc*). *Odf1* was fused to *ECFP*. 24 h post-transfection cells were subjected for Co-IP.

Co-IP with testis tissue was performed essentially as described in 2.2.1.3.5 with the following modifications. Testis was frozen in liquid nitrogen and ground in a mortar. The cell lysate was prepared by resuspension in PBS containing 1% Nonidet P40, 100 µg/ml PMSF, and 1µg/ml protease inhibitors and then sonicated 3 times for 45 sec each. The supernatant was obtained by centrifugation for 15 min at 1,000x g.

2.2.4 Specific methods of ODF2 protein investigation

2.2.4.1 Reporter gene assay

Reporter gene *OT* contains firefly-luciferase under control of promoter with Tcf4 binding site. Once the complex containing β-catenin and its co-factor Tcf4 binds to the Tcf4 binding site, the reporter gene is immediately activated. Subsequently the luciferase activity is measured by luminometer TriStar LB 941 (Berthold Technologies, Germany). In contrast to *OT*, as negative control *OF* vector has a mutated Tcf4 binding site. As internal control renilla-luciferase gene (*phRL*) was

considered to control transfection efficiency. The influence of ODF2 on canonical Wnt signaling pathway or rather on β-catenin was investigated by co-transfection of *Odf2 (13.8NC)-GFP* and *β-catenin*. 24 h post-transfection cells were scratched from the bottom of the wells of 12-well plate and centrifuged for 10 min at 800x g. The pellet was resuspended and lysed in 30 μl lysis buffer for 30 min at room temperature. Then the suspension was centrifuged at 13,000x g for 1 min at room temperature. The supernatant was transferred into well of 96-well plate and subsequently added with 50 μl of firefly-luciferase substrate (buffer A). After firefly-luminescence measurement the reaction was prevented by adding 50 μl renilla-luciferase substrate (buffer B). Renilla-luminescence was also measured by luminometer.

All experiments were performed in triplicate. The value of firefly-luminescence was divided by renilla-luminescence and then multiplied by 1000 to obtain relative firefly-luciferase activity. The values measured by luminometer are demonstrated in the supplement.

2.2.4.2 Micro injection into embryos of *Xenopus laevis*

The eggs of *Xenopus laevis* were collected and mixed with the testis mixture. After the *in vitro* fertilization the eggs were dejellied. After dejellying, the fertilized eggs were transferred to 0.1x MBS containing 1% Ficoll prior to injection. At the 3.stage (4-cell) the embryos were injected in its marginal zone of ventral area where the nature *Xwnt-8* is enriched. The injection was performed for every time with three groups: only *Xwnt-8*, *Xwnt-8* and *Odf2*, and only *Odf2*. For co-injection of *Xwnt-8* and *Odf2* different RNA amount combinations of both genes were carried out. 100 to 200 embryos were injected for each combination of co-injection or single injection to implement statistic analysis. After injection, the embryos were incubated at 14°C and had to be controlled twice a day by microscopy. Only living embryos were allowed to stay further and transferred into fresh 0.1x MBS buffer. In about 4 days the embryos entered into tadpole stages, and the tadpoles with secondary dorsal axis were counted.

2.2.4.3 Quantitative real time PCR

HEK293 cells were transiently transfected with following constructs: *13.8NC-GFP*, *13.8NCΔGFP*, *pEGFP-1*, *pEGFP-N1*, *shODF2,* respectively. Total RNA was extracted from these transiently transfected cells, untransfected cells and cells stably transfected with *13.8NC-GFP* using peqGOLD RNAPure and digested with RQ1 DNase. RNA was reverse transcribed using RevertAid H Minus First Strand cDNA synthesis kit and oligo(dT)$_{18}$ primer. PCR was performed with primers hHPRT1_2f_390 / hHPRT1_2r_631 and hCmyc_2f_344 / hCmyc_2r_615. 10 μl final reaction volume contains 0.3 μl forward primer (10 pmol/μl), 0.3 μl reverse primer (10 pmol/μl), 1 μl cDNA (equivalent of 20 ng RNA), 5 μl iQ^{TM} SYBR$^®$ Green Supermix and 3.4 μl nuclease-free H$_2$O. The PCR was performed using the standard reaction program of CFX96^{TM} Real-Time System (Bio-Rad) with annealing temperature at 58 °C and elongation for 30 sec.

2.2.4.4 Wound healing assay

NIH3T3, MCF7 and MDA-MB-231 cell lines were examined using wound healing assay. Untransfected cells, cells stable transfected with empty vector *pEGFP-N1* and cells stably transfected with *13.8NC-GFP* were applied for each cell line. 100% confluent cells were scratched and cultured in serum starvation medium. The width of wound was measured after certain hours and analysed with ImageJ software.

3. Results

3.1 ODF1 protein

3.1.1 ODF1 protein is essential for tight linkage of sperm head to tail and male fertility in mice

3.1.1.1 The generation of mice with disruption of the *Odf1* gene

The *Odf1* gene consists of two exons separated by one large intron. Transcription and translation start sites are both in exon 1 (Burfeind and Hoyer-Fender, 1991; Burfeind *et al*., 1993; Gastmann *et al*., 1993). The targeting vector used to disrupt *Odf1* was designed with a neomycin cassette to replace exon 1 and the promoter region (Fig. 3.1 A). After electroporation of the linearized targeting vector into mouse ES cells recombinant colonies were established by selection with G418 and ganciclovir. Next, Southern blot hybridization with HindIII digested genomic DNA of individual ES cell clones and 3` external probe was performed. Out of 96 ES cell clones tested, 20 clones showed the expected hybridization pattern of a band of ~5.4 kb that refers to the wild-type allele and a band of ~7.2 kb that refers to the homologous recombined allele (Fig. 3.1 B). One ES cell clone that showed the expected hybridization pattern after repeated Southern blot hybridization with the external 3` probe was chosen for microinjection into blastomeres of 3.5-day-old embryos of C57BL/6 mice. After reimplantation of embryos, several chimeras were born, most of them with a high chimerism (>90%). Male chimeras mated with C57BL/6 females transmitted the targeted allele to their offspring. Offspring were genotyped by PCR on genomic DNA isolated from tail tip biopsy specimens using primer pair Neomy/Odf1-I (Fig. 3.1 C). Heterozygous mice were crossed with C57BL/6 mice to establish the heterozygous $Odf1^{+/-}$ line. Eventually, heterozygous male and female mice were crossed to generate *Odf1*-deficient mice. Genotyping was generally performed on tail tip biopsy specimens using the primer pair Neomy/Odf1-I for detection of the recombined allele and with primer pair Odf1-N/Odf1-I for detection of the wild-type allele (Fig. 3.1 C).
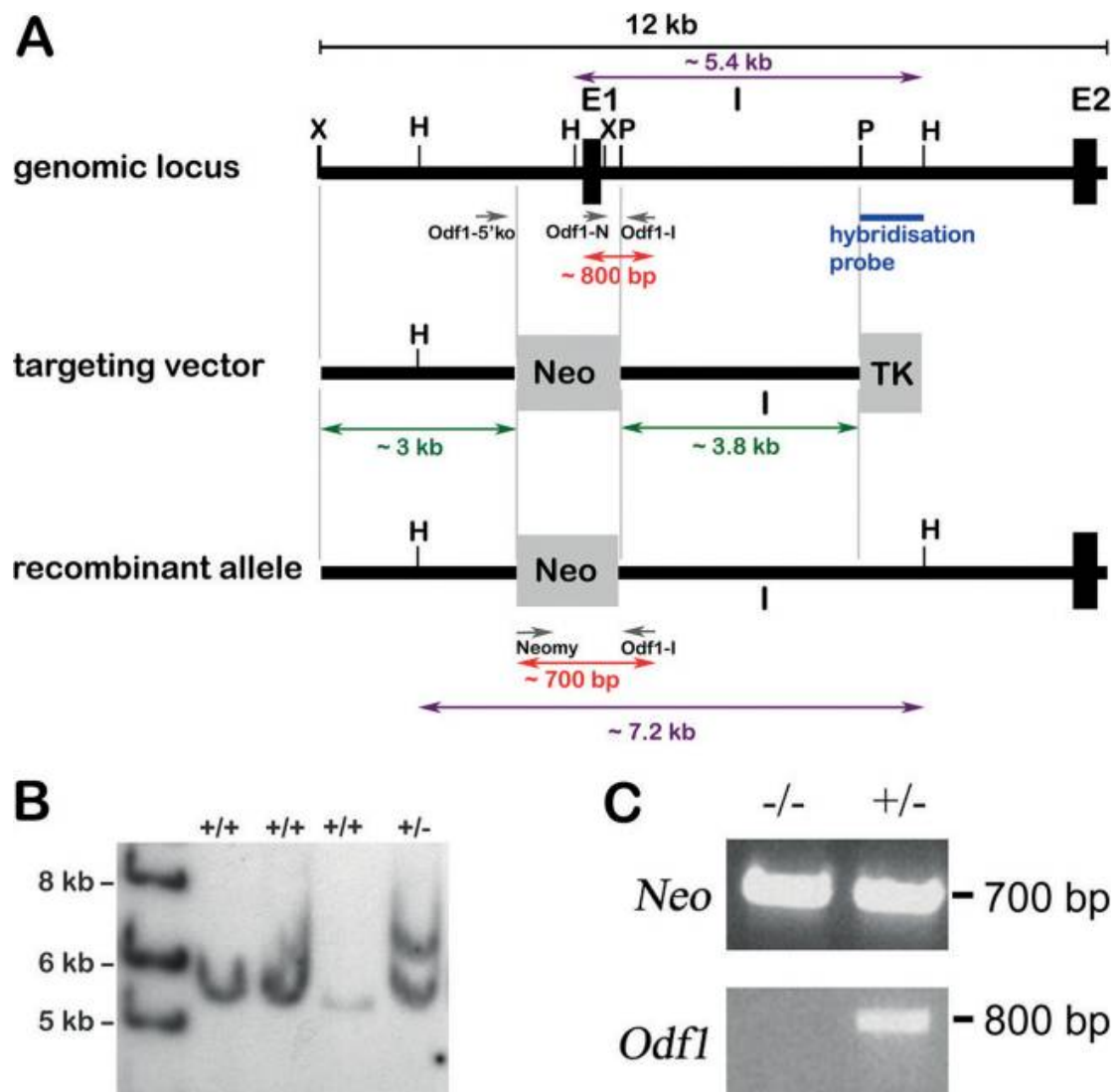
Fig 3.1: Targeted disruption of the promoter region and of exon 1 of the *Odf1* gene. (A), structure of the wild-type allele, targeting vector, and recombinant allele are shown, together with relevant restriction sites, primer positions, and external hybridization probe position. The targeting vector consists of 5` upstream region (~3 kb) and intronic sequences (~3.8 kb) flanking the pgk-neomycin selection cassette (Neo). TK, thymidine kinase cassette; X, XbaI; H, HindIII; P, PstI; E1, exon 1; E2, exon 2; I, intron; Odf1-5`ko, Odf1-I, Odf1-N, and Neomy, primers used for genotyping. Southern blot hybridization of HindIII-digested genomic DNA with the 3` external probe resulted in an ~5.4-kb fragment of the wild-type allele and an ~7.2-kb fragment of the recombined allele. Genotyping with primer pair Odf1-N/Odf1-I resulted in an ~800-bp fragment of the wild-type allele, and genotyping with the primer pair Neomy/Odf1-I resulted in an ~700-bp

fragment of the recombined allele. **(B)**, Southern blot hybridization of HindIII-digested genomic DNA isolated from individual ES cell colonies generated by electroporation with the targeting construct, followed by selection with G418 and ganciclovir. Hybridization with the 3´ external probe to a fragment of ~7.2 kb revealed homologous recombination. The fragment of the wild-type allele is shown at ~5.4 kb. +/+, no homologous recombination; +/-, homologous recombination. **(C)**, genotyping using the primer pair Neomy/Odf1-I for detection of the recombined allele (*Neo*) and the primer pair Odf1-N/Odf1-I for detection of the wild-type allele (*Odf1*) in homozygous (-/-) and heterozygous (+/-) mice.

3.1.1.2 *Odf1*-deficient male mice are infertile

Heterozygous and homozygous *Odf1*-deficient male mice were first inspected regarding their overall morphological features taking into consideration testes weight related to body length and weight. However, no significant difference between both groups could be found. Phenotypic differences mostly rely on individual deviations irrespective of the presence of ODF1. Testis weight especially was related to body length and weight but not to the presence or absence of ODF1. Therefore, *Odf1* deficiency did not obviously influence these morphological criteria.

However, the infertility in homozygous *Odf1*-deficient male mice has been observed, whereas fecundity was not impaired in *Odf1*-deficient female mice or in heterozygous male mice. To further confirm the infertility of $Odf1^{-/-}$-male mice, 11 $Odf1^{-/-}$-male mice were mated with wild-type females. Over a time period of at least 3 months, none of these pairings gave birth to offspring or even resulted in pregnancy. In contrast, their heterozygous $Odf1^{+/-}$ male littermates ($n = 6$) gave rise to offspring generally after about 4 weeks of mating with wild-type females. In test matings, no sperm in the uterus of the female mouse was found when mated to *Odf1*-deficient male, although the vaginal plug inspection was positive. The litter size of matings of wild-type C57BL/6 females with heterozygous $Odf1^{+/-}$ males ($n = 29$ litters; average litter size of 6.7) was comparable to that of wild-type breeding (litter size of 6.2).

Furthermore, offspring of heterozygous males have sex ratios of approximately Mendelian ratio (57 male and 43 female pups were born), suggesting that *Odf1* deficiency in the heterozygote state did not impair embryonic development. In addition, *Odf1*-deficient female mice (*Odf1*$^{-/-}$) are not impaired in fertility (Tab. 3.1). Therefore the *Odf1*-deficient mouse line was established by mating of *Odf1*-deficient females (*Odf1*$^{-/-}$) with heterozygous males.

Genotype	Male fertility	Average litter size (males)	Mean testis / body weight (x10^{-3}) ± SD	Female fertility	Average litter size (females)
+ / +	28/28	6.2	Not determined	28/28	6.2
+ / -	29/29	6.7	3.1±0.37 (n=3)	19/19	5.8
- / -	11/0	0	2.92±0.31 (n=6)	10/10	5.2

Tab. 3.1: Fertility, fecundity, and testis weight of wild-type and *Odf1* mutant mice. To test fertility, sexually mature mice were bred for at least 3 months. Litter size was recorded for each mating. Testis weight and body weight were measured from mice older than 5 months of age.

3.1.1.3 Spermatogenesis in *Odf1*-deficient mice

Histological analyses of testes from heterozygous and homozygous *Odf1*-deficient adult mice revealed that spermatogenesis proceeded normally in all heterozygous mice (*n* = 4) (Fig. 3.2 B g). However, three different phenotypes were observed in *Odf1*$^{-/-}$ mice. One of nine homozygous mice analyzed showed an obvious wild-type phenotype with elongating spermatids in the seminiferous tubules (Fig. 3.2 B h). Six mice had displaced germ cells in the lumen (Fig. 3.2 B, arrow in panel i), and two mice had multinuclear cells in the lumen (Fig. 3.2 B, arrow in panel j). Mature sperm were barely found.

To investigate whether spermatogenesis is also affected, I inspected testis sections of one to three individuals each aged 10, 15, and 19 days *post partum* (dpp). Histological analyses of testis sections from 10 dpp onward revealed no obvious differences

between heterozygous and homozygous *Odf1*-deficient mice (Fig. 3.2 A). Spermatogenesis proceeded normally as previously described (Nebel *et al.*, 1961). Meiosis starts around day 10, and early round spermatids are present ~10 days later. Fig. 3.2 A (b, d, and f) demonstrates that the spermatogenesis of *Odf1*-deficient males proceeded normally, and at 19-dpp round spermatids were observed in heterozygous as well as in homozygous mutants (arrows in Fig. 3.2 A, e and f). The early elongating spermatid stage then is reached at about day 26 and elongating spermatids were also detected in most of the *Odf1*-deficient testes (Fig. 3.2 B, h and i).

Furthermore, I investigated testis composition and spermatogenic progression by reverse transcription-PCR (RT-PCR) of marker genes. *Insl3* was chosen as a marker gene for Leydig cells, *Mis* (Müllerian inhibiting substance) as a marker gene for Sertoli cells, *Stra8* as a marker gene for spermatogonia, *Sycp3* (*Scp3*, synaptonemal complex protein 3) as a marker gene for meiosis, *Hanp1/ H1T2* as a marker gene to monitor spermiogenic progression, and *Odf2* as a ubiquitously expressed gene that is upregulated during spermiogenesis (Adham *et al.*, 1993; Brohmann *et al.*, 1997; Cui, 2010; Hüber and Hoyer-Fender, 2007; Lim *et al.*, 1998; Marmor and Grob-Menendez, 1991; Matzuk and Lamb, 2008; Otani *et al.*, 1988; Oulad-Abdelghani *et al.*, 1996; Tanaka *et al.*, 2005). In addition, expression of *Odf1* by RT-PCR was checked to confirm the correct genotyping and absence of *Odf1* in homozygous *Odf1*-deficient mice (Fig. 3.3). I performed RT-PCR for all marker genes using cDNA generated from testes of two wild-type mice, nine heterozygous mice, and 17 homozygous *Odf1*-deficient mice. Besides *Odf1*, which was absent in homozygous *Odf1*-deficient mice, all marker genes were expressed in all cases, including mice that have undifferentiated or multinuclear cells present in their testis tubules (see Fig. 3.2 B). Fig. 3.3 shows the expression of *Hanp1* and *Odf1* as an example of RT-PCR (other PCR results not shown).

Although there is normal progression of spermatogenesis up to the spermatid stage, examination of semithin sections revealed a disorganized seminiferous epithelium, and strong reduction of mature spermatozoa in caput epididymides of *Odf1*-deficient mice (Fig. 3.4). Instead, an increase of non-mature germ cells and a high percentage

of dysplastic sperm were found in the epididymides (Fig. 3.4).
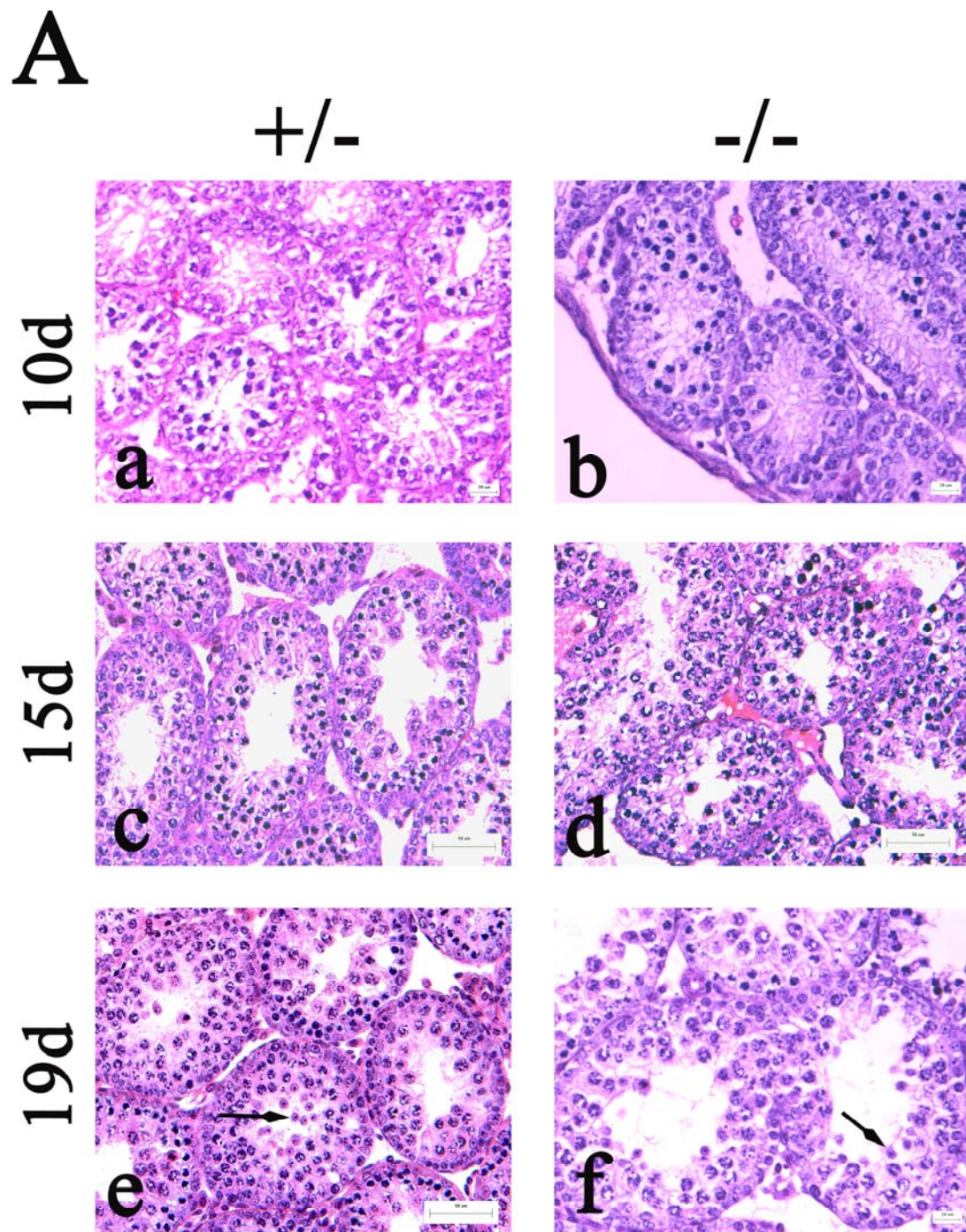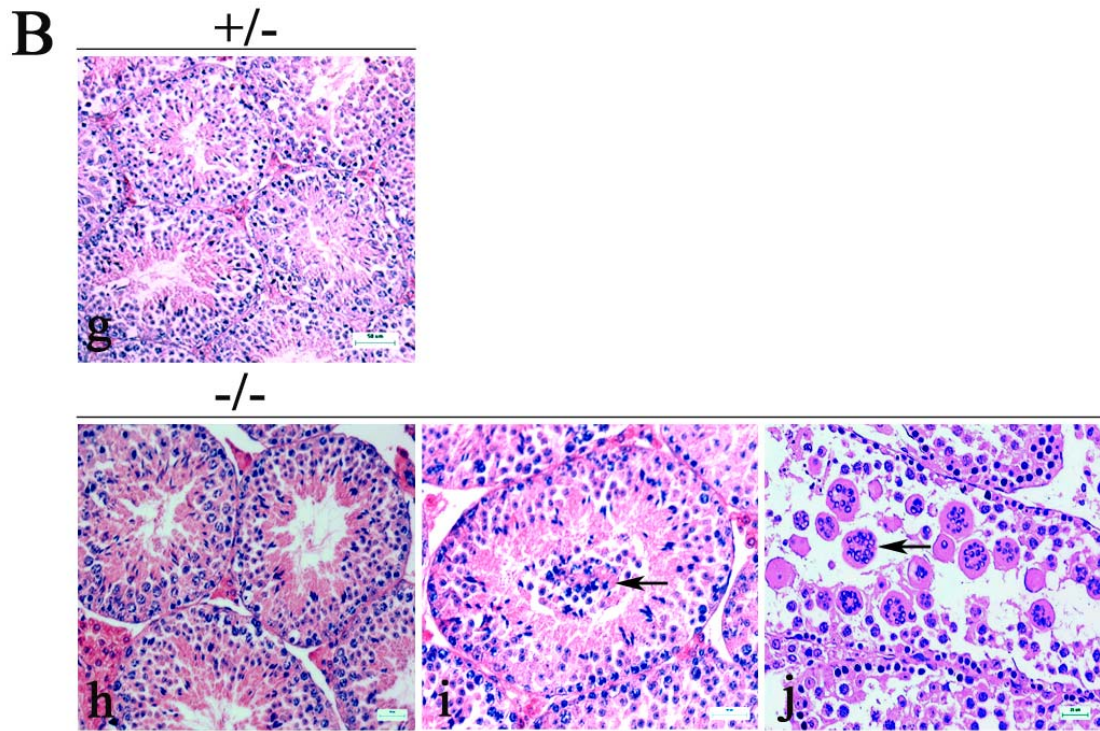
Fig. 3.2: Testicular histology of heterozygous and homozygous *Odf1*-deficient mice. Testis sections were stained with hematoxylin and eosin. **(A)**, spermatogenesis in heterozygous and homozygous *Odf1*-deficient mice. Testes from 10-day-old mice (10d), 15-day-old mice (15d), and 19-day-old mice (19d) were examined. No differences in spermatogenic progression between heterozygous and homozygous mice were observed. Round spermatids are found in 19d testes of heterozygous and homozygous *Odf1*-deficient mice (arrows in panels e and f). For each developmental stage, the testes of one to three mice were prepared. Bars: 20 μm (a, b, and f), 50 μm (c to e). **(B)**, spermatogenesis proceeded normally in adult heterozygous mice (g). In adult homozygous mice three different phenotypes were observed. One in nine animals showed an obvious wild-type phenotype (h); six animals also had undifferentiated cells prematurely released in the lumen of the seminiferous epithelium (i; arrow), and in testes of two animals the seminiferous epithelium was flat and highly disorganized, and numerous multinuclear cells were found in the lumen (j; arrow). Bars: 50 μm (g to i), 25 μm (j).
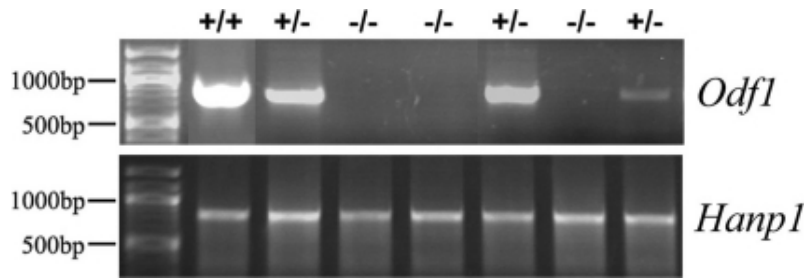
Fig. 3.3: Marker gene expression revealed spermatogenic progression irrespective of the presence or absence of ODF1. RT-PCR for *Odf1* or *Hanp1* was performed on cDNA generated from the testes of wild-type (+/+), heterozygous (+/-), and homozygous *Odf1*-deficient (-/-) mice.
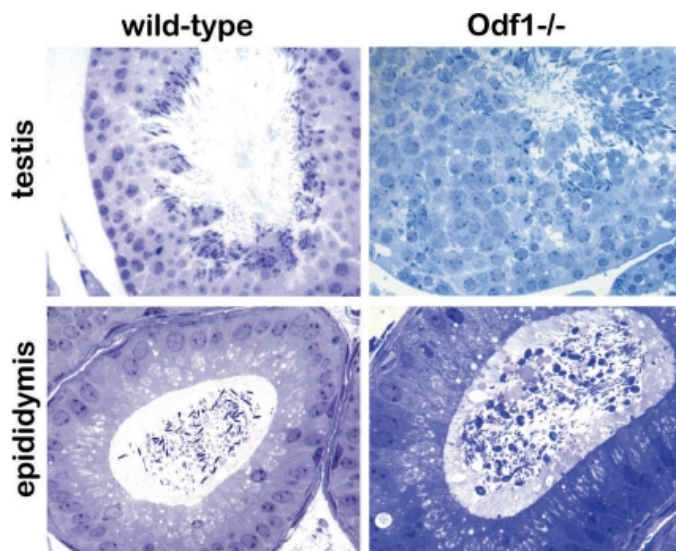
Fig.3.4: Semithin sections of wild-type and homozygous *Odf1*-deficient mouse testes and epididymides. Sections were stained with toluidine blue. Seminiferous tubules of wild-type and of *Odf1*-deficient mouse testis showed spermatogenic progression up to elongated spermatozoa and sperm tails. Sections of caput epididymides showed mature spermatozoa in the wild-type genotype, whereas in *Odf1*-deficient mice mature spermatozoa were barely found. Magnifications: testis, x400; epididymis, x630 (cooperation with Prof. Andreas Meinhardt, department of anatomy and cell biology, Giessen, Germany).

3.1.1.4 Sperm analyses of *Odf1*-deficient mice

Histological analyses, as well as expression profiling, revealed that *Odf1* deficiency did not affect the premeiotic, meiotic, and early postmeiotic phases of spermatogenesis. Even elongated spermatozoa, including the formed sperm tail, could be detected in the testes of homozygous mice. Therefore, the epididymal spermatozoa were more closely analyzed. Sperm motility was measured after capacitation *in vitro*, taking into consideration the sperm velocity parameters (curvilinear velocity [VCL], average path velocity [VAP], straight line velocity [VSL], and also the straightness of the movement [STR]) and parameters describing the head behavior (amplitude of the lateral head displacement [ALH] and the beat cross frequency [BCF]). Homozygous *Odf1*-deficient spermatozoa showed significantly reduced velocities (VAP, VCL, and VSL) and a reduction in lateral head displacement (ALH) compared to wild-type and heterozygous *Odf1*-deficient spermatozoa (Fig. 3.5). BCF and STR were significantly increased in homozygous mutants. Heterozygous *Odf1*-deficient spermatozoa revealed properties generally in between wild-type and homozygous spermatozoa (Fig. 3.5).

Then the capability of spermatozoa was analyzed to perform the acrosome reaction. Whereas in wild-type sperm as well as in heterozygous *Odf1*-deficient sperm a clear acrosome reaction could be monitored, homozygous sperm did not show any acrosome reaction at all and were of a conspicuously different phenotype (Fig. 3.6 A). *Odf1*-deficient spermatozoa were characterized by their coiling sperm tail (Fig. 3.6 A c). Immunocytology using anti-α-tubulin antibodies revealed that the axoneme is formed in heterozygous (Fig. 3.6 B), as well as in homozygous *Odf1*-deficient spermatozoa (Fig. 3.6 C). PL-FITC staining showed the presence of the acrosome in heterozygous spermatozoa but not in probes of *Odf1*$^{-/-}$ mice. Furthermore, sperm heads were generally missing in the epididymal probes of *Odf1*$^{-/-}$ mice (Fig. 3.6 C)
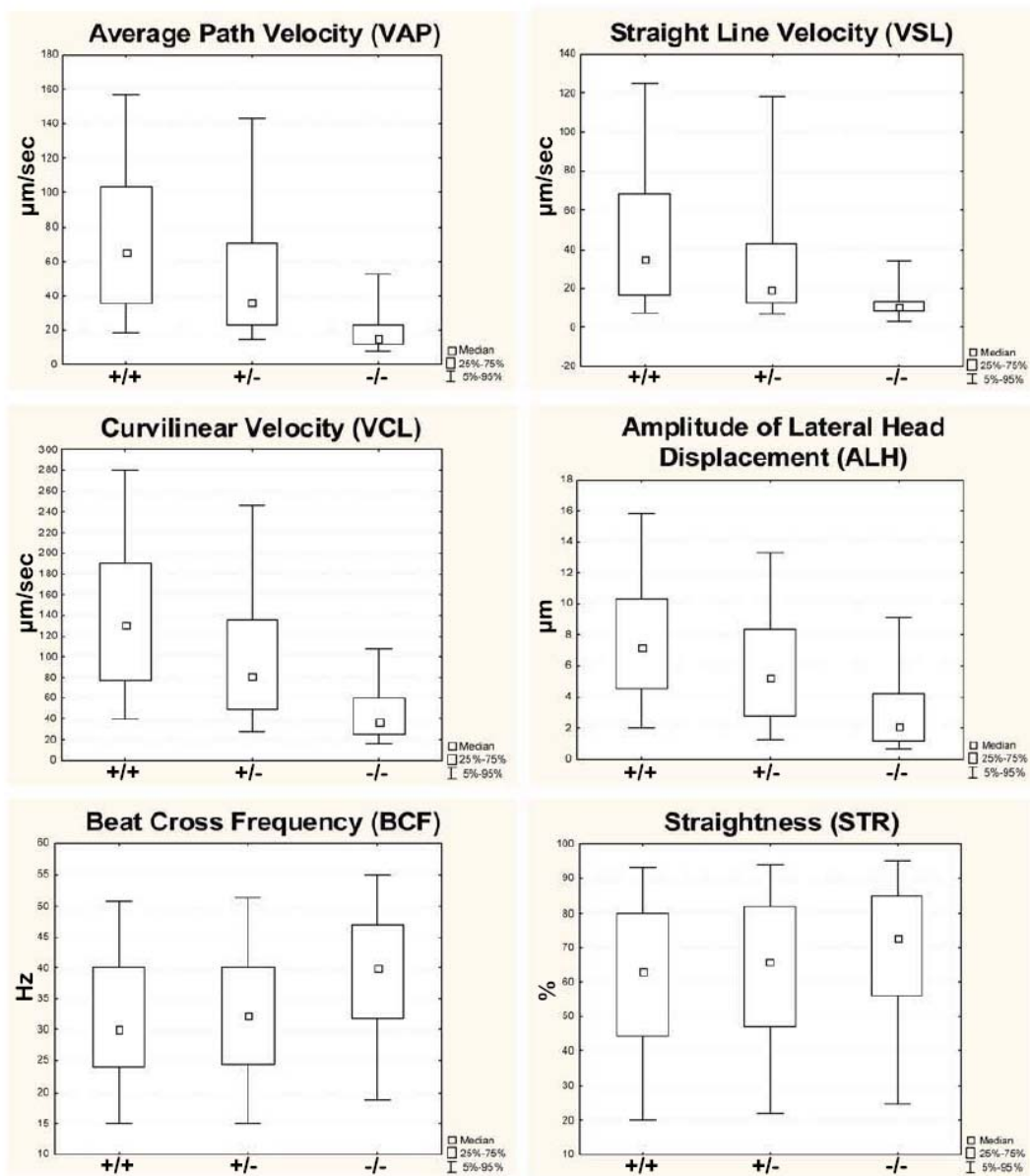
Fig. 3.5: Computer-assisted analysis of sperm motility. The parameters of wild-type (+/+), heterozygous (+/-) and homozygous (-/-) *Odf1*-deficient spermatozoa are shown. Sperm velocities (µm/sec), straightness of the movement (percent), lateral amplitude of the sperm head (µm), and beat frequency (Hz) were measured. For all measurements the medians and the percentiles (25%-75% and 5%-95%) are shown. Homozygous *Odf1*-deficient spermatozoa exhibit significantly reduced velocities and ALH and an increased BCF and STR compared to wild-type. Velocities and amplitude of the lateral head displacement of heterozygous spermatozoa demonstrated the middle values between wild-type and homozygous spermatozoa (cooperation with Dr. Pawel Grzmil, worked at department of human Genetics, university medicine,

59

Georg-August-Universität Göttingen, Göttingen, Germany; working at department of genetics and evolution, institute of zoology, Jagiellonian University, Cracow, Poland).
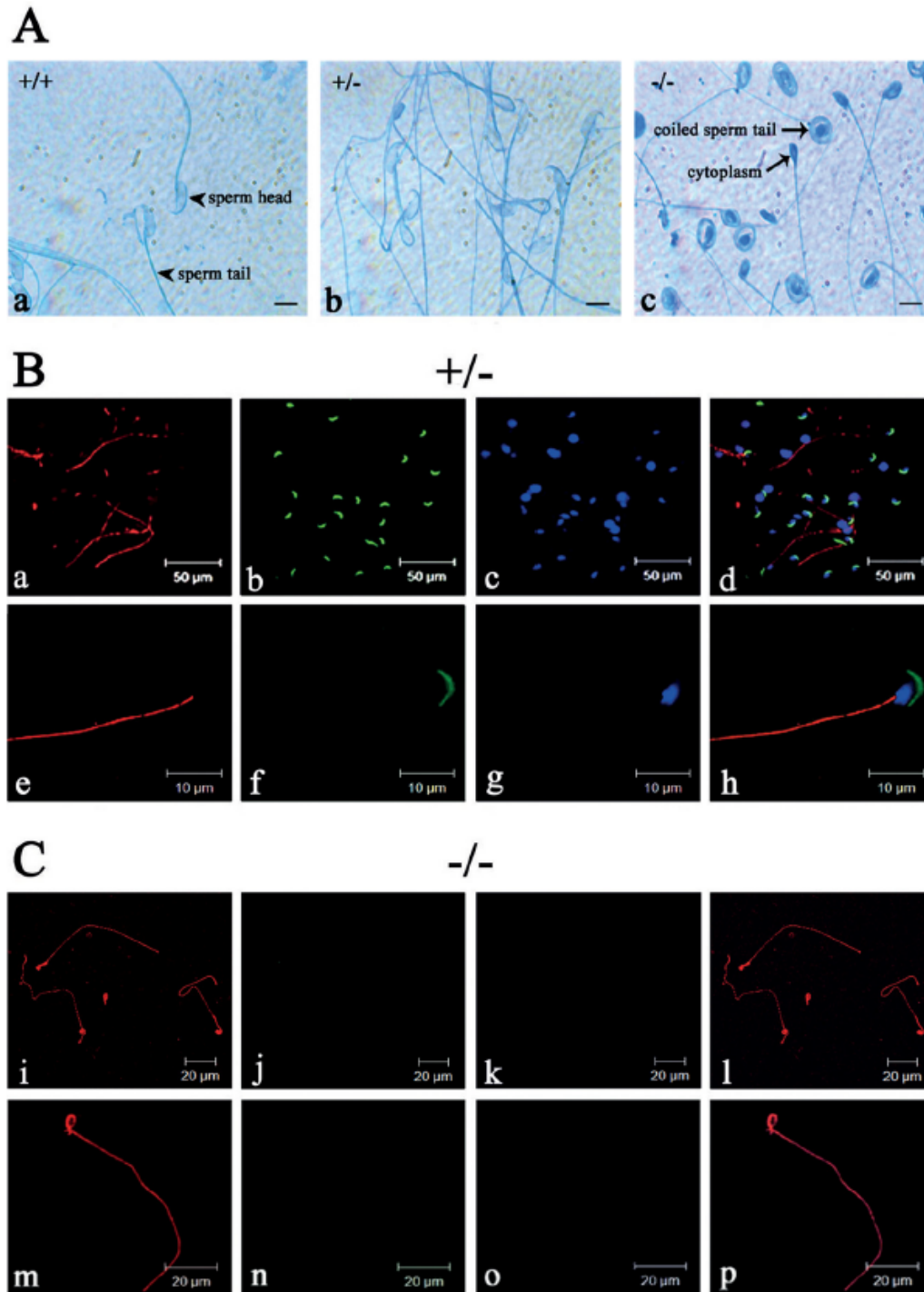
Fig. 3.6: Acrosome and axoneme in *Odf1*-mutant sperm. (A), acrosome reaction in epididymal sperm of wild-type (+/+), heterozygous (+/-), and homozygous (-/-) mice. A characteristic light

blue staining of the reacted acrosome is visible in wild-type (a; +/+) and heterozygous (b; +/-) sperm, whereas in $Odf1^{-/-}$ sperm (c; -/-) no acrosome reaction was found. In addition, a remarkable sperm coiling in $Odf1^{-/-}$ sperm is visible. Bars: 10 μm. **(B)** and **(C)**, detection of the axonemal microtubules in heterozygous (B) and homozygous (C) $Odf1$-deficient spermatozoa. Sperm were released from the cauda epididymides of heterozygous (B, +/-) and homozygous (C, -/-) mice and stained for the acrosome with PL-FITC (in green) and for tubulin with anti-α-tubulin antibodies (in red). Nuclear counterstain with DAPI is shown in panels c, g, k, and o (in blue). In heterozygous and homozygous sperm the sperm tail was detected with anti-α-tubulin antibodies demonstrating the presence of the axonemal structure (a, e, i, and m). In homozygous sperm the tail showed a conspicuous coiling (i, m, l, and p). The acrosome is present in heterozygous sperm (b and f) but absent in homozygous sperm (j and n). In addition, characteristic DAPI-stained sperm heads are also barely visible in homozygous preparations (k and o).

3.1.1.5 Loss of *Odf1* affects the ultrastructure of the spermatozoon

Inspection of transmission electron micrographs (EM) prepared from wild-type and homozygous *Odf1*-deficient mice, respectively, revealed a disturbed ultrastructure in homozygous mice (Fig. 3.7 B). Most remarkably, the organization of the mitochondrial sheath in the midpiece of spermatozoa discernible in longitudinal sections and cross-sections is disturbed (Fig. 3.7 B, arrowheads). In the midpiece of wild-type spermatozoa the mitochondria are elongated, crescent-shaped organelles that are aligned end-to-end to form helices and are enclosed by a rigid capsule, the mitochondrial sheath (Otani *et al.*, 1988). This orderly mitochondrial array is visible in longitudinal sections and in cross-sections of wild-type spermatozoa (Fig. 3.7 A, arrowheads). A disturbed mitochondrial organization is found in epididymal sperm (Fig. 3.7 B a to c, arrowhead) as well as in testicular sections of $Odf1^{-/-}$ mice (Fig. 3.7 B d to f, arrowhead). In addition, the well-structured pattern of the ODFs is disturbed. ODFs are no more tightly aligned to their corresponding microtubule doublet. The disturbed structural organization of the sperm tail is evident in cross-sections of the

61

midpiece when the mitochondrial sheath surrounds the sperm tail cytoskeleton (Fig. 3.7 B c to f, arrows) but is also found in the principal piece of the sperm tail characterized by its surrounding fibrous sheath (Fig. 3.7 B b, arrow). In the principal piece, the ODFs are neither correctly aligned to their corresponding tubule doublets nor dislodged from them (Fig. 3.7 B b, arrow). In addition, in the cytoplasm of a single cell more than one axonemal cross-section could be found very often, sometimes together with a longitudinal section through the axoneme, or two longitudinal sections through axonemata in parallel (Fig. 3.7 B a, asterisks). In contrast, in wild-type sperm tail cross-sections a highly regular pattern was found with tight association of the ODFs to their corresponding tubule doublets (Fig. 3.7 A b and c, arrow). Wild-type sperm showed a tight linkage of the sperm head to the tail and the well-known ultrastructural organization comprising basal plate, capitulum, segmented columns, and even the proximal centriole (Fig. 3.7 A d and e). Sperm of heterozygous mice likewise did not reveal obvious disturbances. Mitochondria, ODFs, and the connecting piece are well structured (Fig. 3.7 C a to c). However, in ODF1-deficient epididymides no sperm heads could be found but instead only detached tails. It was thus not possible to analyze the ultrastructure of the neck region.
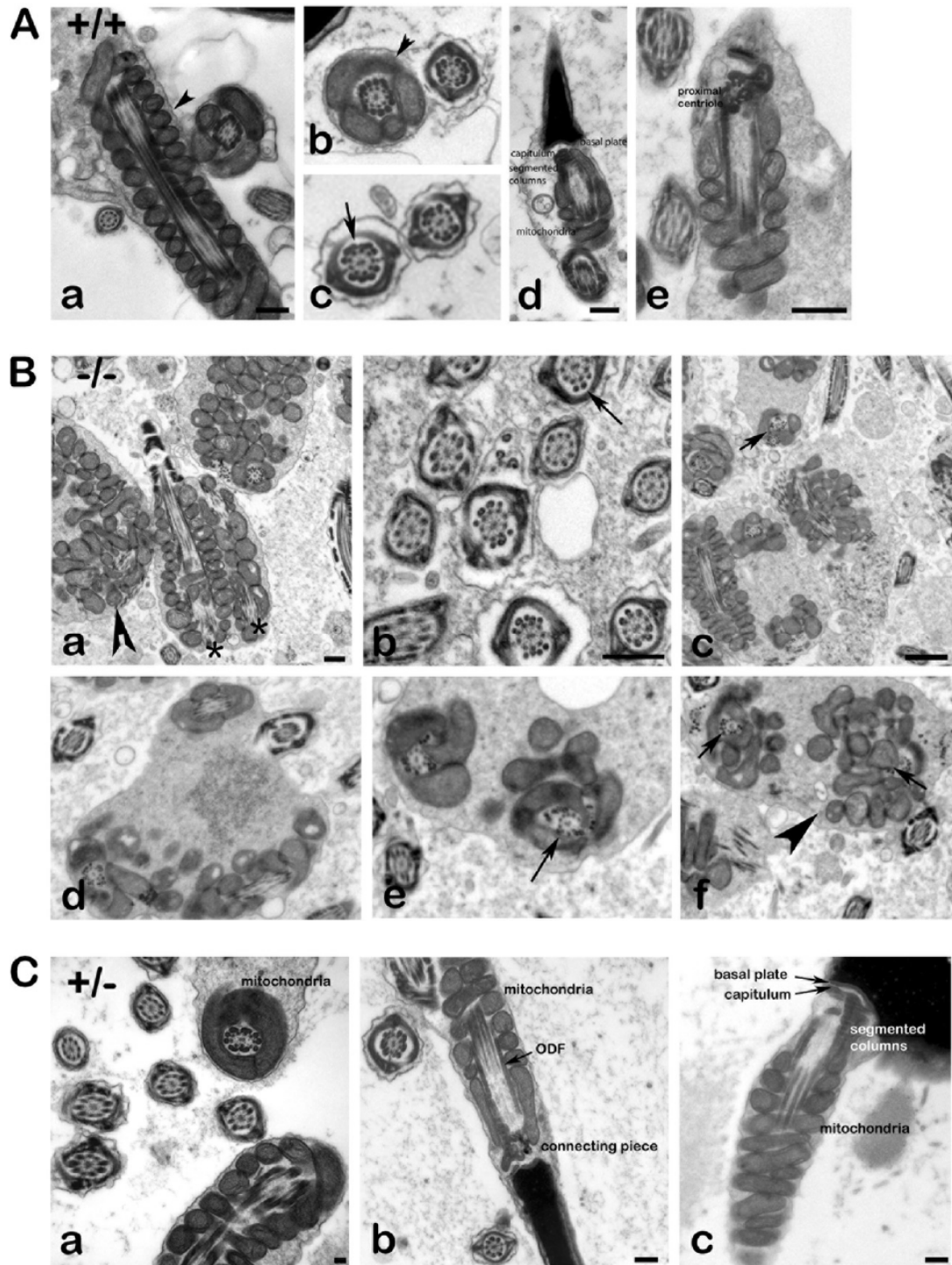
Fig. 3.7: Ultrastructure of spermatozoa. (A), transmission electron microscopy of epididymal spermatozoa from wild-type mice. The well-structured organization of the sperm is shown, including the mitochondrial sheath (a, b, d, and e, arrowheads), the outer dense fibers (c, arrow), and the neck region (d and e). Bars: 250 nm (a and d), 500 nm (e). **(B)**, transmission electron microscopy of *Odf1*⁻/⁻ sperm. Epididymides (a to c) and testes (d to f) from *Odf1*-deficient mice

were prepared, and sections analyzed by electron microscopy. Sperm are highly disorganized including the mitochondrial sheath (a, c to f, arrowheads), as well as the outer dense fibers in the midpiece (c to f, arrows) and in the principal piece (b, arrow). In addition, very often in the cytoplasm of one cell more than one axonemal section was found (two longitudinal sections of axonemata in panel a, asterisks). Arrowheads, disturbed mitochondrial sheath; arrows, disturbed alignment of ODFs. Bars: 500nm (a and b), 1,000nm (c). **(C)**, transmission electron microscopy of sperm from heterozygous mice. No obvious disturbances were found but instead well-organized mitochondria (a to c), ODFs (a and b), and connecting piece (b and c). Bars: 100 nm (a), 250 nm (b and c) (cooperation with Prof. Andreas Meinhardt, department of anatomy and cell biology, Giessen, Germany).

3.1.2 *Odf1*-deficient congenic heterozygous mice (129/Sv background) have impaired male fertility

3.1.2.1 Incipient congenic heterozygous male mice are subfertile

Odf1 deficiency on C57BL/6//129/Sv mixed background resulted in male infertility due to sperm decapitation. Additionally, *Odf1* deficient sperm suffer from disorganized mitochondrial sheath and outer dense fibers. Heterozygous males are fertile but show reduced sperm motility (see 3.1.1.4 and Yang *et al.*, 2012). In order to generate an isogenic *Odf1*-deficient mouse strain heterozygous *Odf1*-deficient mice were backcrossed with wild-type mice of strain 129/Sv for seven generations. I observed that litter size was dependent on the gender of the parent that carries the *Odf1 knock out* allele. Whereas heterozygous *Odf1$^{+/-}$*-female mice from backcross generations zero to six (N0 to N6; N0 is the first mating with stain 129/Sv) gave birth to an average of 5 pups per mating (all up 40 pups in 8 litters), i.e. a litter size that is in the range of wild-type 129/Sv pairings (359 pups in 65 litters that is a mean litter size of 5.5), litter size of backcrosses using *Odf1$^{+/-}$*-male mice is reduced to approximately 50% (a total of 34 pups in 12 litters) (Fig. 3.8 A). Matings of heterozygous *Odf1$^{+/-}$* males and females of backcross generation N7 are severely

impaired in fertility. In six matings only two pups were born after more than 5 months of continuous cohabitation. Analysing litter size during successive backcrossing revealed that fertility of female heterozygotes dropped to ~3 pups per litter in backcross generation N6 and N7 whereas male heterozygotes already have a reduced litter size in backcross generation N0. Moreover, although the fertility was impaired when heterozygous $Odf1^{+/-}$ males and females of backcross generation N7 were mated, mating between heterozygous females and wild-type males of backcross generation N7 have a mean litter size of 3 pups (all in all 12 pups in 4 matings) (Fig. 3.8 B).
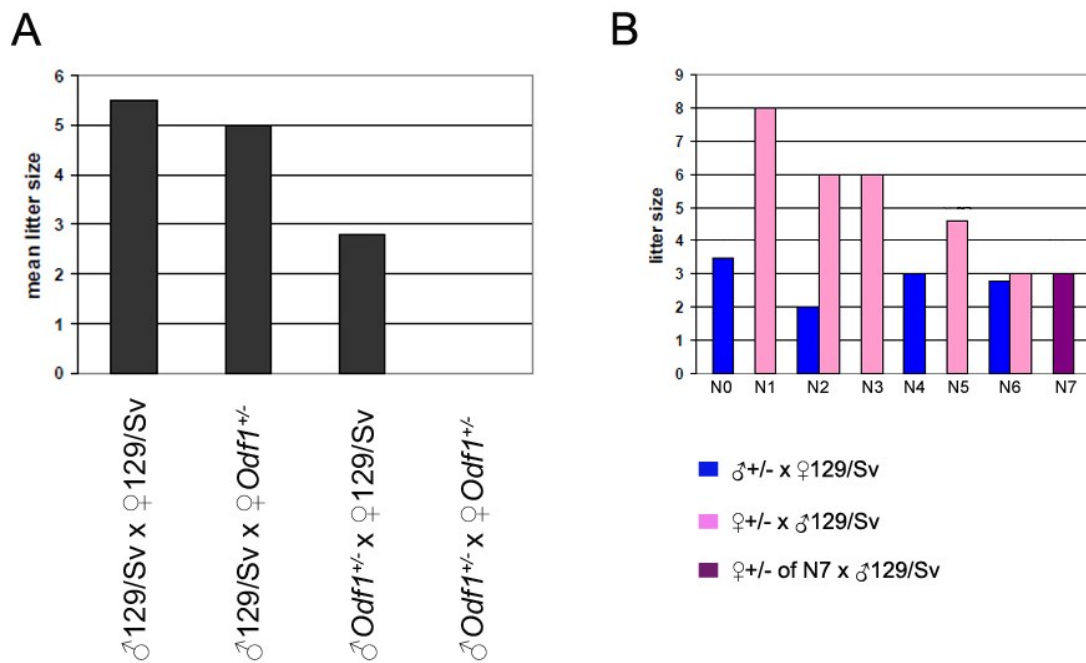
Fig. 3.8: Impaired fertility of congenic heterozygous *Odf1*-deficient males. (A), litter size of matings on 129/Sv background. Matings of 129/Sv males and females gave rise to 5 pups per litter on average (all in all 359 pups in 65 litters). A similar litter size was found in matings of heterozygous *Odf1*-deficient females with 129/Sv males from backcross generation N0 to N6 (all up 40 pups in 8 litters). However, litter size was reduced to roughly 50% in backcrosses between 129/Sv females and heterozygous *Odf1*-deficient males (a total of 34 pups were born in 12 litters from backcross generation N0 to N6). Finally, matings between congenic heterozygous *Odf1*-deficient mice of backcross generation N7 are severly impaired in fertility giving rise to only

2 pups in six matings and a mating period of 5 months. **(B)**, male fertility is reduced in all backcross generations whereas female fertility steadily drops from 6 to 8 pups per litter (N1 to N3) to 3 pups per litter in N6 and N7. Matings of heterozygous females of generation N7 and wild-type males gave birth to approximately 3 pups per litter.

3.1.2.2 Insemination capacity and sperm parameters are not altered in heterozygous males

To figure out the underlying causes of reduced male fertility mating behaviour and sperm parameters were analysed. Heterozygous male mice (n=6; backcross generation N7) were mated with wild-type 129/Sv females and females daily inspected regarding the presence of a vaginal plug. If insemination has occurred females were killed, the liquid of the uterus obtained, and inspected for the presence of sperm. Sperm concentrations were calculated and were always in-between $5x10^6$ to $6x10^7$/ml. As exception, two mates of one specific male did not have sperm in their uteri. Copulation behaviour and insemination capability therefore seem not to be altered in heterozygous $Odf1^{+/-}$ males. I thus wanted to know whether sperm parameters are altered. Sperms were isolated from epididymides of heterozygous $Odf1^{+/-}$ males as well as of wild-type 129/Sv males, respectively, after several weeks of sexual abstinence. No reduction in sperm concentration in the heterozygous condition (between 2 to $6.4x10^4$ sperm/µl; n=3) compared to wild-type males (between 2.6 to $5.2x10^4$ sperm/µl; n=2) has been found. Additionally, motility assays revealed that sperm of heterozygous males are similar to sperm of wild-type males (Fig. 3.9).
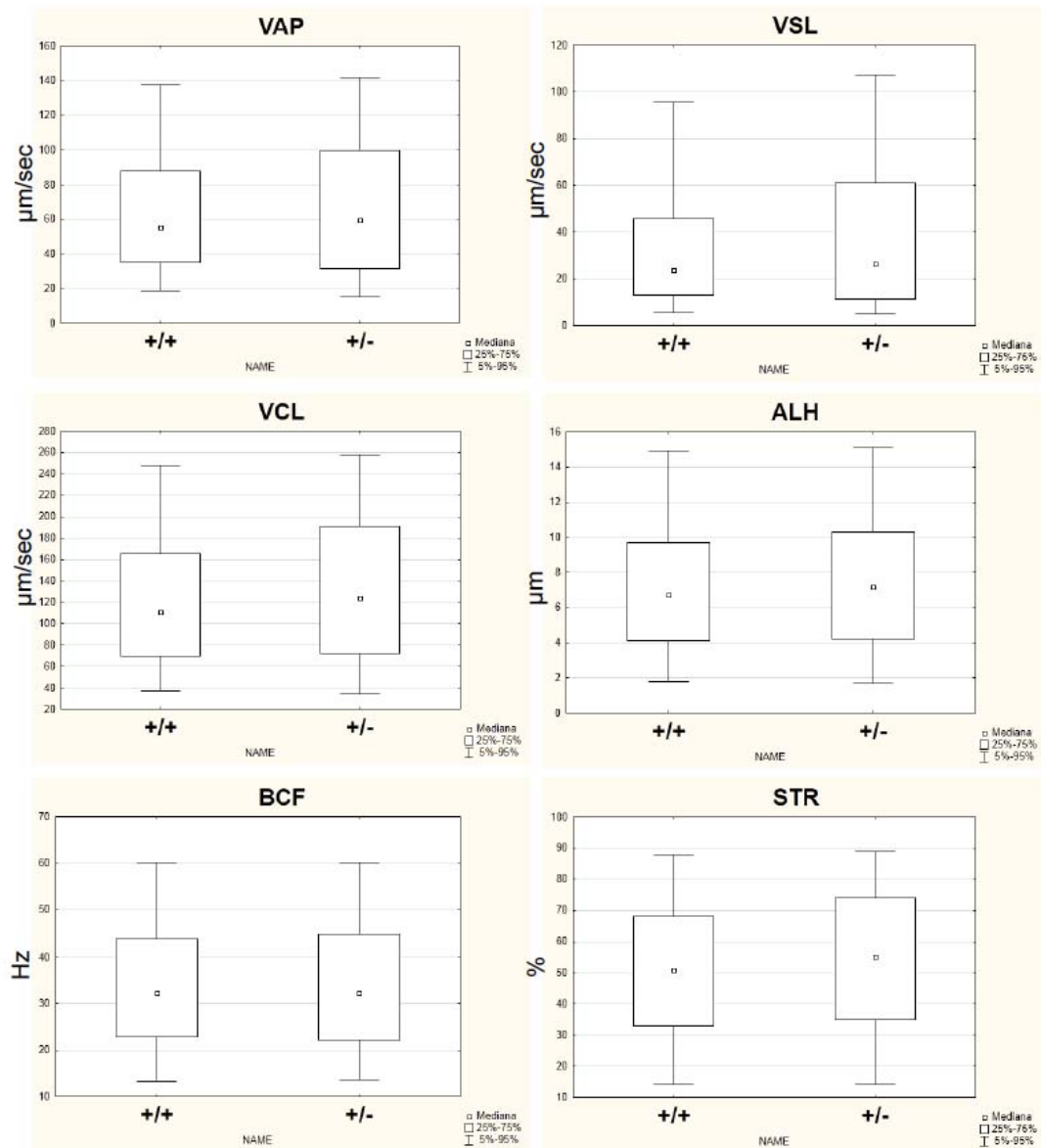
Fig. 3.9: Computer-assisted analysis of sperm motility. The parameters of wild-type (+/+) and heterozygous (+/-) *Odf1*-deficient spermatozoa are shown. Average path velocity (VAP), straight line velocity (VSL), and curvilinear velocity (VCL) (all in μm/sec), straightness of the movement (STR; in %), amplitude of lateral head displacement (ALH; in μm), and beat cross frequency (BCF; in Hz) were measured. For all measurements the medians and the percentiles (25%-75% and 5%-95%) are shown (cooperation with Dr. Pawel Grzmil, worked at department of human Genetics, university medicine, Georg-August-Universität Göttingen, Göttingen, Germany; working at department of genetics and evolution, institute of zoology, Jagiellonian University, Cracow, Poland).

67

3.1.2.3 Fertilization capacity of sperm from heterozygous $Odf1^{+/-}$ males is similar to wild-type sperm

Sperm isolated from epididymides of heterozygous $Odf1^{+/-}$ males of backcross generation N7 (n=3) and from one wild-type male of strain 129/Sv that serves as control were used for the *in vitro* fertilization assay. Sperm were incubated with isolated oocytes from gonadotropin stimulated, super-ovulated female mice. Incubation was performed in *in-vitro*-fertilization medium, and degenerated oocytes as well as 1-cell and 2-cell embryos counted 24 hours later. Wild-type sperm have fertilized more than 80% of oocytes of which 73.9% have developed to the 1-cell stage and 11.6% to the 2-cell stage (n=69 oocytes). Similarly, sperm of $Odf1^{+/-}$ males have also fertilized more than 80% of oocytes with 66.4% developed to the 1-cell stage and 14.5% to the 2-cell stage 24 hours later (n=235) (Fig. 3.10). Thus, although heterozygous $Odf1^{+/-}$ males are severely impaired in reproduction *in vitro* fertilization capability is similar to those of wild-type sperm.
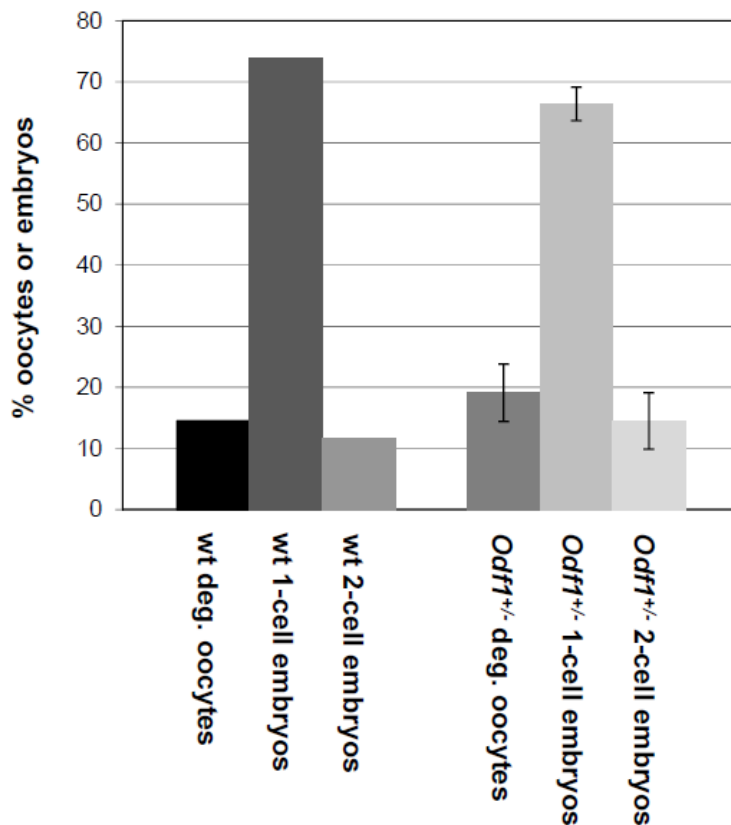
Fig. 3.10: *In vitro* **fertilization capability of wild-type 129/Sv and congenic heterozygous** *Odf1*^{+/-} **sperm.** Sperm were isolated from epididymides of one wild-type (wt) and three heterozygous *Odf1*^{+/-} mice and incubated with isolated oocytes from hyperovulated 129/Sv mice. 24 hours later degenerated oocytes (deg. oocytes), 1-cell and 2-cell embryos were counted. Standard deviations are included. The percentage of successful fertilization is highly similar (cooperation with Dr. Pawel Grzmil, worked at department of human Genetics, university medicine, Georg-August-Universität Göttingen, Göttingen, Germany; working at department of genetics and evolution, institute of zoology, Jagiellonian University, Cracow, Poland).

3.1.2.4 Haplo-deficiency of ODF1 increased the distance between nuclear membrane and capitulum

Odf1-deficient spermatozoa on mixed background suffer from decapitation suggesting that ODF1 is essential for the tight linkage of the spermatozoon head to the tail (see

3.1.1 and Yang *et al*., 2012). I thus wanted to know whether haplo-deficiency of ODF1 on congenic background affects head to tail linkage as well therefore accounting for the observed fertility impairment. The reduced amount of ODF1 in testicular proteins of heterozygous mice was proven by Western blot analysis (Fig. 3.11 A). Electron micrographs were taken from preparations of caput and cauda epididymides as well as from testis of heterozygous mice (generation N7) (Fig. 3.11 B). A regular arrangement of mitochondria in the mid-piece of the sperm tail was observed (Fig. 3.11 B a and b), and a regular assembly of the outer dense fibers was also detected (Fig. 3.11 B b). Additionally, sperm heads are as usual connected with their tails and no structural abnormalities of the connecting piece could be found (Fig. 3.11 B a, c and d). However, more detailed analyses of the sperm-head linkage apparatus revealed that the distance between the nuclear membrane and the capitulum is 1.3 fold increased in congenic heterozygous males (n=52 measurements) compared to that in wild-type males (n=52 measurements) (mean values are 85nm versus 65 nm, respectively) and that the distances are significantly different (p=1,77964 x 10^{-6}) (Fig. 3.11 C and D).
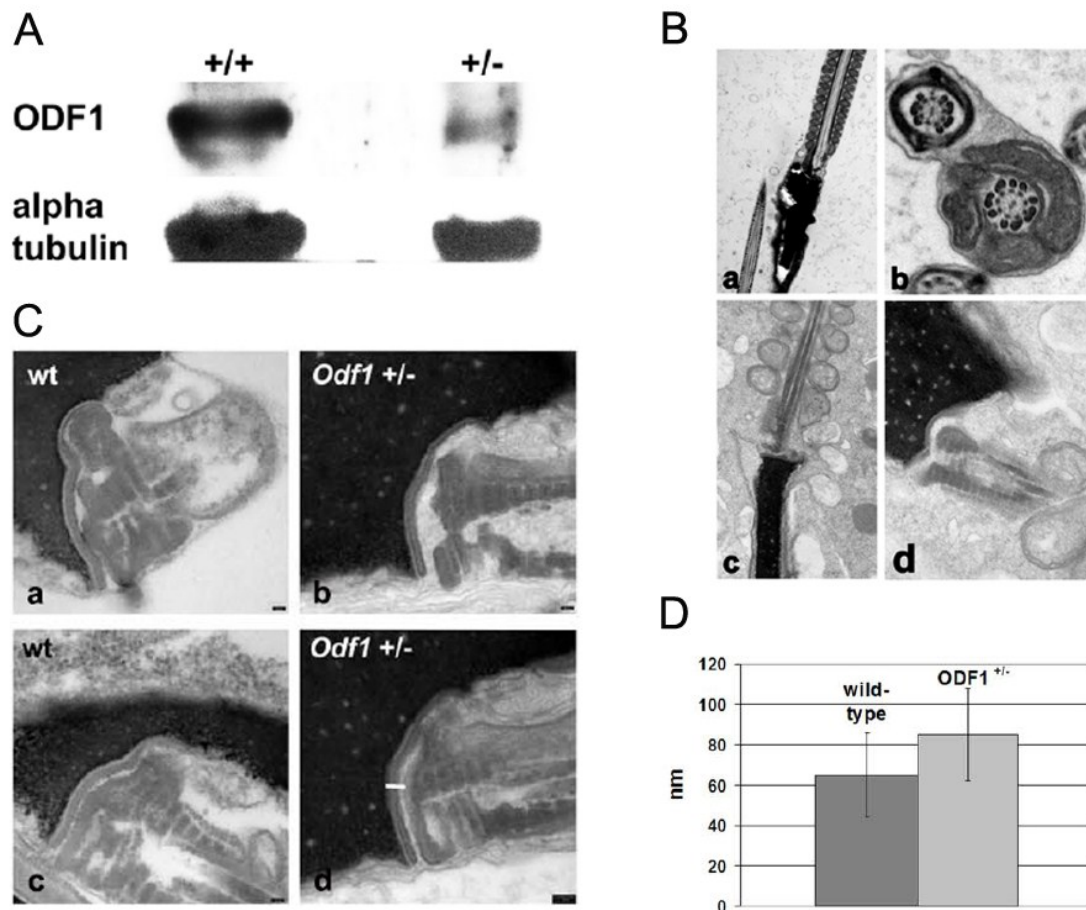
Fig. 3.11: Ultra-structural analyses of spermatozoa from incipient congenic heterozygous
Odf1^{+/-} **mice. (A)**, reduced amount of ODF1 in *Odf1*^{+/-} heterozygous mouse testis. Testis proteins
from wild-type mice (+/+) and 129/Sv heterozygotes (+/-) were analysed for ODF1 expression by
Western blot. Detection of α-tubulin as control. **(B)**, images were taken from probes isolated from
caput (a) and cauda (b) epididymis as well as from testis (c, d). Mitochondria are regularly
organized in the mid-piece region of the sperm tail (a, b). The axonemal structure and the
arrangement of outer dense fibers are not altered (b). Sperm heads are tightly linked to their tails
with a regular formation of the connecting piece (c, d). **(C)**, electron-micrographs were taken from
the connecting piece region of wild-type (a, c; wt) and congenic heterozygous *Odf1*^{+/-} sperm
(generation N7) (b, d; *Odf1+/-*). **(D)**, measurements of distance between the nuclear membrane
and the capitulum in sperm connecting piece. In wild-type sperm the mean distance is 65 nm
whereas in congenic heterozygous *Odf1*^{+/-} males a mean distance of 85 nm was measured.
Statistical analysis by Student's T-test revealed a significant difference ($p < 0.005$). The
approximate region used for taking measurements is marked by a white bar in d. Scale bars in
electron micrographs are of 50 nm.

71

3.2 SPAG4 protein

3.2.1 SPAG4 is a predicted testis specific SUN domain protein

The full length (fl) protein consists of 443 aa with an expected molecular mass of ~48 kDa. One alternatively spliced product was predicted encoding 747 bp that is translated into a protein of 210 aa with a molecular mass of ~23 kDa. According to Sosui and InterProScan, flSPAG4 consists of a conserved SUN domain (aa 267-427), a coiled-coil region (aa 194-251), and two transmembrane domains (aa 137-159 and 170-192). Amino acid sequence alignment of SPAG4l-2 (Frohnert *et al.*, 2011) and the putative open reading frame of SPAG4 revealed that both proteins are indeed distinct with highest similarities in the conserved SUN domain (Fig. 3.12). To investigate the expression pattern of *Spag4* RT-PCR analyses were performed (Fig. 3.13). Total RNA was extracted from mouse tissues as well as from the established cell lines F9, mouse spermatogonial stem cells (SSC), and mouse embryonic stem cells (ES). RNA was digested with RNase free DNase prior to cDNA synthesis. PCR reactions were performed with primer pair Spag4 650 for/Spag4 C KpnI to amplify ~800 bp of the 3`-region of *Spag4*. Amplification of *Gapdh* was used as control. No expression of *Spag4* was found in somatic tissues (heart, kidney, lungs, ovary, spleen, and epididymis; Fig. 3.13 A) whereas Spag4 is explicitly expressed in testis. To investigate *Spag4* expression during spermatogenic progression, cDNA from testes of mice aged 5-dpp to 25-dpp was prepared. Spermatogenic progression is a highly ordered process that starts postnatally leading to the appearance of progressively more mature germ cells at specific times after birth (Nebel *et al.*, 1961). Meiosis starts around day 10, early round spermatids are present approximately ten days later, and the early elongating spermatid stage is reached at about day 26 in the mouse. RT-PCR revealed that transcription of *Spag4* started around day 20 to 25 postnatally and proceeded to the adult testis (Fig. 3.13 B). Expression of *Spag4* therefore correlated with the formation of spermatids. Moreover, no transcription of *Spag4* in embryonic stem cells (ES), in spermatogonial stem cells (SSC), and in the teratocarcinoma stem

cell line F9 could be found (Fig. 3.13 C). *Spag4* therefore seems to be specifically expressed in male germ cells. Additionally the primer pair used for amplification was verified to be specific for *Spag4* and did not amplify *Spag4l* (Fig. 3.13 D). A clear product has been found with testis cDNA as template whereas no product was generated using *Spag4l* cDNA as template.

```
Spag4      MRRSPRSGSAASSHNHTPNFYSENSNSSHSATSGDSNGRRSAGPELGEPE
Spag4l-2   MPRTRNIGALCTLPEDT----------THSGR-----------PRRG---
           * *: . *: .: :.*          :**.            *. *

Spag4      GRRARGSSCGEPALSPGMPGGDTWAGSSRPKLAPRSHNGQTACGAATVRG
Spag4l-2   VQRSYISRMAEPAP-----------------------------------
            :*: * .***

Spag4      GASEPSGSSVVLEEQLNLLPILDLRQEMPTPRVSKSFLSLLFQVLSMVLS
Spag4l-2   -------------ANMNDPLLLPL--RMNTPGLS--LVQILLGYMSWLTY
                        ::*    :* *  .* ** :* ::.:*: :* :

Spag4      LA---------VDGLVCVCREICSIRFLFTAVSLLSIFLAALWWGLLYLI
Spag4l-2   LACFLRTQTQQVFLNTCRCKLFCQK--VMEKMGLLVLCVFGFWMFSMHLP
           **     . * *: :*.     ::  :. :.** : : ::*    ::*

Spag4      PPLE-------NEPTEMLTLSQYHHRVHSQGQQLQQLQAELNKLHKEVSS
Spag4l-2   SKVEVWQDDSINGP--LQSLRMYQEKVRHHTGEIQDLRGSMNQLIAKLQK
           . :*      **  : :*  *:.:*: : ::*:*:..:*:*   ::..

Spag4      VRAAHSE-RVAKLVFQRLNEDFVRKPDYALSSVGASIDLEKTSSDYEDQN
Spag4l-2   MEAISDEQKMAQKIMKMIQGDYIEKPDFALKSIGASIDFEHTSATYNHDK
           :.*   .* ::*: ::: :: *::.***:**.*:*****:*:**. *:.::

Spag4      TAYFWNRLSFWNYARPPSVILEPDVFPGNCWAFEGDKGQVVIRLPGHVQL
Spag4l-2   ARSYWNWIRLWNYAQPPDVILEPNVTPGNCWAFASDRGQVTIRLAQKVYL
           :  :** : :****:**.*****:* ******* .*:***.***. :* *

Spag4      SDITLQHPPPTVAHTGGASSAPRDFAVYGLQADDETEVFLGKFIFDVQKS
Spag4l-2   SNITLQHIPKTISLSGSPDTAPKDIVIYGLESLPREEVFLGAFQFQPE-N
           *:***** * *:: :*...:**:*:.:***::  . ***** * *: : .

Spag4      EIQTFHLQNDPPSAFPKVKIQILSNWGHPRFTCLYRVRAHGVRTSEWADD
Spag4l-2   VIQMFQLQNLPPRSFAAVKVKISSNWGNPRFTCMYRVRVHGSVTPP-KDS
           ** *:*** ** :*. **::* ****:*****.****.** *. *.

Spag4      NATGVTGGPH
Spag4l-2   HLEP----LS
           :
```

Fig. 3.12: Amino acid sequence alignment and domain organization of SPAG4 and SPAG4L-2 from *Mus musculus*. Both proteins showed a similar structural organization with two putative transmembrane domains (in grey), one coiled-coil domain (in pink), and the SUN domain (in blue). Despite their related nomenclature, SPAG4 and SPAG4L are distinct proteins. SPAG4 encoding the N-terminal part (SPAG4-N) stops at aa MLTL (blue arrow), SPAG4 encoding the C-terminal part (SPAG4-C) starts with aa EPTE (green arrow).
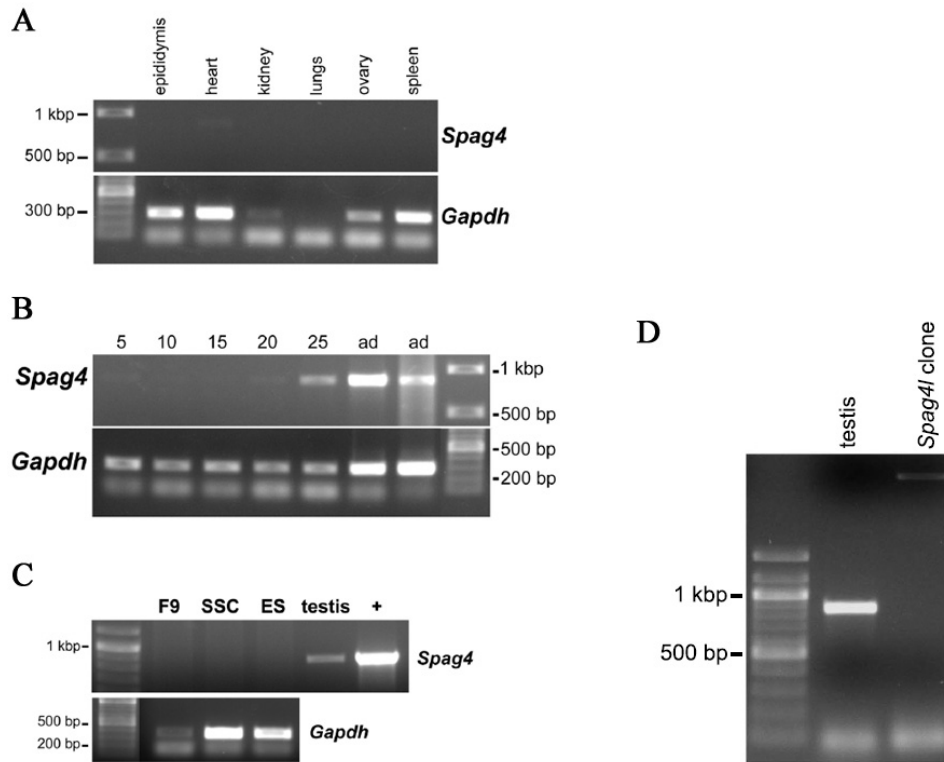
Fig. 3.13: *Spag4* **is specifically transcribed in male germ cells.** RT-PCR was performed to amplify ~800bp of *Spag4,* and *Gapdh* as control. **(A)**, *Spag4* is not transcribed in somatic tissues. **(B)**, *Spag4* is transcribed in testis starting around day 20 after birth. Transcription lasts to adult testis (ad). **(C)**, *Spag4* is not transcribed in ES, SSC, and F9 cells. As positive controls, testis cDNA (testis), and *Spag4* cDNA clone (+) were used. Amplification of *Gapdh* was always used as control for the integrity of cDNAs. **(D)**, specificity of amplification of *Spag4* but not *Spag4l*. Amplification with primer pair Spag4 650 for/Spag4 C KpnI was performed on testis cDNA (testis) as well as on *Spag4l* cDNA clone.

3.2.2 The over-expressed SPAG4 in somatic cells locates to nuclear membrane

Full length *Spag4* cDNA was cloned into pcDNA3.1 to yield a protein with the HA-tag at its N-terminal end and the Myc-tag at its C-terminal end. The plasmid was transfected into HEK293 cells and the fusion protein detected with anti-HA and

anti-Myc antibodies, respectively. In either case, HA-SPAG4-Myc was detected at the nuclear membrane (Fig. 3.14). Furthermore, HA-SPAG4-Myc located also to the cytoplasm probably due to its abundant over-expression in the somatic cell line. Additionally, anti SPAG4 antibody specifically detected HA-SPAG4-Myc at the nuclear membrane whereas HA-SPAG4L2-Myc (Frohnert *et al*., 2011) was not detected thus confirming the specificity of the antibody. The full length SPAG4 protein therefore is located at the nuclear membrane.

All SUN domain proteins characterized so far are transmembrane proteins spanning the inner nuclear membrane (INM) with their N-terminal region oriented towards the nucleoplasm and the C-terminally located SUN domain positioned in the luminal space between outer nuclear membrane (ONM) and inner nuclear membrane (INM). To further substantiate the topology of SPAG4, *pHA-Spag4-Myc* was transfected into NIH3T3 cells and in situ digested with proteinase K (Frohnert *et al*., 2011). Cells were either incubated with proteinase K in KHM buffer (Fig. 3.15 S1, P1), or with proteinase K in KHM buffer containing Triton X-100 (Fig. 3.15 S2, P2). Cells incubated in buffer without Triton X-100 might be largely inaccessible for proteinase K treatment whereas Triton X-100 rendered the cells permeable thus enabling proteolytic digestion. Proteinase K digestion in the presence of Triton X-100 resulted in a nearly complete degradation of proteins. Only a very faint band of SPAG4 at ~40 kDa could be detected with anti-Myc antibodies but not with anti HA-antibodies (Fig. 3.15, P2) suggesting that proteolytic degradation started from the N-terminal end with the HA-tag. A C-terminal fragment of about 40 kDa is expected when the N-terminal part up to the transmembrane domain is degraded. However, proteolytic degradation took also place in the absence of Triton X-100. Besides full length SPAG4 of > 55 kDa, several degradation products were detected with anti-Myc antibodies as well as with anti-HA antibodies (Fig. 3.15, S1, P1). The full length SPAG4 is shown in the control (Fig. 3.15, C). Since the C-terminal end of SPAG4 was tagged with Myc and the N-terminal end with HA, C-terminal or N-terminal degradation products could specifically be identified with anti-HA or anti-Myc, respectively. Anti-myc antibodies clearly detected the full length protein of > 55 kDa in the supernatant (S1) as well as

in the pellet (P1) along with smaller proteolytic fragments suggesting that degradation started from the N-terminal end leaving the C-terminal myc-tag sheltered. Using anti-HA antibodies, proteolytic fragments were detected as well, with a protein fragment of ~40 kDa as the largest fragment whereas the full length protein was no longer present. These fragments contain the N-terminal HA-tag and are therefore derived from successive C-terminal digestion. Strong proteolytic degradation probably resulted from liberated proteins caused by experimentally induced destruction of cells. Therefore, proteolytic fragments might also include C-terminally Myc-tagged and N-terminally HA-tagged fragments. These results suggest that the N-terminal HA-tag is more accessible to proteinase K digestion than the C-terminal Myc–tag. The flSPAG4 protein therefore seems to have a similar orientation within the nuclear membrane as other SUN domain proteins with the C-terminal end located in the perinuclear space. Due to experimental conditions of ectopic over-expression of SPAG4 a conspicuous amount of SPAG4 is also degraded from the C-terminal end but leaves the N-terminal HA-tag intact (see also Fig. 3.14).

Dimerization of SUN domain proteins has been described in the literature. I therefore wanted to know whether SPAG4 is also able to form homodimers. HEK293 cells were co-transfected with *EYFP-SPAG4-Myc* and *HA-SPAG4-Myc* expression plasmids thus enabling detection of two different SPAG4 molecules individually. Cells were lysed and soluble proteins were subjected to immunoprecipitation using anti-GFP antibodies which were raised in rabbit. The bead bound protein fraction was then analyzed by Western blot using monoclonal anti-HA antibodies. HA-tagged SPAG4 (at ~55kDa) was detected not only in the soluble protein fraction and the protein pellet (Fig. 3.16, lanes s and p, respectively) but was also found to co-precipitate with SPAG4-EYFP fusion protein (Fig. 3.16 lane b). In contrast, no SPAG4 was found in the control beads in which anti-GFP antibodies have been omitted (Fig. 3.16, lane bc). These results thus demonstrate that SPAG4 forms homodimers.
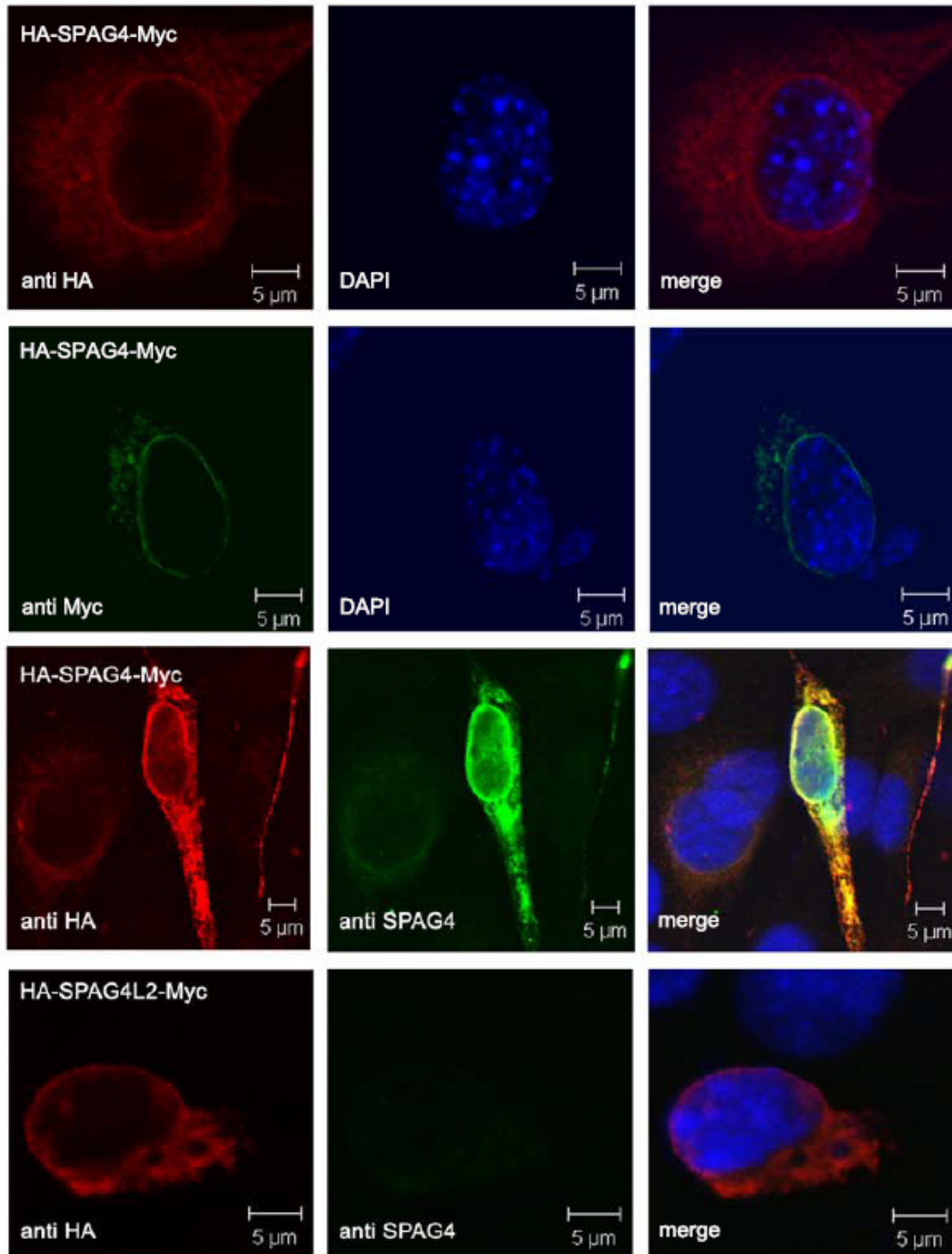
Fig. 3.14: Ectopic expression of SPAG4 in HEK293 cells revealed nuclear membrane localization. A plasmid encoding SPAG4 tagged with HA at its N-terminal end and Myc at its C-terminal end was transfected into HEK293 cells and detected with anti-HA (in red), anti-Myc (in green), and anti SPAG4 antibodies (in green), respectively. Anti SPAG4 antibody specifically detected SPAG4 but did not react with transfected SPAG4L2 (tagged with HA at its N-terminal

77

end and with Myc at its C-terminal end; HA-SPAG4L2-Myc) although expression of HA-SPAG4L2-Myc was proven by anti-HA antibodies (in red). Nuclear counterstaining with DAPI in blue.
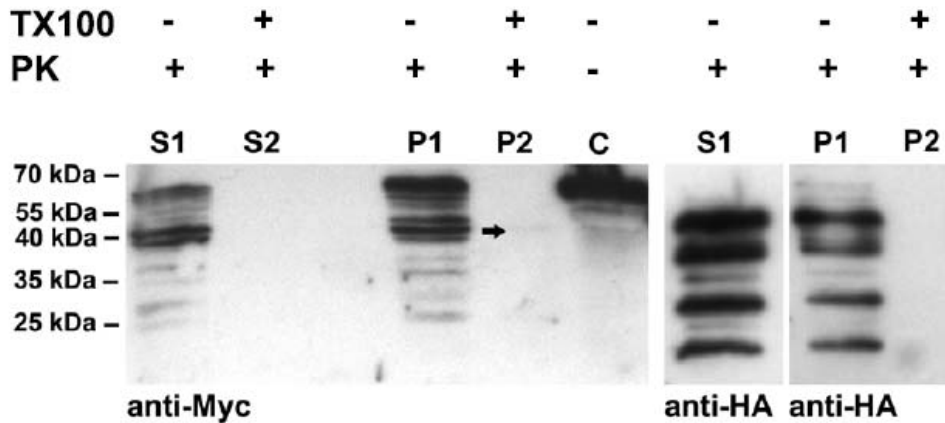
Fig. 3.15: The N-terminal end of SPAG4 is prone to in situ proteinase K digestion. *pHA-Spag4-Myc* was transfected into NIH3T3 cells and subjected to in situ proteinase K digestion. Scraped cells were exposed to proteinase K either in the absence (S1, P1) or in the presence of Triton X-100 (S2, P2). Proteins were separated on denaturing SDS-gels, blotted onto nitrocellulose membranes, and probed with the indicated antibodies anti-Myc or anti-HA. The full length SPAG4 protein is shown in the control (C). Proteinase K digestion started from the N-terminal end tagged with HA since no full length protein could be detected with anti-HA antibodies. In contrast, anti-Myc antibodies detected the full length protein of ~70 kDa. In P2 a very faint band of about 40 kDa could be detected with anti-Myc antibodies but not with anti-HA antibodies (arrow). Presence (+) or absence (-) of proteinase K (PK) or Triton-X100 (TX100) are indicated (This experiment was performed by Prof. Dr. Sigrid Hoyer-Fender).

Fig. 3.16: Confirmation of SPAG4 self-interaction by co-immunoprecipitation. HEK293 cells were co-transfected with *EYFP-SPAG4-Myc* and *HA-SPAG4-Myc* expression plasmids. After cell lysis soluble proteins were subjected to immunoprecipitation using anti-GFP antibodies (raised in rabbit). Bead bound proteins were then dissolved in denaturation buffer and separated on SDS-polyacrylamide gels. After Western blot target proteins were detected with anti-HA antibodies (raised in mouse) at ~55 kDa. There are two closely standing bands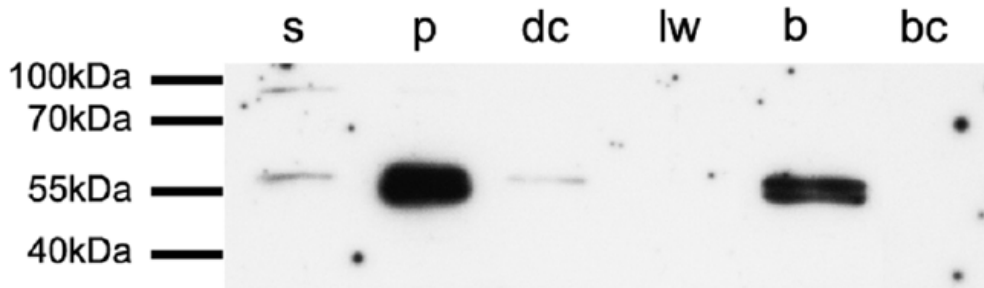 on lane b. They are supposed to be the complete fusioned HA-SPAG4-MYC protein and the main part HA-SPAG4 lost its Myc-tag. s, supernatant of cell lysate; p, pellet, insoluble cellular fraction; dc, depletion control, proteins of the supernatants after separation of protein G agarose beads; lw, last wash; b, proteins bound to beads after incubation with fishing antibody; bc, control, proteins bound to beads without the presence of the fishing antibody.

3.2.3 The distribution of endogenous SPAG4 in male germ cells during spermiogenesis

From 3.2.1 and 3.2.2 it is known that SPAG4 is a novel SUN domain protein located in the nuclear membrane and restricted to spermatids. Subsequently, the next question was, do the endogenous SPAG4 proteins also associate with the nuclear membrane of male germ cells? Fig. 3.17 shows that the protein revealed dynamic distribution during spermiogenesis albeit always associated with the nuclear membrane. In early round spermatids SPAG4 is first scattered over the nuclear membrane and then became more and more restricted towards the distal pole where the transient manschette is forming (Fig. 3.17 A and B). In elongating spermatids SPAG4

distribution is similar to the location of the manchette (Fig. 3.17 C and D). In later spermatid stages the manchette gradually disintegrated and SPAG4 became concentrated towards the distal pole at a position where the sperm tail inserts (Fig. 3.17 E-G).
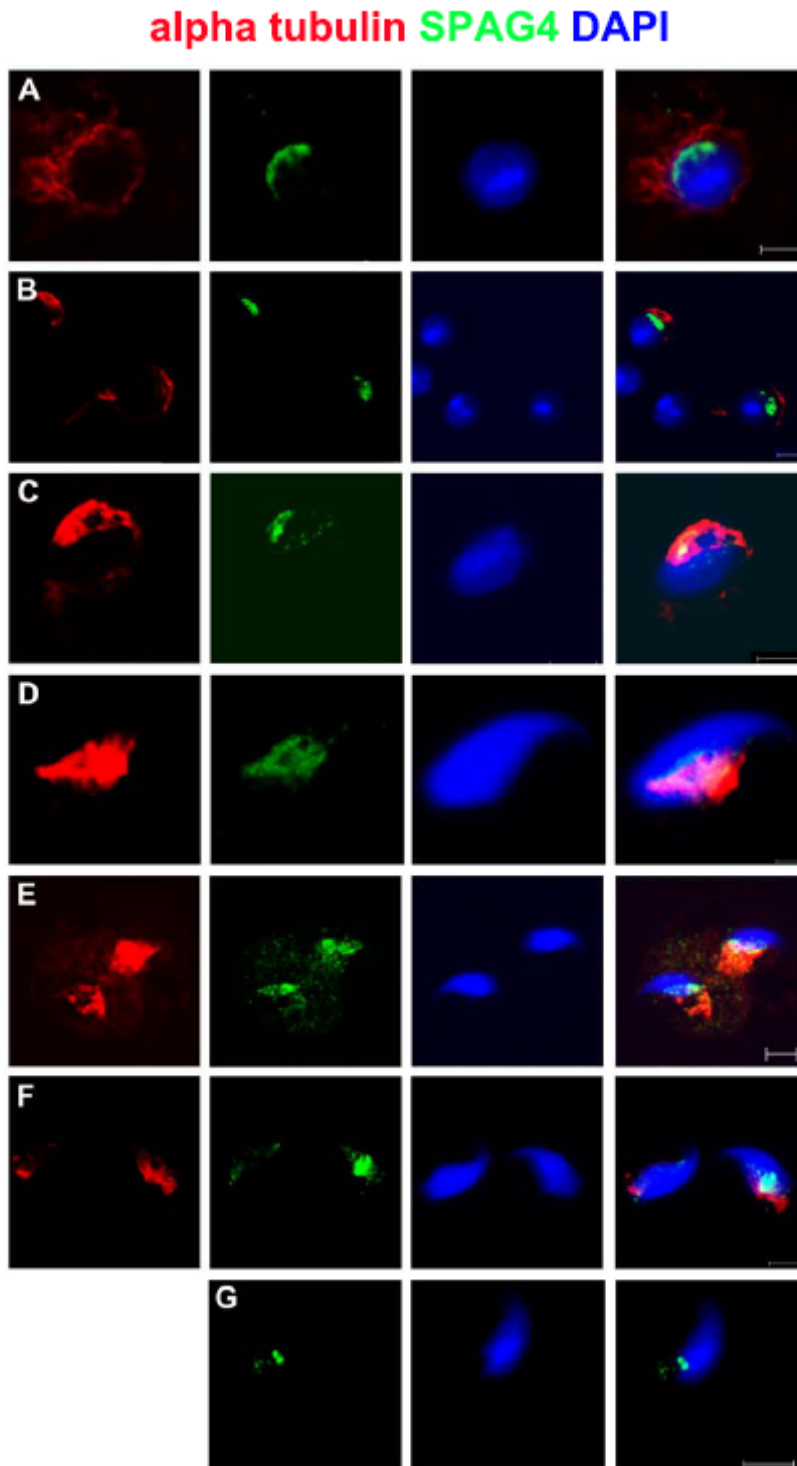
Fig. 3.17: Endogenous expression of SPAG4 in spermatids. Suspension preparations from mouse testis were incubated with anti-SPAG4 antibodies (green) and anti-α tubulin antibodies (red). SPAG4 is first scattered over the round spermatid nucleus (A) and later on became restricted towards the posterior pole where the manchette is forming (B). In elongating spermatids SPAG4 is associated with the manchette (C, D). In later spermatid stages the manchette disintegrated and SPAG4 became concentrated at the distal pole (E-G). DAPI counterstain in blue. Scale bars in A, B, C, E, F, G: 5 μm, in D: 2 μm.

3.2.4 SPAG4 interacts with ODF1

SPAG4 (sperm associated antigen 4) was originally identified as a sperm specific protein that interacts with the sperm tail outer dense fiber protein ODF1 without being incorporated into the sperm tail (Shao *et al.*, 1999). Due to its wide expression in human neoplastic tissues SPAG4 was described moreover as a potential cancer marker (Kennedy *et al.*, 2004). SPAG4/ODF1 interaction thus first is verified by co-immunoprecipitation out of mouse testis. Endogenous SPAG4 was precipitated with goat anti-SPAG4 antibodies and endogenous ODF1 detected by Western blot using rabbit anti-ODF1 antibodies. ODF1 (at ~ 35 kDa) was detected in the beads bound protein fraction (Fig. 3.18 A, lane b). Only a very faint signal was also found in the beads only control fraction (Fig. 3.18 A, lane bc) thus demonstrating interaction between SPAG4 and ODF1. Specificity was further proven using testicular proteins from *Odf1*$^{-/-}$ mice for co-IP (see 3.1 and Yang *et al.*, 2012). SPAG4 was precipitated first and Western blots incubated with anti-ODF1 antibodies (Fig. 3.18 B). As expected, no ODF1 could be found. Additionally, the ~35 kDa protein band observed in co-precipitated proteins from wild-type testis (Fig. 3.18 A) was also missing demonstrating that this band indeed represents ODF1 and that ODF1 interacts with SPAG4 in testicular cells. Moreover, as positive control for anti-ODF1 antibody specificity bacterially expressed ODF1 fused to MBP (mODF1-MBP) was used that was detected by the antibody. To identify the protein region of SPAG4 responsible for

interaction with ODF1 co-IP of transfected cells were performed. To this end, ODF1 fused to ECFP was either co-transfected with a plasmid encoding the C-terminal end of SPAG4 fused to HA (HA-SPAG4-C) or with a plasmid encoding the N-terminal end of SPAG4 fused to HA (HA-SPAG4-N). In both constructs the HA-tag is fused to the N-terminal end. Proteins were precipitated using anti-GFP antibodies, and bound proteins separated on denaturing polyacrylamide gels. Co-precipitation of both the C-terminal region of SPAG4 with ODF1 (Fig. 3.18 C) as well as the N-terminal region of SPAG4 with ODF1 (Fig. 3.18 D) was confirmed by immunodetection of the HA-tag. SPAG4-C (~35 kDa) and SPAG4-N (~25 kDa) were clearly identified in the bead bound fractions (Fig. 3.18 C and D, lanes b) but not in the control bead fractions in which the anti-GFP antibody was omitted (Fig. 3.18 C and D, lanes bc). Additionally, SPAG4-C and SPAG4-N were also detected in the soluble protein fraction (Fig. 3.18, lane s), in the insoluble protein fraction (Fig. 3.18, lane p), and in the depletion control fractions obtained after protein G agarose mediated protein precipitation (Fig. 3.18, lanes dc). Incubation of Western blots with anti-GFP antibodies confirmed the presence of ODF1 in all fractions. Additionally, very faint signals were also obtained in the control experiments (Fig. 3.18, lanes bc). These results indicate that ODF1 is able to interact with both the C-terminal as well as the N-terminal end of SPAG4.
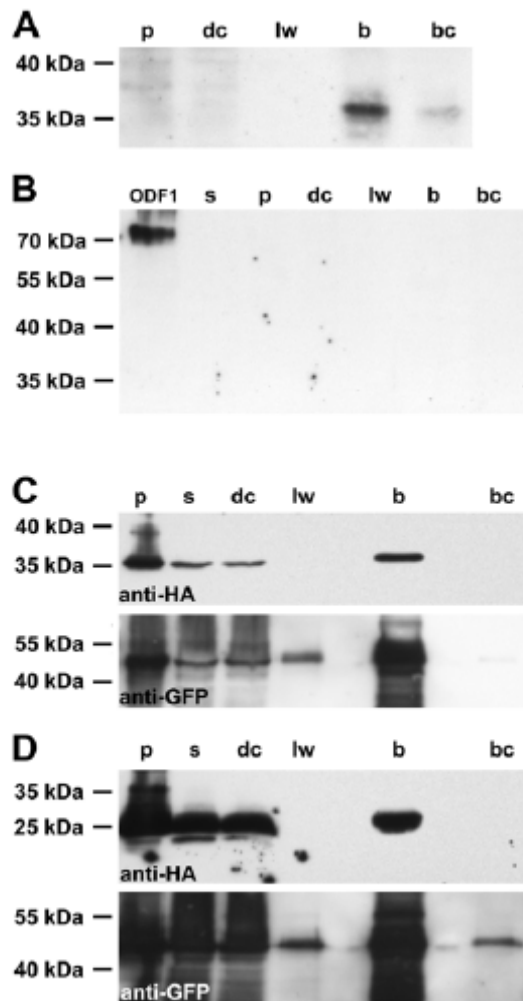
Fig. 3.18: Interaction of ODF1 and SPAG4. (A) and **(B)**, interaction of endogenous proteins. SPAG4 was immunoprecipitated from wild-type testis (A) or *Odf1*$^{-/-}$ testis (B) and bound ODF1 detected on Western blots. In wild-type testis ODF1 co-precipitated with SPAG4 and was therefore detected in the bead bound fraction (A, lane b) whereas in ODF1-deficient testis no signal of similar molecular mass was found (B). The antibody however reacted with bacterially expressed ODF1 fused to MBP (B, lane ODF1). **(C)** and **(D)**, interaction of ODF1 with both the C-terminal as well as the N-terminal part of SPAG4. Plasmids encoding ODF1 fused to ECFP (*pODF1-ECFP*) and either the C-terminal part of SPAG4 fused to HA (*pHA-Spag4-C*) (C) or the N-terminal part of SPAG4 fused to HA (*pHA-Spag4-N*) (D) were transfected into HEK293 cells and co-immunoprecipitation performed using anti-GFP antibodies. Co-precipitation with ODF1-ECFP was found for both SPAG4-C (C, lane b) and SPAG4-N (D, lane b). In the control bead bound fractions (lanes bc) no SPAG4 proteins were found. s, supernatant of cell lysate; p,

83

pellet, insoluble cellular fraction; dc, depletion control, proteins of the supernatants after separation of protein G agarose beads; lw, last wash; b, proteins bound to beads after incubation with fishing antibody; bc, control, proteins bound to beads without the presence of the fishing antibody.

3.2.5 The recruitment of SPAG4 to the posterior pole of elongating spermatids is independent of ODF1

To investigate whether absence of ODF1 affects the recruitment of SPAG4 to the nuclear membrane in round spermatids and more specifically the redistribution to the posterior pole in elongating spermatids the SPAG4 distribution in $Odf1^{-/-}$ male germ cells was analysed. Suspensions were prepared from *Odf1 knock out* testis and cells incubated with anti-SPAG4 antibodies and anti-α-tubulin antibodies (Fig. 3.19). SPAG4 showed a similar distribution as in germ cells from wild type testis (Fig. 3.17) with scattered nuclear membrane localization in round spermatids (Fig. 3.19 A) and progressive redistribution towards the posterior pole in elongating spermatids (Fig. 3.19 B to E). Additionally, SPAG4 is located in close vicinity to the forming manschette as already found in wild type germ cells (Fig. 3.17). It is also obviously to be seen that a substantial amount of SPAG4 is present in the cytoplasma of elongating spermatids (Fig. 3.17 E; Fig. 3.19 C and D). With these results it seems that the recruitment of SPAG4 to the posterior pole of elongating spermatids is independent of ODF1.
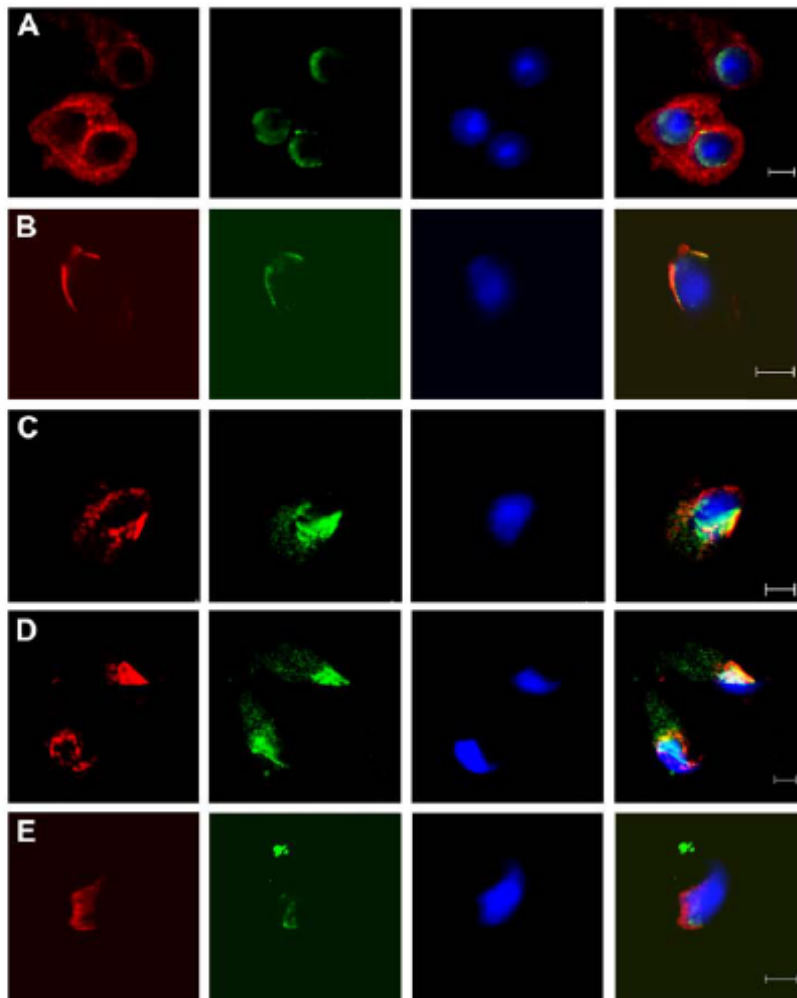
Fig. 3.19: Redistribution of SPAG4 towards the posterior pole of elongating spermatids is not mediated by ODF1. Testicular suspension preparations from *Odf1 knock out* mice were incubated with anti-SPAG4 antibodies (in green) and anti-α tubulin antibodies (in red). SPAG4 is first scattered over the round spermatid nucleus (A) and redistributed towards the posterior pole where the manschette is forming (B-E). An approximate colocalization with the manschette is found in elongating spermatids (C, D). In yet later spermatid stages the manschette disintegrated and SPAG4 became concentrated at the most distal pole (E). DAPI counterstain in blue. Scale bars are of 5 μm each.

3.2.6 ODF1 is recruited to the nuclear membrane by SPAG4

It was shown that recruitment of SPAG4 to the nuclear membrane and its concentration towards the posterior pole in elongating spermatids is not affected by absence of ODF1. Then the recruitment of ODF1 via SPAG4 to the nuclear membrane was also investigated. NIH3T3 cells were transfected with SPAG4 and ODF1 expression constructs and protein localization was analysed by immunocytology (Fig. 3.20). Whereas ODF1 (fused to ECFP) located to the cytoplasm but not to the nuclear membrane in cells without SPAG4 expression (Fig. 3.20 A), co-expression of full length SPAG4 (HA-SPAG4-Myc) recruited ODF1 to the nuclear membrane. Co-expression of the C-terminal part of SPAG4 (HA-SPAG4-C) demonstrated co-localization with ODF1 in the cytoplasm but no nuclear membrane staining (Fig. 3.20 C). In contrast, the N-terminal part of SPAG4 (HA-SPAG4-N) is localized to the nuclear membrane causing in turn recruitment of ODF1 to the nuclear membrane as well (Fig. 3.20 D). These results thus demonstrate that ODF1 and SPAG4 interact, that the N-terminal part of SPAG4, which comprises the predicted transmembrane domains, is indeed targeted to the nuclear membrane, and that SPAG4 recruits ODF1 to the nuclear membrane.

These investigations further revealed that ectopic expression of ODF1 resulted in a distinct concentration of ODF1 in the vicinity of the nucleus that reminds to the centrosome (Fig. 3.20 A, C, D, arrow). Therefore the cells transfected with *Odf1* was costained with anti-γ tubulin antibody which detects the centrosomal protein γ tubulin (Fig. 3.20 E). The arrow in panel E indicates that ODF1 is concentrated in a tiny dot near the nucleus that is γ tubulin positive demonstrating that ODF1 is recruited to the centrosome.
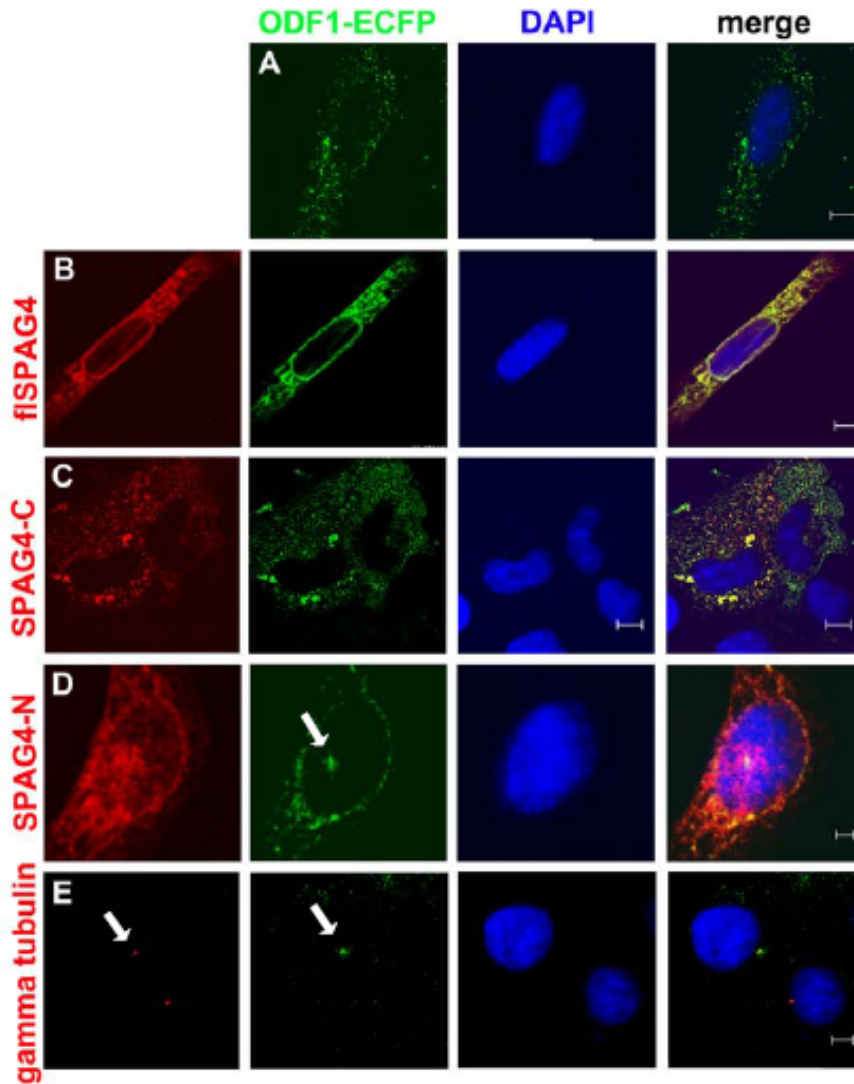
Fig. 3.20: Ectopically expressed ODF1 located at the centrosome and is recruited to the nuclear membrane by SPAG4 (full length, flSPAG4) and its N-terminal region. Cells were transfected with expression plasmids encoding ODF1 fused to ECFP (*pOdf1-ECFP*) and SPAG4. SPAG4 proteins were detected by anti-HA (in red) and ODF1 by anti-ODF1 or anti-GFP antibodies (in green). ODF1 is recruited to the nuclear membrane by the full length SPAG4 (B) as well as by the N-terminal region of SPAG4 (D). The C-terminal region of SPAG4 is located in the cytoplasm and co-localized with ODF1 (C). Without SPAG4 ODF1 is cytoplasmic (A). ODF1 is concentrated in a tiny dot near the nucleus (arrows in D and E) that co-localizes with γ tubulin (E, in red). DNA counterstain with DAPI. Scale bars are of 2 μm (D), 5 μm (A, B, E) or of 10 μm (C).

3.3 ODF2 protein

3.3.1 The influence of centrosomal protein ODF2 on canonical Wnt pathway key protein β-catenin

3.3.1.1 Ectopic expression of ODF2 promotes the degradation of over-expressed β-catenin

Previous results from pull-down and co-immunoprecipitation showed that ODF2 interacts with β-catenin (colleagues of our group). I subsequently investigated the influence of ODF2 on β-catenin. Mammalian cell lines NIH3T3 and HEK293 were used for transfection of different plasmid DNA constructs, then reporter gene assay was performed. The reporter gene *Topflash* (*OT*) is firefly-luciferase which has a promoter with Tcf4 binding sites. When the canonical Wnt signaling pathway is activated, β-catenin goes into the nucleus and binds to the Tcf4 binding site with Tcf4 together and the reporter gene will be subsequently activated. Then the luciferase activity may be measured by luminometer.

The over-expressed β-catenin can cause an obvious increasing of firefly-luciferase activity. After the co-transfection of *β-catenin* and *Odf2* (*13.8NC-GFP*) the relative activity of luciferase reporter is strongly reduced from 100% down to 51% and to 39% in NIH3T3 and HEK293 cells, respectively, compared to single transfection of *β-catenin* (Fig. 3.21 A and B). This result suggests that over-expression of ODF2 affects β-catenin stability.

β-catenin is a key protein of canonical Wnt pathway. When canonical Wnt pathway is not activated, cytoplasmic β-catenin will be targeted for degradation by a destruction complex containing APC, CK1, Axin and GSK-3β. Therefore, I examined whether the influence of ODF2 on the canonical Wnt pathway is mediated by the β-catenin destruction complex. Lithium potently inhibits GSK-3β activity, but is not a general inhibitor of other protein kinases (Klein and Melton, 1996). The cells were treated with 20mM lithium acetate for 16 hours. Once GSK-3β is inhibited by lithium, β-catenin will not be degraded and acts as a transcriptional activator. Fig. 3.21 A and

B show that in lithium-treated cells (NIH3T3 and HEK293) over-expressed ODF2 obviously reduces the activity of the luciferase reporter from 100% down to 72% and to 40% in NIH3T3 and HEK293 cells, respectively, compared to single transfection of *β-catenin*. This reduction demonstrates that the influence of ODF2 on β-catenin is not exclusively mediated by GSK-3β.

To support the results of reporter gene assays, I investigated subsequently β-catenin expression quantified by Image J software using α-tubulin expression as loading control. Western blot analyses showed that over-expressed ODF2 did not affect the endogenous β-catenin neither in NIH3T3 nor in HEK293 cells. Therefore, *β-catenin* was over-expressed in HEK293 cells. The results indicated that co-transfection of *Odf2* and *β-catenin* together triggered a decrease of β-catenin, which was 76% of *β-catenin* found in cells transfected exclusively with *β-catenin* (Fig. 3.21 C, D). Moreover, the endogenous β-catenin was not affected by ectopically over-expressed ODF2. The relative amount of degraded β-catenin fragments inversely corresponded to the relative amount of intact β-catenin: less intact β-catenin could be detected and more degraded β-catenin exists in cells which were transfected with *β-catenin* and *13.8NC-GFP*. This result demonstrates that over-expressed ODF2 could abet the degradation of over-expressed β-catenin.

C

1. untransfected HEK293
2. HEK293 transfected with *β-catenin*
3. HEK293 transfected with *β-catenin* and *13.8NC-GFP*
4. HEK293 transfected with *13.8NC-GFP*

D

Quantification of Western blot in HEK293

- untranstected HEK293
- HEK293 transfected with β-catenin
- HEK293 transfected with β-catenin and 13.8NC-GFP
- HEK293 transfected with 13.8NC-GFP
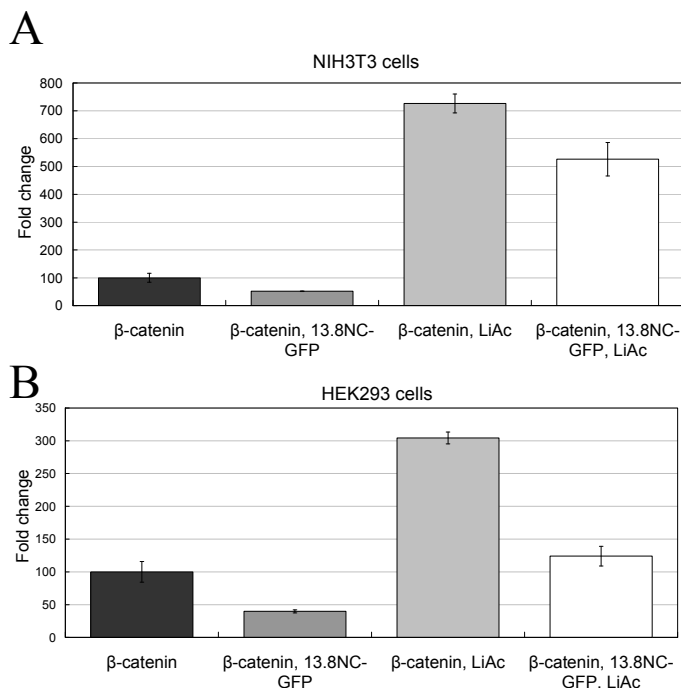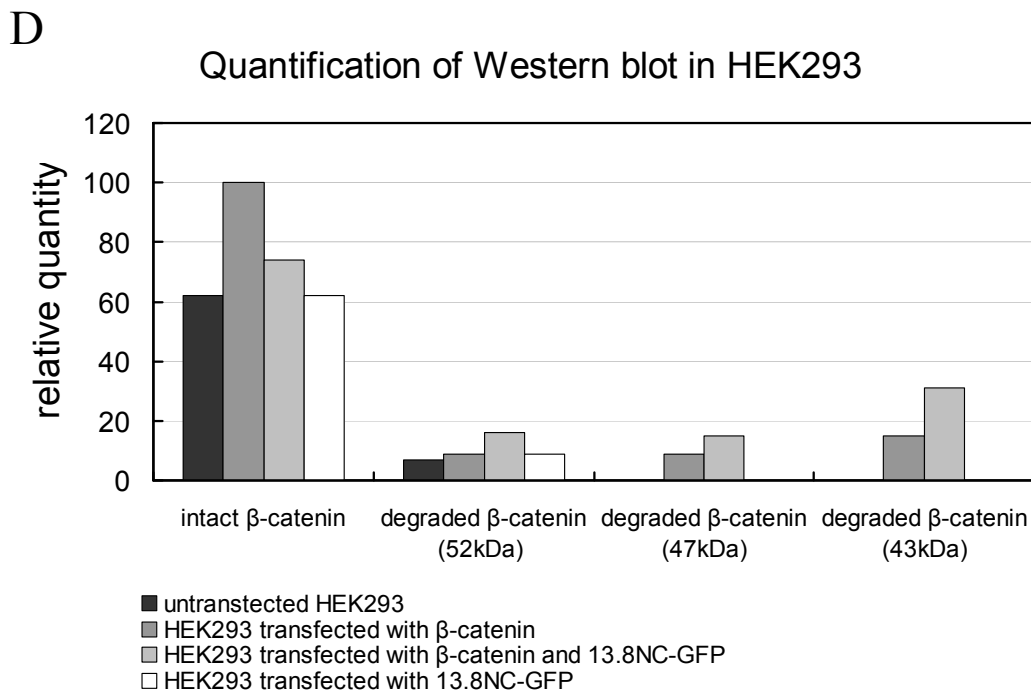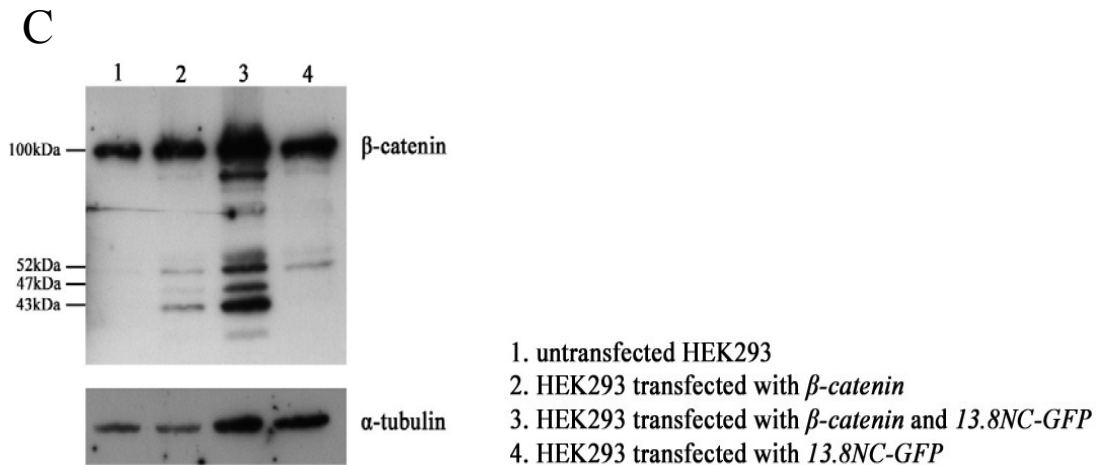
Fig. 3.21: The influence of over-expressed ODF2 on β-catenin activity. (A) and **(B),** reporter gene assay in NIH3T3 cells (A) and HEK293 cells (B). Over-expressed ODF2 decreases the activity of luciferase reporter in both cell lines and as well by lithium-treatment. **(C)**, the expression of β-catenin in differently transfected HEK293 cells. The intact β-catenin is ~100kDa. The main degraded β-catenin fragments are ~52kDa, ~47kDa and ~43kDa. α-tubulin is the loading control. **(D)**, the relative quantity results of β-catenin expression normalized to α-tubulin according to Western blot of figure 3.21 C. Quantifications are divided into four groups according to the β-catenin fragment size.

3.3.1.2 A high ODF2 expression level abets the degradation of endogenous β-catenin

Cycloheximide is an inhibitor of protein biosynthesis in eukaryotic organisms and exerts its effect by interfering with the translocation step in protein synthesis thus blocking translational elongation. HEK293 cells were transfected with *13.8NC-GFP* and incubated for 18 hours until a large amount of exogenous ODF2 fused to GFP was translated. Afterwards untransfected and transfected cells were treated with cycloheximide (100μg/ml) for 0, 4, 8, 12 and 24 hours, respectively. After cycloheximide treatment, the proteins extracted from cells were examined by Western blotting (Fig. 3.22 A). Since cells were treated with cycloheximide, protein synthesis was inhibited.

Fig. 3.22 B shows that transfected cells had an increasing relative exogenous ODF2 expression level in all cycloheximide treatments from 0 hour to 24 hours. This increase might be caused by a faster degradation of α-tubulin rather than over-expressed ODF2. Interestingly, in transfected cells, a higher ODF2 expression level corresponds to a lower β-catenin expression level (at 0, 12, and 24 hours) and vice versa (at 4 and 8 hours). Moreover, β-catenin was more degraded in transfected cells than in untransfected cells obviously from 8 to 24 hours. These results indicate that high ODF2 expression level promotes the degradation of endogenous β-catenin.

A

untransfected cells | cells transfected with 13.8NC-GFP

0h 4h 8h 12h 24h   0h 4h 8h 12h 24h

β-catenin

α-tubulin

13.8NC-GFP

B

Cycloheximide treatment

Relative quantity

(y-axis: 0, 0.2, 0.4, 0.6, 0.8, 1, 1.2, 1.4, 1.6)

(x-axis: 0h, 4h, 8h, 12h, 24h)

— relative β-catenin expression of untransfected cells
— relative β-catenin expression of cells transfected with 13.8NC-GFP
— relative 13.8NC-GFP of cells transfected with 13.8NC-GFP
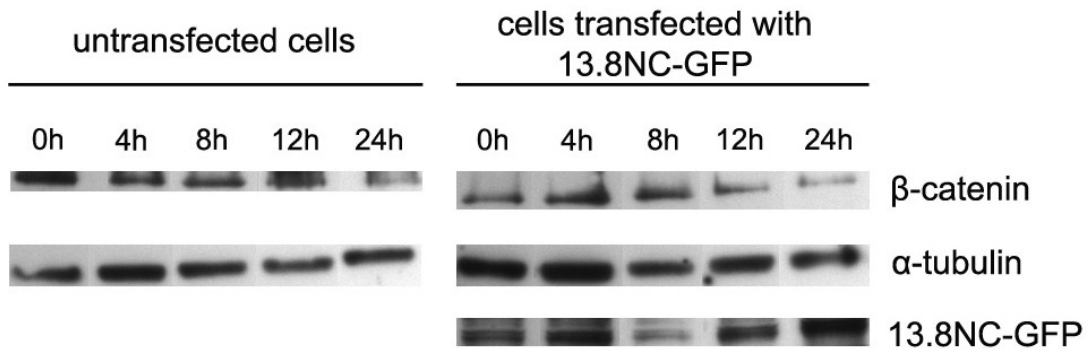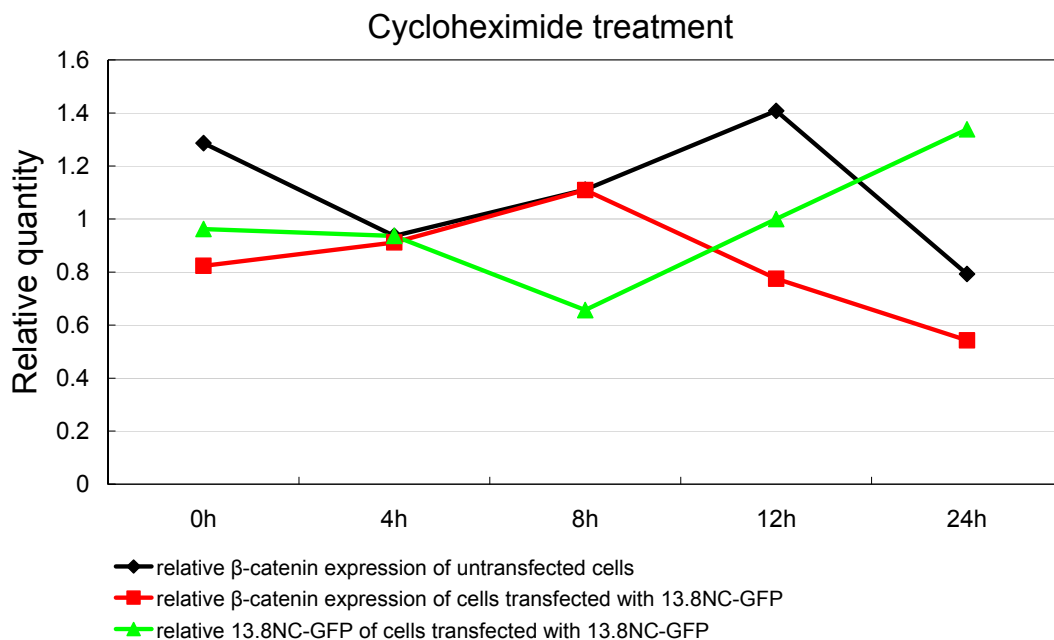
Fig. 3.22: Relative quantity of β-catenin in HEK293 cells treated with cycloheximide. (A), detection of intact endogenous β-catenin (~100kDa) in untransfected cells and cells transfected with *13.8NC-GFP* after cycloheximide treatment (0h, 4h, 8h, 12h and 24h, respectively). α-tubulin as loading control. The ectopic ODF2 expression level of cells transfected with *13.8NC-GFP* was inspected with anti-GFP antibody. **(B)**, relative quantities of β-catenin and ODF2, respectively, normalized to α-tubulin according to the Western blot of figure 3.22 in panel A.

3.3.2 Investigation of ODF2 protein domains responsible for canonical Wnt pathway inhibition

ODF2 and Cenexin are alternative splice products distinguished by a novel exon 3b encoding 42 amino acids present exclusively in Cenexin isoforms (cenexin insertion) (Hüber and Hoyer-Fender, 2007). The cenexin insertion is necessary for targeting ODF2/Cenexin to the centrosome and primary cilium, and also for the formation of ODF2/Cenexin fibers that are associated with acetylated microtubules (Hüber *et al.*, 2008). Reporter gene assays were employed to investigate whether the cenexin insertion is also necessary for the down-regulation of canonical Wnt pathway. A series of deletion constructs were generated and fused to GFP by former lab members in our group (Fig. 3.23 A, Donkor *et al.*, 2004; Hüber *et al.*, 2008). Each construct was co-transfected with β-catenin into HEK293 cells and reporter gene assays were performed (Fig. 3.23 B).

Among these constructs, the first 86 amino acids of N-terminus of ODF2 protein and the human testis-isoform of ODF2 that missed cenexin insertion (42 aa) have a minimal down-regulative effect on the activity of the reporter gene compared to the control (*phRL, OT, β-catenin*) and any other of the co-transfections (Fig. 3.23 B). The coiled-coil part (shown in black in Fig. 3.23 A) showed a strong repression. The cenexin insertion by itself repressed canonical Wnt pathway whereas the first 44 amino acids of N-terminal end seems to reduce the overall repressive effect.

A

B

Odf2 constructs

Fig. 3.23: The influence of different ODF2 protein domains translated from a series of deletion constructs on canonical Wnt pathway. (A), schematic drawing of a series of deletions translated from ODF2 constructs. 13.8NC: ODF2 protein starting with MSASS and comprising cenexin insertion. Human testis: the ODF2 isoform localizing specially in sperm. cenexin: the

94

N-terminal region of ODF2 isoform expressed in somatic cells. 13.8, N-terminal, cenexin insertion, ODF2NC, ODF2N2C, ODF2NC1 and ODF2NC2: they were encoded by homonymous subclones of *Odf2* (Donkor *et al.*, 2004; Hüber *et al.*, 2008). Sequences 498-519 and 636-657 are two leucine-zipper motifs. **(B)**, canonical Wnt reporter gene assay using *Odf2* constructs shown in panel A. The different *Odf2* constructs were co-transfected with *β-catenin* into HEK293 cells and the relative reporter gene assay activity quantified 24 hours later (cooperation with bachelor student Annie Angelique Nono Megaptche).

3.3.3 Centrosomal proteins and cytoskeletal proteins down-regulate the canonical Wnt reporter

Since I have shown that ODF2 down-regulates the activity of β-catenin, the question arises: whether other centrosomal proteins also affect the activity of β-catenin. I have chosen the centriolar proteins Ninein, Centrin and ε-tubulin and pericentriolar material proteins γ-tubulin (Paul Chang and Tim Stearns, 2000) to investigate their influences on reporter gene activity in HEK293 cells. Ninein localizes at the subdistal appendages of mother centrioles like ODF2 (Nakawaga *et al.*, 2001; Morgensen *et al.*, 2000). Centrin localizes in the lumen of centrioles (Paoletti *et al.*, 1996). For each experiment the cells were transfected with *β-catenin* alone, and the relative luciferase activity set as 100%. Relative luciferase activity of co-transfection experiments were related to the control value. Fig. 3.24 A shows that over-expressed Ninein, Centrin and ε-tubulin down-regulate the luciferase activity to 35%, 40% and 39%, respectively. γ-tubulin decreases the luciferase activity down to 7%. This result indicates that there might be a tight relationship between the canonical Wnt pathway and centrosomal proteins.

Fig. 3.24 A also shows that over-expressed α-tubulin, which is a main microtubular protein, can strongly inhibit the activity of luciferase reporter from 100% down to 8%.

Nocodazole is a chemical that interferes with the polymerization of microtubules in

cells. When microtubule proteins negatively affect the activity of the reporter, nocodazole probably could rescue it due to disturbing the polymerization of microtubules. The cells were therefore treated by 100ng/ml nocodazole for 16 hours. Nocodazole can indeed increase the reporter luciferase activity at ~20% (Fig. 3.24 B, colorless group). Likewise, the decreased luciferase activities caused by over-expression of either centrin, α-tubulin or γ-tubulin were partially rescued by nocodazole as well (Fig. 3.24 B, yellow, green and red groups, respectively). This result argues that the microtubule system negatively affects canonical Wnt signaling and that the disturbance of microtubule polymerization partially negotiates its inhibitory effect.

In opposite to nocodazole taxol stabilizes microtubules. When microtubules suppress the activity, the stabilization of microtubules should principally enhance this inhibition effect. The HEK293 cells were treated with 100nM taxol for 16 hours. Surprisingly the activity of reporter luciferase did not decrease but conversely had a ~50% increase after the taxol treatment (Fig. 3.24 B, colorless group).

A

centrosomal proteins and tubular proteins

B

Nocodazole and taxol

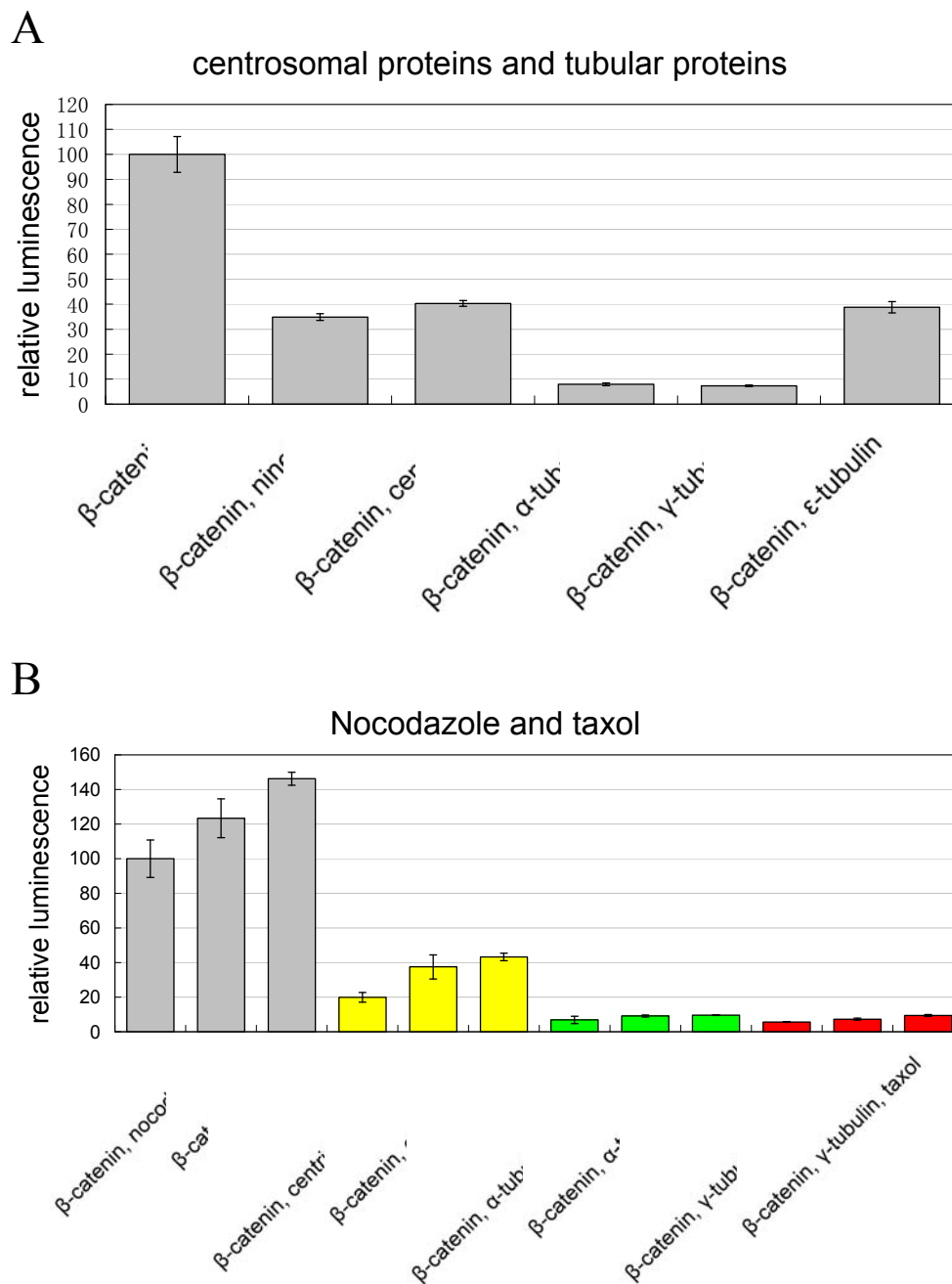**Fig. 3.24: Analysis of the influence of centrosomal and cytoskeletal proteins on canonical Wnt reporter. (A)**, the activity of over-expressed β-catenin can be down-regulated by centrosomal proteins and microtubule proteins. **(B)**, nocodazole and taxol can rescue β-catenin activity to a certain extent that was otherwise inhibited by over-expression of either Centrin, α-tubulin, or γ-tubulin. Nocodazole, 100ng/ml. Taxol, 100nM.

3.3.4 The influence of over-expressed ODF2 on target genes of the canonical Wnt pathway

3.3.4.1 The over-expression of ODF2 does not obviously affect the activation of canonical Wnt pathway target genes *in vivo* (*Xenopus laevis*)

When β-catenin accumulates in the cytoplasm, it will enter into the nucleus and activates as transcriptional co-activator of the transcription factors TCF/LEF target genes of the canonical Wnt pathway. Therefore, I subsequently investigated the effect of over-expressed ODF2 on down-stream target genes of the canonical Wnt pathway. In *Xenopus laevis*, a complete second dorsal body axis can be induced by over-expression of *Xwnt-8*, which belongs to the Wnt family of secreted glycoproteins. Microinjection of *Xwnt-8* mRNA can rescue axial structures in embryos ventralized by UV irradiation (Sokol *et al.*, 1991; Smith and Harland, 1992). I co-injected the mRNA of *Xwnt-8* and *Odf2* into the embryos of *Xenopus laevis* to observe whether the over-expressed ODF2 can avoid or reduce the presence of the secondary axis at their tadpole stages.

About 4 days after injection, the embryos enter the tadpole stages and develop the secondary dorsal axis. Injection of 500pg *Odf2* mRNA caused lethality before they entered into the tadpole stages. Therefore, the amount of *Odf2* mRNA used for injection was reduced to 200pg at the utmost. Fig. 3.25 shows that there is no significant difference between single injection of *Xwnt-8* (8pg) and co-injection of *Xwnt-8* (8pg) and *Odf2* (50pg, 100pg and 200pg, respectively), regarding secondary axis formation. However, an increased *Odf2* mRNA amount injected slightly but gradually reduced secondary dorsal axis formation 71% to 65% (Fig. 3.25). This result demonstrates that over-expressed ODF2 had a moderate effect on *Xwnt-8* induced secondary axis formation in *Xenopus* embryos.
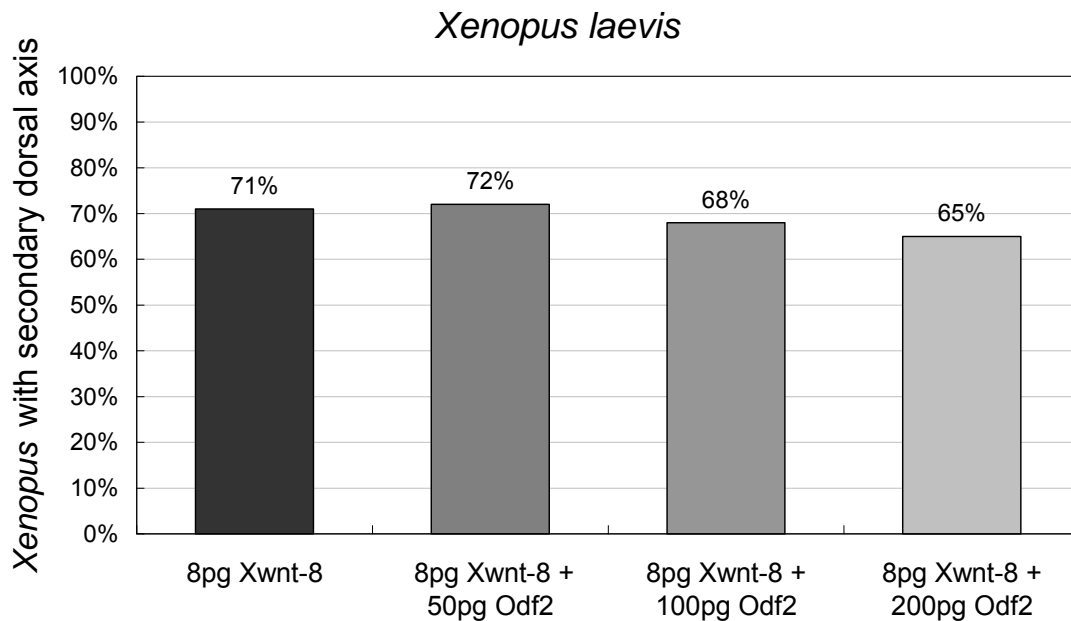
Fig. 3.25: The comparison of single injection of *Xwnt-8* (8pg) mRNA and the co-injection of *Xwnt-8* (8pg) and different amounts of *Odf2* mRNA (50pg, 100pg and 200pg, respectively) on secondary axis formation (cooperation with Dr. B. Rust, Henningfeld's group).

3.3.4.2 Over-expression of ODF2 inhibits *c-Myc* transcription

Here, *c-Myc* was chosen as Wnt target gene and *HPRT* as house keeping gene for expression level analysis using real time PCR. HEK293 cells were transiently transfected with one of five different plasmid constructs, respectively: *13.8NC-GFP*, *Odf2* cloned into *pEGFP-N1* vector; *13.8NCΔGFP*, *Odf2* cloned into *pEGFP-N1* vector without *GFP*; *pEGFP-1*, which does not have a functional promoter; *pEGFP-N1*, the empty *pEGFP-N1* vector; *shODF2*, short hairpin *Odf2* cloned into *pIRES-EGFP* vector. Besides these transient transfections, the construct *13.8NC-GFP* was stably tansfected into HEK293 cells using neomycin selection. Untransfected HEK293 cells were used as blind control in real time PCR.

Two independent relative real time PCR experiments were arranged, each performed in triplicate. Fig. 3.26 shows that cells transfected with *pEGFP-1*, which does not have a functional promoter, have a reduced expression of *c-Myc*. This suggests that

the expression of *c-Myc* was generally affected by the transfection reagent. Ectopically expressed ODF2 (*13.8NC-GFP* and *13.8NCΔGFP*, respectively) down-regulate the transcription of *c-Myc*. However GFP (empty *pEGFP-N1* vector) also has a negative effect on the transcription of *c-Myc*. However, transcription of *c-Myc* was strongly suppressed in cells that were stably transfected with *13.8NC-GFP*. Unexpectedly, the lower expression of ODF2 via *shODF2* interference did not promote the activation of *c-Myc*, but reduced its transcription level when compared to untransfected cells. However, when compared to cells transfected with *13.8NC-GFP*, transcription of *c-Myc* was partially rescued by *shODF2* interference. Taken all together, this result indicates that the down-regulation of β-catenin by over-expression of ODF2 leads to a reduced transcription level of the canonical Wnt target gene *c-Myc*.

It was reported that at least 15% of breast cancers present distinct amplification of *c-Myc* and *c-Myc* is also amplified very frequently in many other tumors (Deming, *et. al*. 2000). This suggests that transcription level of *c-Myc* might be higher in those cancers than in normal tissues. Therefore, the real time PCR was performed in two human breast cancer cell lines, MCF7 and MDA-MB-231, to check their transcription level of *c-Myc* and whether over-expression of ODF2 has also an effect on *c-Myc* in cancer cells. In MCF7 cells, untransfected and stably transfected (*13.8NC-GFP*), *c-Myc* template copies were nearly same and extremely exiguous (~20 copies / 20μg cDNA). In MDA-MB-231 cells, untransfected and stably transfected (*13.8NC-GFP*), there was no *c-Myc* cDNA template to be detected at all (data not shown). Therefore, the influence of over-expressed ODF2 on *c-Myc* could not be confirmed in these two cell lines further.
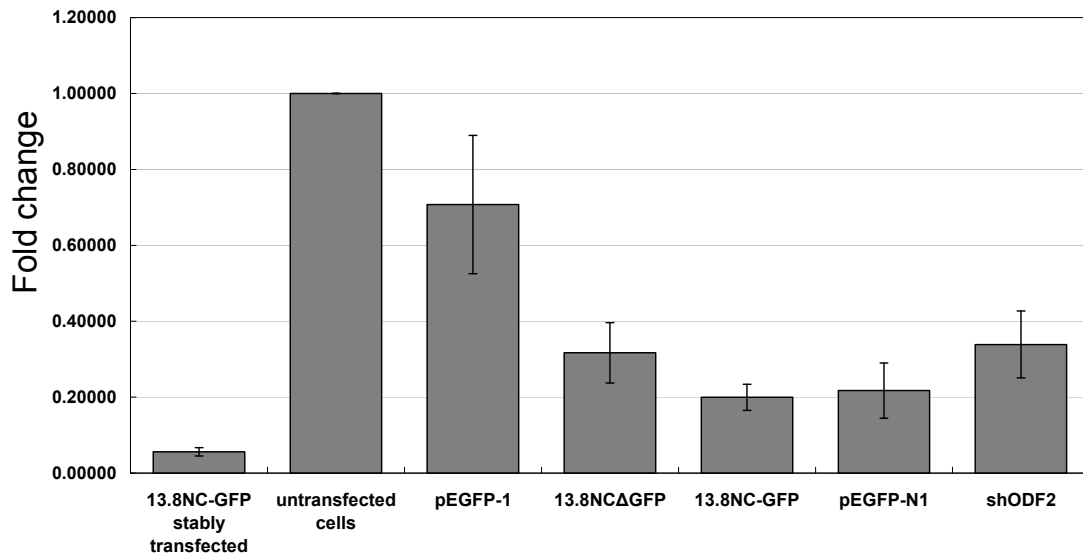
c-Myc gene expression in HEK293 cells

Fig. 3.26: Transcription of *c-Myc* related to *HPRT* in HEK293 cells transfected with different constructs. *13.8NC-GFP*, *Odf2* cloned into *pEGFP-N1* vector; *13.8NCΔGFP*, *Odf2* cloned into *pEGFP-N1* vector without *GFP*; *pEGFP-1*, the *pEGFP* vector without functional promoter; *pEGFP-N1*, the empty *pEGFP-N1* vector; *shODF2*, short hairpin *Odf2* cloned into *pIRES-GFP* vector.

3.3.5 ODF2 over-expression affects the migration of human breast cancer cells

Besides the role in canonical Wnt pathway β-catenin is also very important for cell-cell adhesion. β-catenin links cadherins at the plasma membrane to α-catenin (Cowin *et al*., 1986; Ozawa *et al*., 1989; McCrea *et al*., 1991; Kemler *et al*., 1993; Takeichi *et al*., 1995). Therefore, the influence of over-expressed ODF2 on cell-cell adhesion was also investigated in NIH3T3, MCF7 and MDA-MB-231 cells using the wound healing assay.

To perform the assay, untransfected cells were used as control, cells stably transfected with empty vector *pEGFP-N1* as GFP control, and cells stably transfected with *13.8NC-GFP* were applied to check the influence. In addition, the cell line NIH3T3

was also investigated as control. The 100% confluent cells were scraped to form a wound and the distance between the borders of wound was measured at 0 hour (Fig. 3.27 A). After certain times the distances between the borders of the wound were measured. Fig. 3.27 B shows that the NIH3T3 cells transfected with empty vector and with *13.8NC-GFP* have similarly moving speed, and both of them are faster than untransfected cells. This means that the alteration of cell migration might exclusively be caused by over-expressed GFP but not by ODF2 over-expression. Fig. 3.27 C shows that the MCF7 cells transfected with *13.8NC-GFP* were distinctly affected by over-expressed ODF2 compared with untransfected cells and cells transfected with empty vector. The MCF7 cells transfected with *13.8NC-GFP* migrate faster. Surprisingly Fig. 3.27 D shows that the effect of over-expressed ODF2 on cell migration in MDA-MB-231 cells is inversed compare to MCF7 cells. There is no distinct difference between untransfected cells and cells transfected with empty vector neither in MCF7 cells nor in MDA-MB-231 cells. Thereby GFP did not affect the migration of these two cell lines. These results demonstrate that over-expressed ODF2 has different effects on cell migration in different human breast cancer cell lines but no significant effect in NIH3T3 cells.
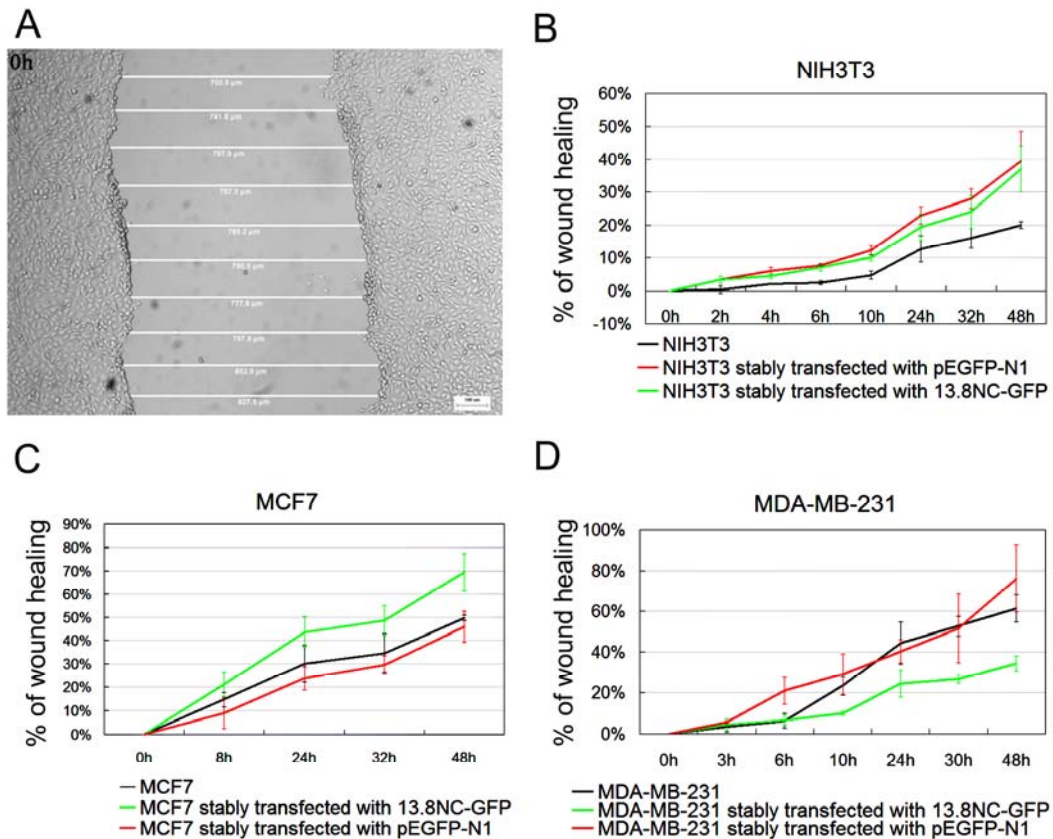
Fig. 3.27: Investigation of the effect of ODF2 over-expression on cell migration by wound healing assay in different cells. (A), an enlarged picture of NIH3T3 cells at 0h as an example for wound healing assay. Each cell line was scratched at three different positions and each wound was measured at ten different positions. **(B)**, **(C)**, and **(D)**, cell migration graphs. The curve with the larger percentage means that the cells migrate faster.

3.3.6 ODF2 interacts with Axin1, Axin2 and TAZ proteins individually

Axin1 and Axin2 are two functionally identical isoforms of Axin that is a scaffold protein cooperating with GSK3β and APC in mediating phosphorylation of β-catenin (Kikuchi, 1999; Chia and Costantini, 2005). Knock in of Axin2 into the deleted Axin1 gene rescues *Axin1*$^{-/-}$ mice (Chia and Costantini, 2005). Moreover, it was demonstrated that Axin colocalized with ODF2 at the centrosome (Fumoto *et al.*, 2009). Therefore it was predicted that ODF2 might bind to Axin and promote its

stability thus affect the degradation of β-catenin. HEK293 cells were co-transfected with *13.8NC-GFP* and *Axin1-myc* or with *13.8NC-GFP* and *Axin2-myc*, respectively. Cells were lysed and soluble proteins were subjected to immunoprecipitation using anti-GFP antibodies which were raised in rabbit. The bead bound protein fractions were then analyzed by Western blot using polyclonal anti-Axin1 and anti-Axin2 antibodies, respectively. Axin1-myc (a doublet band at ~120kDa-130kDa) and Axin2-myc (at ~100kDa) were found to co-precipitate with 13.8NC-GFP fusion protein, respectively (Fig. 3.28 lane b in panel A and B, arrows on upper pictures). In contrast, no Axin1 or Axin2 was found in the control beads in which anti-GFP antibodies have been omitted (Fig. 3.28 lane bc in panel A and B). These results indicate that ODF2 might affect the stability of β-catenin negatively by binding to Axin1 and Axin2 directly.

It was reported that phosphorylated β-catenin serves as a scaffold for TAZ association with β-TrCP/E3 ubiquitin-ligase complex (Azzolin *et al*., 2012). As a transcriptional co-activator of the Hippo pathway that is a growth-limiting and differentiation-promoting signal TAZ promote cell proliferation and inhibit differentiation (Halder and Johnson, 2011; Hong and Guan, 2012; Ramos and Camargo, 2012). Hippo triggers phosphorylation and nuclear export of TAZ for degradation in the cytoplasm. Similar to phosphorylated β-catenin, TAZ is ubiquitinated and degraded by the E3 ligase β-TrCP (Murakami *et al*., 2005; MacDonald *et al*., 2009; *Liu et al*., 2010; *Zhao et al*., 2010; Imajo *et al*., 2012). Due to TAZ's association with many transcription factors via its interaction motifs (WW, coiled coil, SH3, and PDZ) (Hong and Guan, 2012), and the coiled-coil motifs of ODF2, it was investigated whether there is an interaction between TAZ and ODF2, and whether the effect of ODF2 on β-catenin is associated with TAZ. HEK293 cells were co-transfected with *13.8NC-GFP* and *TAZ-HA*. Cells were lysed and soluble proteins were subjected to immunoprecipitation using anti-GFP antibodies which were raised in rabbit. The bead bound protein fractions were then analyzed by Western blot using monoclonal anti-HA antibodies. TAZ-HA (~55kDa) was found to co-precipitate with 13.8NC-GFP fusion protein (Fig. 3.28 C, upper picture). In

contrast, no TAZ was found in the control beads in which anti-GFP antibodies have been omitted (Fig. 3.28 lane bc in panel C). These results indicate that ODF2 might directly bind to TAZ.

Fig. 3.28: Interaction of ODF2 and Axin1, Axin2, and TAZ, respectively. (A), interaction of ODF2 and Axin1. Plasmids encoding Axin1 fused to Myc (*Axin1-myc*) and ODF2 fused to EGFP (*13.8NC-GFP*) were transfected into HEK293 cells and co-immunoprecipitation was performed using anti-GFP antibodies. Axin1-myc (a doublet band at ~120kDa-130kDa) co-precipitated with 13.8NC-GFP detected using anti-Axin1 antibodies (arrow on upper picture). **(B)**, interaction of ODF2 and Axin2. Plasmids encoding Axin2 fused to Myc (*Axin2-myc*) and ODF2 fused to EGFP (*13.8NC-GFP*) were transfected into HEK293 cells and co-immunoprecipitation was performed using anti-GFP antibodies. Axin2-myc (~100kDa) co-precipitated with 13.8NC-GFP detected using anti-Axin2 antibodies (arrow on upper picture). **(C)**, interaction of ODF2 and TAZ. Plasmids encoding TAZ fused to HA (*Taz-HA*) and ODF2 fused to EGFP (*13.8NC-GFP*) were transfected into HEK293 cells and co-immunoprecipitation was performed using anti-GFP antibodies. TAZ-HA (~55kDa) co-precipitated with 13.8NC-GFP detected using anti-HA antibodies. In all panels, ODF2 was proven to be ectopically expressed (~100kDa, arrows on

lower pictures) with anti-GFP antibodies. s, soluble cellular proteins; p, insoluble cellular proteins; dc, proteins of the supernatants after separation of protein G agarose beads (depletion control); lw, proteins of the last washing step; b, proteins of the bead bound fraction. bc, control, proteins bound to beads without the presence of the fishing antibody. These three co-immunoprecipitations were performed by bachelor student Constanza Tapia.

3.3.7 Ectopically expressed ODF2 affects the phosphorylation of Tau

ODF2 is a self-interacting, microtubule-associated protein (Donkor *et al*., 2004). It is thus possible that the positive influence of ODF2 on β-catenin degradation is mediated by stabilizing microtubules subsequently maintaining β-catenin destructure complex. Therefore I investigated the effect of ectopically expressed ODF2 on another microtubule-associated protein Tau. As a microtubule-associated protein, Tau stabilizes microtubule polymers (Brandt and Lee, 1993) and suppresses microtubule dynamics (Panda *et al*., 1995). Normally, phosphorylation of the microtubule-associated proteins by the microtubule-affinity-regulating-kinase causes the microtubule-associated proteins to detach from any bound microtubules (Drewes *et al*., 1998), and the hyperphosphorylation of Tau leads to massive detachment, which in turn greatly reduces the stability of microtubules in nerve cells (Mandelkow and Mandelkow, 1995). The NIH3T3 cells were transfected with *Odf2* siRNA leading a reduced expression of ODF2 (Fig. 3.29 A) and the HEK293 cells were transfected with 13.8NC-GFP causing an over-expression of ODF2 (Fig. 3.29 C). After 48 hours of *Odf2* siRNA transfection and 24 hours of ODF2 over-expression, the cells were lysed and analysed with Western blotting. Relatively quantified results show, that Tau proteins were more phosphorylated when ODF2 was less expressed, and consistently, Tau proteins were less phosphorylated when ODF2 was over-expressed (Fig. 3.29 B and D). These results indicate that ODF2 promotes the stabilization of microtubules and might therefore abet the degradation of β-catenin.
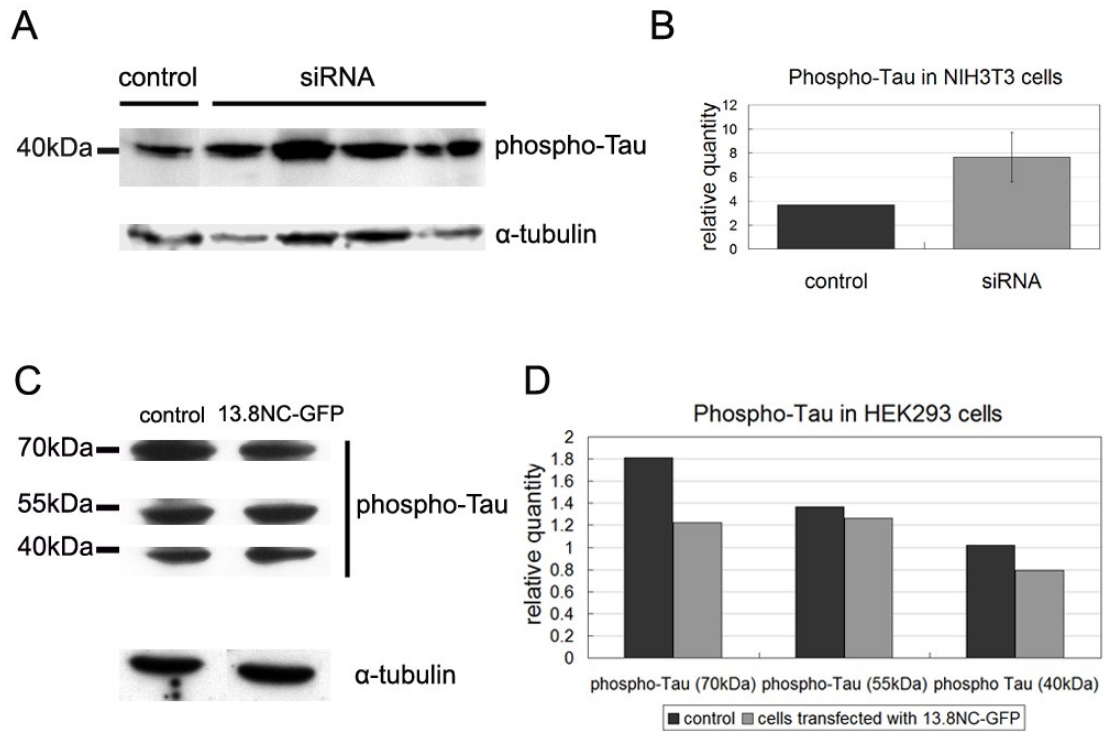
Fig. 3.29: The phosphorylation of Tau was affected by ectopically expressed ODF2. (A), the phosphorylation of Tau increases in NIH3T3 cells in that *Odf2* was knocked down. After using small interfering RNA the soluble proteins were separated on SDS-gels, blotted, and probed with anti-phospho-Tau antibodies. *Odf2* expression was interfered by small interfering RNA constructs, and four independent experiments were performed. The untreated NIH3T3 cells were taken as control. In NIH3T3 cells, many different degraded phospho-Tau fragments were found. α-tubulin was taken as reference protein. **(B)**, the relative quantitative results of main degraded phospho-Tau expression (~40kDa) normalized to α-tubulin according to Western blot result in panel A. **(C)**, the phosphorylation of Tau decreases in ODF2 over-expressed HEK293 cells. Plasmids encoding ODF2 fused to EGFP (*13.8NC-GFP*) were transfected into HEK293 cells, afterwards, the soluble proteins were separated on SDS-gels, blotted, and probed with anti-phospho-Tau antibodies. The untreated HEK293 cells were taken as control. In HEK293 cells, many different degraded phospho-Tau fragments were found. α-tubulin was taken as reference protein. **(D)**, the relative quantitative results of three phospho-Tau degradation fragments (~70kDa, ~55kDa and ~40kDa, respectively) normalized to α-tubulin according to Western blot result in panel A.

4. Discussion

4.1 ODF1 is essential for tight linkage of sperm head to tail and male fertility in mice

Up to 15% of reproductive-aged couples worldwide suffer from infertility according to the World Health Organization. In 50% of cases male infertility has been found to be the cause (Cui, 2010). In male infertility diagnostics, the sperm tail cytoskeleton has received increasing attention over the years since sperm tail-associated defects may impair sperm motility that eventually results in infertility (Marmor and Grob-Menendez, 1991). Likewise, sperm tail defects have been considered as a prognostic factor in assisted conception in humans (Lim *et al.*, 1998).

The sperm tail generates progressive motility necessary to reach the oocyte. Its functional unit is the axoneme, a tubulin-based structure containing microtubule-associated proteins and motor proteins that convert chemically bound energy into progressive mechanical force by ATP hydrolysis (Haimo and Rosenbaum, 1981; King, 2000; Mortimer, 1997; Porter and Sale, 2000). The orderly array of axonemal nine doublet microtubules surrounding a pair of singlet microtubules is complemented by associated ODFs that accompany the microtubule doublets throughout most of the sperm tail. In addition, in the midpiece of the sperm tail the mitochondrial sheath wraps around the ODFs, and in the principal piece the fibrous sheath surrounds the axoneme and the residual seven ODFs (Fawcett, 1975). Both the ODFs and the fibrous sheath provide structural rigidity to the tail (Baltz *et al.*, 1990). The fibrous sheath additionally is involved in the generation of ATP (Miki *et al.*, 2004). A main protein component of mammalian ODFs is ODF1. Moreover, ODF1 is exclusively expressed in spermatids and restricted to the ODF compartment (Morales *et al.*, 1994). Not surprisingly, it was observed that *Odf1*-deficiency did not affect female mice. Loss of ODF1 exclusively affected male mice resulting in infertility.

In testes it was found that spermatogenesis in general was not impaired. The expression of all marker genes characteristic for the various germ cell types

demonstrated that spermatogenesis proceeded normally from spermatogonia to spermatids. Expression of *Hanp1* especially substantiated spermiogenic progression in *Odf1*-deficient mice because *Hanp1* transcription is restricted to spermatids (Tanaka *et al*., 2005). Histological examinations of testes likewise revealed no hints of disturbed spermatogenesis up to at least 19 days after birth. Perturbations of the germinal epithelium were found not until sexual maturity when two-thirds of mice exhibited undifferentiated cells, and two of nine mice showed multinuclear cells in the lumen of their seminiferous tubules. However, in most cases elongated spermatids were present.

Semithin sections of epididymides from *Odf1*$^{-/-}$ mice revealed an increase of nonmature germ cells and a high percentage of dysplastic sperm. Sperm heads were barely found, thus accounting for observed infertility. The presence of large multinucleate cells found in some tubules suggests that the lack of ODF1 also might affect germ cell separation, leading eventually to the coalescence of adjacent germ cells. Measurement of sperm parameters revealed that *Odf1*-deficient epididymal sperm are motile, although with strongly reduced velocities but increased beat cross frequencies and straightness, both of which might be caused by the absence of the normally built sperm head. In addition, half-reduction of the amount of ODF1 in sperm of heterozygous mice, originating from the syncytial nature of the germinal epithelium (Braun *et al*., 1989), affected their motility but eventually did not impact fecundity. At the light microscopic level, *Odf1*-deficient sperm are characterized by their remarkable tail coiling, as well as by their missing heads. At the ultra-structural level, disturbed mitochondrial organization in the midpiece of the sperm tail and disturbed organization of ODFs not only in the midpiece but also in the principal piece were observed. Most remarkably, however, is the absence of intact spermatozoa. These results thus strongly support the view that ODF1 is essential for the tight connection of the sperm head to the tail and for the orderly arrangement of the mitochondria and the ODFs in the sperm tail.

Besides the observation of mitochondrial disorganization in *Odf1*$^{-/-}$ mice, loss of either Nectin-2, a Ca^{2+}-independent immunoglobulin-like cell-cell adhesion molecule, or

Gopc (Golgi-associated PDZ- and coiled-coil motif-containing protein) showed impairment of tight packaging of mitochondria into a helical sheath (Bouchard *et al.*, 2000; Suzuki-Toyota *et al.*, 2007). However, neither Nectin-2 nor Gopc have previously been identified as ODF1 binding partners. Instead, a promising candidate that could be responsible for mediating the tight packaging of mitochondria and their association to the ODFs in the midpiece of the sperm tail is the kinesin light chain, KLC3. KLC3 has not only been shown to interact with ODF1 but also to associate with mitochondria in the sperm tail (Bhullar *et al.*, 2003; Zhang *et al.*, 2004). Lack of its binding partner ODF1 could thus affect the tight mitochondrial association to the ODFs eventually resulting in its disturbed arrangement.

It has also been found that the ODFs associate to the axonemal microtubule doublets no more tightly in midpiece and principal piece in *Odf1*$^{-/-}$ mice. Lack of ODF1 seems to result in reduction or even loss of the central part of ODF, the medulla, and eventually in hollow fibers (Fig.3.7 B b). Beyond that, the most striking phenotype was the detachment of the tail from the nucleus. It resembles a type of oligoteratoasthenospermia in humans with sperm tail fragility and decapitated sperm heads (Baccetti *et al.*, 2001; Chemes *et al.*, 1999; Kamal *et al.*, 1999). Detachment might occur during sperm passage from testis to epididymidis due to the loosening of the sperm head-to-tail linkage by missing ODF1 that eventually could not withstand mechanical forces.

Whereas the heterozygous male mice, that were generated from mixed genetic background (C57BL/6//129/Sv), are fully fertile albeit having reduced sperm motility, the incipient congenic heterozygous male mice, generated by successive backcrossing of *Odf1*-depleted mice of mixed background (either heterozygous females or males) to inbred 129/Sv mice, are strongly reduced in fertility. In six individual matings, incipient congenic male mice of backcross generation N7 gave birth to only two pups after more than 5 months of continuous cohabitation. Moreover, male fertility rate is already reduced to ~50% in backcross matings compared to wild-type crosses. Whereas fertility of heterozygous females continuously drops during progressive

backcrosses, male fertility is already severely reduced in generation N0. The decline in female fertility by successive backcrossing to 129/Sv suggests that the genetic background strongly affects fertility success. However, severe subfertility of male mice could not be explained exclusively by the genetic background since heterozygous females of generation N7 gave birth to 3 pups per litter when mated to wild-type males (Fig. 3.8 B). Both together, severe subfertility of heterozygous male mice and reduced fertility of female mice might account for the infertility observed in generation N7 pairings. The generally much higher litter size of strain C57BL/6 might explain why haplo-deficiency of ODF1 seemed not to affect male fertility on mixed genetic background (C57BL/6//129/Sv).

Although normal sperm count, sperm motility and no ultra-structural sperm anomalies of congenic heterozygous males were detected, a significant increase of the distance between the nuclear membrane and the capitulum was yet observed, when ODF1 is reduced. A larger distance between nucleus and capitulum reflects a weakening of sperm head-tail linkage that eventually causes decapitation when strong shearing forces are applied as e.g. during sperm movement through the female genital tract.

The impact of ODF1 on the structural organization of the spermatozoon is illustrated in Fig. 4.1, emphasizing known interaction partners. Linking ODFs to microtubules might occur via ODF1/SPAG5/SPAG4 interaction and to mitochondria via ODF1/KLC3 interaction. ODF1/ODF2 binding might account for rigidity of ODFs, basal plate, capitulum, and striated columns (Schalles *et al*., 1998). The results of ODF1 investigation suggest that ODF1 is essential for the rigid junction of sperm head and tail and that a loss of function of ODF1 might account for some of the cases of human infertility with decapitated sperm heads.
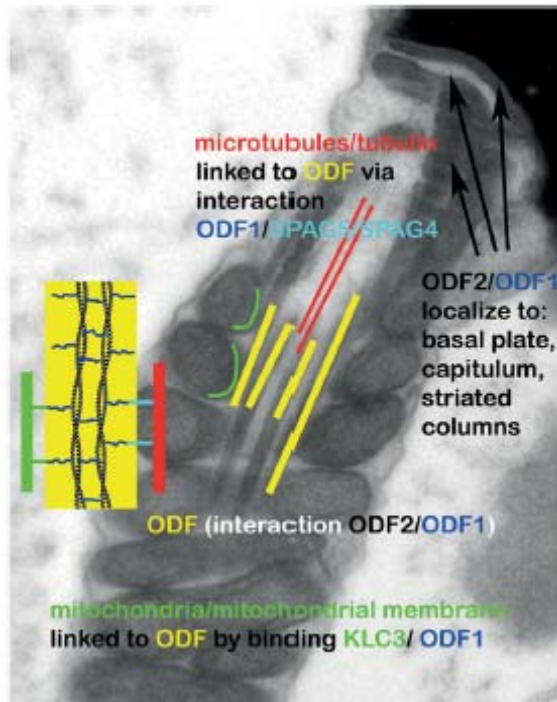
Fig. 4.1: The localization of ODF1 and its reported interaction partners that might account for observed disturbances in ODF1-deficient sperm. ODF1 interacts with ODF2, and both are located to the ODFs, basal plate, capitulum, and striated columns (Schalles *et al.*, 1998). Linking of ODF to axonemal microtubules might be mediated via binding of ODF1 to SPAG5/SPAG4 and of ODF to mitochondria via KLC3 binding.

4.2 Interaction of ODF1 and SPAG4 defines a novel germ cell specific LINC complex involved in sperm head to tail attachment

The most striking phenotype observed in *Odf1 knock out* mice was sperm decapitation causing male infertility. ODF1, therefore, has been turned out to be an important component of the head-to-tail coupling apparatus (HTCA) in sperm (see 3.1 and Yang *et al.*, 2012). ODF1 most likely ensures the connection to capitulum and sperm tail by interaction with ODF2 that is a fiber forming protein and the main component of the sperm tail outer dense fibers (Shao *et al.*, 1997; Petersen *et al.*, 1999). ODF1 thus belongs to the cytoskeletal compartment of the HTCA. But which protein (or proteins)

might then be responsible for mediating the tight connection of the capitulum to the nuclear membrane by binding to ODF1? Presumably, the respective counterpart has to be expressed in male germ cells and preferentially localized to the nuclear membrane. In somatic cells the cytoskeleton is linked to the nucleoskeleton by nuclear membrane proteins with conserved SUN or KASH domains. SUN domain proteins with predominant expression in testis have already been identified although meticulous analyses are still missing. One of these proteins is SPAG4. SPAG4 has been described as an interaction partner of ODF1 that localizes to the microtubules of manchette and axoneme (Shao *et al.*, 1999). However, albeit proven by immunoelectron microscopy the cytoskeletal localization is quite uncommon for SUN domain proteins that are usually nuclear membrane proteins. I therefore started to investigate expression and localization of SPAG4 in depth. Full-length *Spag4* was cloned from mouse testis. The protein consists of the N-terminal region followed by the putative transmembrane domain, a coiled-coil domain and the conserved SUN domain and thus revealed its affiliation to the SUN domain protein family. Its domain organization additionally indicated a membranous association. I could indeed show that SPAG4 is a nuclear membrane protein just as other SUN domain proteins. When ectopically over-expressed a conspicuous amount of SPAG4 is cytoplasmic although no hints to microtubule association were found. *In vivo* proteinase K treatment demonstrated that the C-terminal region is more resistant against proteolytic degradation demonstrated by the fact that only antibodies directed against the C-terminally located Myc-tag were able to detect the full-length protein as well as a resistant fragment of ~40 kDa. These data thus indicate that SPAG4 is located in the nuclear membrane with its C-terminal region most likely residing in between the outer and inner nuclear membrane. The *Spag4* gene is exclusively expressed in testis. Expression was found neither in somatic tissues nor in ovary. Additionally, spermatogonial stem cells (SSC), embryonic stem cells (ES) or the teratocarcinoma cell line F9 did not express *Spag4*. Transcription of *Spag4* in testis starts around day 20 to 25 in mice which corresponds to the emergence of the early round spermatid stage. Transcription of *Spag4* therefore seems to be restricted to the male germ cell lineage starting at the round spermatid

stage. Immunocytology on testicular cell preparations confirmed previous data. SPAG4 protein was identified exclusively in male germ cells from round spermatids to late elongating spermatids. The protein was always found at the nuclear membrane and became concentrated towards the posterior pole of the spermatids during spermiogenesis. SPAG4 was located in proximity to the manchette but did not show exact co-localization. When the manchette started to disintegrate a specific amount of SPAG4 scattered into the residual cytoplasm. In mature sperm SPAG4 was no longer detectable most likely due to its amount below the detection limit. I could never verify SPAG4 in the sperm tail. However, it might be possible that immunoelectron microscopy is even more sensitive to enable detection of the protein in the sperm tail and the manchette (Shao *et al.*, 1999). Eventually, these results demonstrate that SPAG4 is a nuclear membrane protein restricted to haploid male germ cells and localized to the posterior pole of spermatids - a region in which the sperm tail attaches to the nucleus. Furthermore, I verified that SPAG4 interacts with ODF1 endogenously in testis as well as when ectopically over-expressed. Interaction was proven for both the N-terminal fragment of SPAG4 including the transmembrane domain as well as the C-terminal part. Interaction with ODF1 was demonstrated by co-IP as well as by immunocytology. The C-terminal fragment missed the transmembrane domain and therefore displayed an aberrant cytoplasmic localization. The N-terminal fragment comprising the transmembrane domain localized to the nuclear membrane and caused the recruitment of ODF1 to the nuclear membrane as well as was also shown for the full length SPAG4 protein. These results therefore suggest that the nuclear membrane protein SPAG4 most likely recruits ODF1 to the nuclear membrane via its N-terminal end that resides in the cytoplasm. Location of SPAG4, vice versa, is not provoked by ODF1. However, I have to admit that cytoplasmic location of the N-terminal end of the SUN domain protein SPAG4 is quite uncommon for a member of this protein family. Beyond, by ectopic over-expression of ODF1 I found that ODF1 is concentrated at the centrosome, which was identified by γ-tubulin staining. When simultaneously over-expressed, SPAG4 is also concentrated at the centrosomal area. Since the centrosome comprises ODF2 and can be transformed into the basal body to

grow a cilium it could be viewed as an equivalent to the connecting piece in sperm: via binding to ODF2 ODF1 is recruited to the centrosome/connecting piece and via interaction ODF1-SPAG4 the centrosome/connecting piece is linked to the nuclear membrane (Yang *et al.*, in preparation). My data therefore suggest that the interaction between ODF1 (in the capitulum) and SPAG4 (in the nuclear membrane at the implantation fossa) is the molecular equivalent of the HTCA. The interaction of ODF1 and SPAG4 is illustrated in Fig. 4.2. This model is supported by the fact that the presumed *Drosophila* ortholog of SPAG4 is likewise required for the attachment of the basal body to the spermatid nucleus (Kracklauer *et al*., 2010). However, the final proof will be attained by the generation of *Spag4* deficient mice and their observed phenotype. In conclusion, it is suggested that SPAG4-ODF1 interaction defines a novel LINC complex in spermatids that mediates the attachment of the sperm head to the tail.
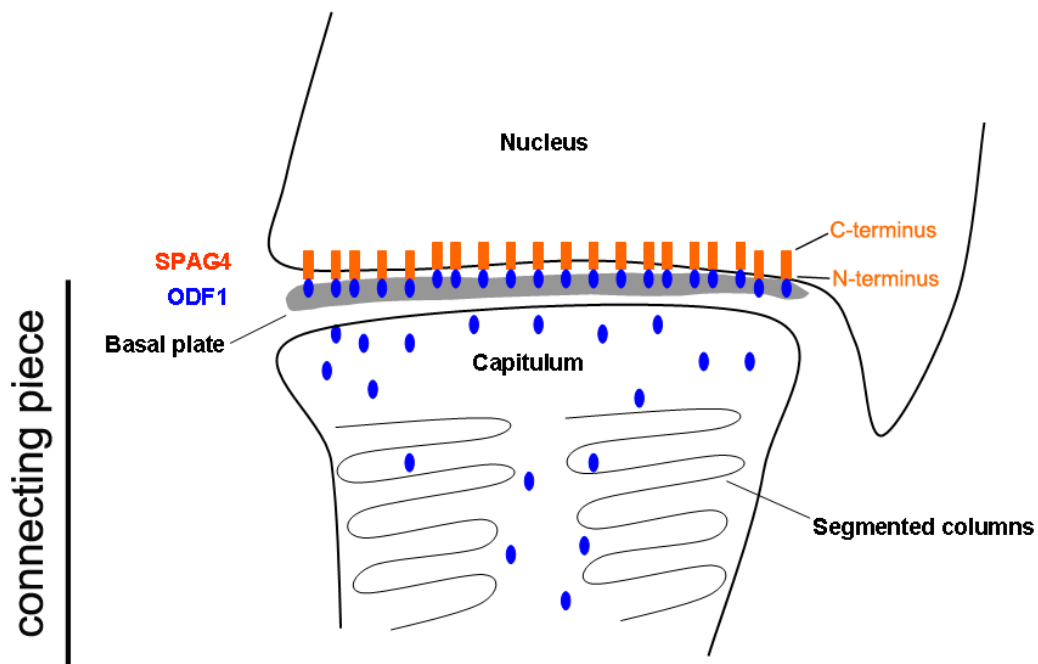

Fig. 4.2: The interaction between ODF1 and SPAG4 defines a novel LINC complex in spermatids that mediates the attachment of the sperm head to the tail. ODF1, that locates at the basal plate of the connecting piece of spermatids, is linked to the nuclear membrane via the N-terminal end of SPAG4.

4.3 ODF2 positively affects degradation of β-catenin due to influencing its destruction complex

Whereas ODF1 is exclusively expressed in spermatids and restricted to the ODF compartment (Morales *et al.*, 1994), ODF2 is not only expressed in male germ cells (Brohmann *et al.*, 1997; Shao *et al.*, 1997; Turner *et al.*, 1997; Hoyer-Fender *et al.*, 1998; Schalles *et al.*, 1998; Petersen *et al.*, 1999) but also localizes generally to the appendages of the mother centriole in somatic cells (Nakagawa *et al.*, 2001; Hoyer-Fender *et al.*, 2003; Donkor *et al.*, 2004). Ishikawa's group reported that the *Odf2* gene is essential for the formation of distal/subdistal appendages and the generation of primary cilia. Using immunofluorescence and ultrathin-section electron microscopy, they showed that in *Odf2$^{-/-}$* F9 cells, distal/subdistal appendages disappear from mother centrioles, and the formation of primary cilia is completely suppressed (Ischikawa *et al.*, 2005). In recent years, it has been found that primary cilia are involved in several signaling pathways essential for growth and differentiation, including the Hedgehog (Hh), Wnt, and PDGF pathways (Eggenschwiler and Anderson, 2007; Berbari *et al.*, 2009). Furthermore, many components (Dvl, Inversin, APC, GSK3β, Axin1, Axin2, and β-catenin) of canonical Wnt pathway have been detected to localize to the centrosome, and some of them take part in regulating centrosomal functions (Kaplan *et al.*, 2004; Louie *et al.*, 2004; Fumoto *et al.*, 2006; Hadjihannas *et al.*, 2006; Huang *et al.*, 2007; Corbit *et al.*, 2008; Bahmanyar *et al.*, 2008; Park *et al.*, 2008; Kim *et al*, 2009; Fumoto *et al.*, 2009). Correspondingly, basal bodies and primary cilia simultaneously regulate both canonical and non-canonical Wnt pathways (Simons *et al.*, 2005; Gerdes *et al.*, 2007; Kishimoto *et al.*, 2008; Corbit *et al.*, 2008; reviewed in Bisgrove and Yost, 2006). Due to the tight association of the canonical Wnt pathway and all three organelles (centrosomes, basal bodies and primary cilia), the influence of centrosomal protein ODF2 on canonical Wnt pathway was investigated.

Former colleagues of our group analysed many possible interactions between ODF2 and components of the canonical Wnt pathway, among them, using pull-down and

co-immunoprecipitation it has been detected that ODF2 interacts with β-catenin. Therefore, I was focusing on the effect of ODF2 on the canonical Wnt key protein, β-catenin. Using reporter gene assays in cultured cells I found that over-expression of ODF2 negatively affects the canonical Wnt signaling. In addition, the result of a quantitative Western blot analysis shows that over-expressed ODF2 could conspicuously abet the degradation of over-expressed β-catenin. In fact, not only the degradation of over-expressed β-catenin was affected, when ODF2 over-expression level is extremely high, the degradation of endogenous β-catenin can also be promoted. Furthermore, the transcription level of a Wnt target gene, *c-Myc*, was reduced by the over-expression of ODF2. In support of these results, a microinjection assay was performed in *Xenopus* embryos. This result shows that over-expressed ODF2 moderately inhibited *Xwnt-8* induced secondary axis formation in *Xenopus* embryos. Altogether, these results suggest that ODF2 inhibits the canonical Wnt pathway possibly due to promoting the degradation of β-catenin.

ODF2 protein domains, which might be responsible for canonical Wnt pathway inhibition, were investigated. The cenexin insertion in the N-terminal region as well as an overall coiled-coil structure in the C-terminal region showed a strong repression on the canonical Wnt pathway. So far, no enzymatic function of ODF2 has been found, and based on its overall coiled-coil domain, ODF2 is most likely a structural protein. This view is consistent with the result of a former colleague of our group, that ODF2 is a self-interacting, microtubule-associated protein (Donkor *et al*., 2004). In my work, I found that ODF2 interacts with Axin1 and Axin2. Axin1 and Axin2 are isoforms of Axin that is a scaffold protein cooperating with GSK3β and APC mediating phosphorylation of β-catenin (Kikuchi, 1999; Chia and Costantini, 2005). Therefore, due to interactions between ODF2 and β-catenin, Axin1 and Axin2 each, it seems that ODF2 takes part of the scaffolding protein complex and stabilizes bound β-catenin, resulting in an increased degradation of β-catenin. Inhibition of GSK3β by lithium increased β-catenin-dependent activation of a reporter vector. However, activation of the reporter in the presence of over-expressed ODF2 was not fully restored by lithium suggesting that a part of β-catenin might be bound to ODF2,

therefore this part of β-catenin could not function as transcriptional activator. In mitosis, β-catenin localizes to centrosomes, and deletion of β-catenin results in monopolar spindles with duplicated but unseparated centrosomes (Kaplan *et al*., 2004). Consistently, stabilization of β-catenin increases the distance between centrosomes in interphase cells and between centrioles in G1/S phase of the cell cycle (Bahmanyar *et al*., 2007). Additionally, Axin colocalizes with ODF2 to centrosome (Fumoto *et al*., 2009). Therefore, the scaffolding protein complex of ODF2 and Axin might be involved in the regulation of centrosome cohesion via promoting the degradation of β-catenin.

A microtubule-associated protein Tau was less phosphorylated in the presence of over-expressed ODF2 and vice versa pointing to a function of ODF2 by stabilization of microtubule. It seems that ODF2 stabilizes the destruction complex by linking scaffolding proteins Axin and β-catenin, further by binding this destruction complex to microtubules. Interference of microtubule polymerization by nocodazole increased β-catenin-dependent activation of a reporter vector as well as taxol-mediated over-stabilization of microtubules. Moreover, activity of the canonical Wnt pathway could be down-regulated by centrosomal and cytoskeletal proteins. This result suggests that the canonical Wnt pathway tightly associates with centrosome and microtubules.

It was reported that hSav1-Mst2-Nek2A complex including two Hippo pathway components, the mammalian sterile 20-like kinase 2 (Mst2) and the scaffold protein Salvador (hSav1), functions in centrosome disjunction (Mardin *et al*., 2010). In my work, I found that ODF2 interacted with TAZ, a major transcriptional co-activator of the Hippo pathway, ubiquitinated by the E3 ligase β-TrCP mediated by phosphorylated β-catenin as its scaffold (Murakami *et al*., 2005; MacDonald *et al*., 2009; *Liu et al*., 2010; *Zhao et al*., 2010; Imajo *et al*., 2012; Azzolin *et al*., 2012). This finding suggests that like the canonical Wnt pathway, more and more components of the Hippo pathway are involved in regulating functions of centrosome.

As a multifunctional protein, besides the roles in canonical Wnt pathway (Wieschaus *et al*., 1984) and the centrosome cycle (Kaplan *et al*., 2004), β-catenin also plays an

important role in cell-cell adhesion (Ozawa *et al*., 1989). When canonical Wnt pathway is inactivated, β-catenin locates at the cytoplasmic side of the membrane as a component of cadherin-based cell-cell connections. Using MCF7, a human breast cancer cell line retaining characteristics particular to the mammary epithelium, I found that cells migrated faster in the presence of over-expressed ODF2. The increasing migration speed of cells was most likely induced by an instable cell-cell connection probably mediated by reduced β-catenin. This view supports the conclusion that over-expressed ODF2 promotes the degradation of β-catenin. However, in two further cell lines, NIH3T3 and MDA-MB-231, the results were not consistent with those in MCF7. In NIH3T3 cells, over-expressed ODF2 has no significant effect on cell migration. In MDA-MB-231 cells, a human breast cancer cell line retaining mesenchymal-like phenotype, cells migrated slower in the presence of over-expressed ODF2. Because mesenchymal cells lose their cell-cell adhesion, reduced migration speed of MDA-MB-231 cells could not be caused by influencing the degradation of β-catenin by over-expressed ODF2. The reason for the effect of ODF2 on cell migration in MDA-MB-231 is still unknown.

Taken all together, besides the structural function of ODF2 in ciliogenesis, ODF2 inhibits the canonical Wnt pathway probably due to promoting the degradation of β-catenin. The increase of degradation of β-catenin caused by ODF2 is possibly mediated by stabilizing β-catenin bound to a scaffolding protein complex including ODF2 and Axin and further by binding this destruction complex to microtubules. In addition, ODF2 is predicted to contain overall CKII and PKC phospho-sites (http://myhits.isb-sib.ch/cgi-bin/motif_scan). CKII positively regulates the canonical Wnt pathway via phosphorylation of β-catenin at its Thr[393], leading to proteasome resistance and increased protein and co-transcriptional activity (Song *et al*., 2003). Therefore, ODF2 might also be an antagonist of β-catenin through competing CKII to promote the degradation of β-catenin.

5. List of figures and tables

6. References

Adham, I. M., Burkhardt, E., Benahmed, M., & Engel, W. (1993). Cloning of a cDNA for a novel insulin-like peptide of the testicular Leydig cells. *Journal of Biological Chemistry*, *268*(35), 26668-26672.

Austin, C. (1951). Observations on the penetration of the sperm into the mammalian egg. *Australian Journal of Biological Sciences*, *4*(4), 581-596.

Azzolin, L., Zanconato, F., Bresolin, S., Forcato, M., Basso, G., Bicciato, S., Cordenonsi, M., & Piccolo, S. (2012). Role of TAZ as mediator of Wnt signaling. *Cell*,*151*(7), 1443-1456.

Baccetti, B., Capitani, S., Collodel, G., Di Cairano, G., Gambera, L., Moretti, E., & Piomboni, P. (2001). Genetic sperm defects and consanguinity. *Human Reproduction*, *16*(7), 1365-1371.

Bahmanyar, S., Kaplan, D. D., DeLuca, J. G., Giddings, T. H., O'Toole, E. T., Winey, M., Salmon, E. D., Casey, P. J., Nelson, W. J., & Barth, A. I. (2008). β-Catenin is a Nek2 substrate involved in centrosome separation. *Genes & development*, *22*(1), 91-105.

Baltz, J. M., Williams, P. O., & Cone, R. A. (1990). Dense fibers protect mammalian sperm against damage. *Biology of reproduction*, *43*(3), 485-491.

Bhullar, B., Zhang, Y., Junco, A., Oko, R., & van der Hoorn, F. A. (2003). Association of kinesin light chain with outer dense fibers in a microtubule-independent fashion. *Journal of Biological Chemistry*, *278*(18), 16159-16168.

Bilić, J., Huang, Y. L., Davidson, G., Zimmermann, T., Cruciat, C. M., Bienz, M., & Niehrs, C. (2007). Wnt induces LRP6 signalosomes and promotes dishevelled-dependent LRP6 phosphorylation. *Science*, *316*(5831), 1619-1622.

Bimboim, H. C., & Doly, J. (1979). A rapid alkaline extraction procedure for screening recombinant plasmid DNA. *Nucleic acids research*, *7*(6), 1513-1523.

Bisgrove, B. W., & Yost, H. J. (2006). The roles of cilia in developmental disorders and disease. *Development*, *133*(21), 4131-4143.

Borg, C. L., Wolski, K. M., Gibbs, G. M., & O'Bryan, M. K. (2010). Phenotyping male infertility in the mouse: how to get the most out of a 'non-performer'. *Human reproduction update*, *16*(2), 205-224.

Brohmann, H., Pinnecke, S., & Hoyer-Fender, S. (1997). Identification and characterization of new cDNAs encoding outer dense fiber proteins of rat sperm. *Journal of Biological Chemistry*, *272*(15), 10327-10332.

Boddy, M. N., Howe, K., Etkin, L. D., Solomon, E., & Freemont, P. S. (1996). PIC 1, a novel ubiquitin-like protein which interacts with the PML component of a multiprotein complex that is disrupted in acute promyelocytic leukaemia. *Oncogene*, *13*(5), 971-982.

Bouchard, M. J., Dong, Y., McDermott, B. M., Lam, D. H., Brown, K. R., Shelanski, M., Bellvé, A. R., & Racaniello, V. R. (2000). Defects in nuclear and cytoskeletal morphology and mitochondrial localization in spermatozoa of mice lacking nectin-2, a component of cell-cell adherens junctions. *Molecular and cellular biology*, *20*(8), 2865-2873.

Brandt, R., & Lee, G. (1993). Functional organization of microtubule-associated protein tau. Identification of regions which affect microtubule growth, nucleation, and bundle formation in vitro. *Journal of Biological Chemistry*, *268*(5), 3414-3419.

Braun, R. E., Behringer, R. R., Peschon, J. J., Brinster, R. L., & Palmiter, R. D. (1989). Genetically haploid spermatids are phenotypically diploid. *Nature*, *337*(6205), 373-376.

Burfeind, P., Belgardt, B., Szpirer, C., & Hoyer-Fender, S. (1993). Structure and chromosomal assignment of a gene encoding the major protein of rat sperm outer dense fibres. *European Journal of Biochemistry*, *216*(2), 497-505.

Burfeind, P., & Hoyer-Fender, S. (1991). Sequence and developmental expression of a mRNA encoding a putative protein of rat sperm outer dense fibers. *Developmental biology*, *148*(1), 195-204.

Burmester, S., & Hoyer-Fender, S. (1996). Transcription and translation of the outer dense fiber gene (Odf1) during spermiogenesis in the rat. A study by in situ analyses and polysome fractionation. *Molecular reproduction and development*, *45*(1), 10-20.

Calvin, H. I., Hwang, F. H. F., & Wohlrab, H. (1975). Localization of zinc in a dense fiber-connecting piece fraction of rat sperm tails analogous chemically to hair keratin. *Biology of reproduction*, *13*(2), 228-239.

Chang, M. C. (1951). Fertilizing capacity of spermatozoa deposited into the fallopian tubes. *Nature*, *168*(168), 697-698

Chemes, H. E., Puigdomenech, E. T., Carizza, C., Olmedo, S. B., Zanchetti, F., & Hermes, R. (1999). Acephalic spermatozoa and abnormal development of the head–neck attachment: a human syndrome of genetic origin. *Human Reproduction*, *14*(7), 1811-1818.

Chemes, L. B., Glavina, J., Alonso, L. G., Marino-Buslje, C., de Prat-Gay, G., & Sánchez, I. E. (2012). Sequence evolution of the intrinsically disordered and globular domains of a model viral oncoprotein. *PloS one*, *7*(10), e47661.

Chia, I. V., & Costantini, F. (2005). Mouse axin and axin2/conductin proteins are functionally equivalent in vivo. *Molecular and cellular biology*, *25*(11), 4371-4376.

Corbit, K. C., Shyer, A. E., Dowdle, W. E., Gaulden, J., Singla, V., & Reiter, J. F. (2008). Kif3a constrains β-catenin-dependent Wnt signalling through dual ciliary and non-ciliary mechanisms. *Nature Cell Biology*, *10*(1), 70-76.

Cowin, P., Kapprell, H. P., Franke, W. W., Tamkun, J., & Hynes, R. O. (1986). Plakoglobin: a protein common to different kinds of intercellular adhering junctions. *Cell*, *46*(7), 1063-1073.

Cui, W. (2010). Mother or nothing: the agony of infertility. *Bull.World Health Organ.* *88*(12), 881-882.

Deming, S. L., Nass, S. J., Dickson, R. B., & Trock, B. J. (2000). C-myc amplification in breast cancer: a meta-analysis of its occurrence and prognostic relevance. *British journal of cancer*, *83*(12), 1688.

Donkor, F. F., Mönnich, M., Czirr, E., Hollemann, T., & Hoyer-Fender, S. (2004). Outer dense fibre protein 2 (ODF2) is a self-interacting centrosomal protein with affinity for microtubules. *Journal of cell science*, *117*(20), 4643-4651.

Drewes, G., Ebneth, A., & Mandelkow, E. M. (1998). MAPs, MARKs and microtubule dynamics. *Trends in biochemical sciences*, *23*(8), 307-311.

Fawcett, D. W., Anderson, W. A., & Phillips, D. M. (1971). Morphogenetic factors influencing the shape of the sperm head. *Developmental biology*,*26*(2), 220-251.

Fawcett, D. W., & McNutt, N. S. (1969). The ultrastructure of the cat myocardium I. Ventricular papillary muscle. *The Journal of cell biology*,*42*(1), 1-45.

Fawcett, D. W., & Phillips, D. M. (1969). Observations on the release of spermatozoa and on changes in the head during passage through the epididymis. *J Reprod Fertil Suppl*, *6*, 405-418.

Fawcett, D. W. (1975). The mammalian spermatozoon. *Developmental biology*, *44*(2), 394-436.

Fawcett, D. W. (1958). The structure of the mammalian spermatozoon.*International Review of Cytology*, *7*, 195-234.

Feinberg, A. P., & Vogelstein, B. (1983). A technique for radiolabeling DNA restriction endonuclease fragments to high specific activity. *Analytical biochemistry*, *132*(1), 6-13.

Fitzgerald, C. J., Oko, R. J., & van der Hoorn, F. A. (2006). Rat Spag5 associates in somatic cells with endoplasmic reticulum and microtubules but in spermatozoa with outer dense fibers. *Molecular reproduction and development*, *73*(1), 92-100.

Fontaine, J. M., Rest, J. S., Welsh, M. J., & Benndorf, R. (2003). The sperm outer dense fiber protein is the 10th member of the superfamily of mammalian small stress proteins. *Cell stress & chaperones*, *8*(1), 62.

Friend, D. S., & Fawcett, D. W. (1974). Membrane differentiations in freeze-fractured mammalian sperm. *The Journal of cell biology*, *63*(2), 641-664.

Fumoto, K., Hoogenraad, C. C., & Kikuchi, A. (2006). GSK-3β-regulated interaction of BICD with dynein is involved in microtubule anchorage at centrosome. *The EMBO journal*, *25*(24), 5670-5682.

Fumoto, K., Kadono, M., Izumi, N., & Kikuchi, A. (2009). Axin localizes to the centrosome and is involved in microtubule nucleation. *EMBO reports*, *10*(6), 606-613.

Gastmann, O., Burfeind, P., Güunther, E., Hameister, H., Szpirer, C., & Hoyer-Fender, S. (1993). Sequence, expression, and chromosomal assignment of a human sperm outer dense fiber gene. *Molecular reproduction and development*, *36*(4), 407-418.

Gerdes, J. M., Liu, Y., Zaghloul, N. A., Leitch, C. C., Lawson, S. S., Kato, M., Beachy, P. A., Beales, P., DeMartino, G. N., Fischer, S., Badano, J. L., & Katsanis, N. (2007). Disruption of the basal body compromises proteasomal function and perturbs intracellular Wnt response. *Nature genetics*, *39*(11), 1350-1360.

Goto, M., O'Brien, D. A., & Eddy, E. M. (2010). Speriolin is a novel human and mouse sperm centrosome protein. *Human reproduction*, *25*(8), 1884-1894.

Hadjihannas, M. V., Brückner, M., Jerchow, B., Birchmeier, W., Dietmaier, W., & Behrens, J. (2006). Aberrant Wnt/β-catenin signaling can induce chromosomal instability in colon cancer. *Proceedings of the National Academy of Sciences*, *103*(28), 10747-10752.

Haidl, G., Becker, A., & Henkel, R. (1991). Poor development of outer dense fibres as a major cause of tail abnormalities in the spermatozoa of asthenoteratozoospermic men. *Human Reproduction*, *6*(10), 1431-1438.

Haimo, L. T., & Rosenbaum, J. L. (1981). Cilia, flagella, and microtubules. *The journal of cell biology*, *91*(3), 125s-130s.

Halder, G., & Johnson, R. L. (2011). Hippo signaling: growth control and beyond. *Development*, *138*(1), 9-22.

Hanahan, D. (1983). Studies on transformation of *Escherichia coli* with plasmids. *Journal of molecular biology*, *166*(4), 557-580.

Hishiya, A., & Takayama, S. (2008). Molecular chaperones as regulators of cell death. *Oncogene*, *27*(50), 6489-6506.

Hofferbert, S., Burfeind, P., Hoyer-Fender, S., Lange, R., Haldl, G., & Engel, W. (1993). A homozygous deletion of 27 basepairs in the coding region of the human outer dense fiber protein gene does not result in a pathologic phenotype. *Human molecular genetics*, *2*(12), 2167-2170.

Hong, W., & Guan, K. L. (2012, September). The YAP and TAZ transcription co-activators: key downstream effectors of the mammalian Hippo pathway. In*Seminars in cell & developmental biology* (Vol. 23, No. 7, pp. 785-793). Academic Press.

Hoyer-Fender, S., Burfeind, P., & Hameister, H. (1995). Sequence of mouse Odf1 cDNA and its chromosomal localization: extension of the linkage group between human chromosome 8 and mouse chromosome 15. *Cytogenetic and Genome Research*, *70*(3-4), 200-204.

Hoyer-Fender, S., Petersen, C., Brohmann, H., Rhee, K., & Wolgemuth, D. J. (1998). Mouse Odf2 cDNAs consist of evolutionary conserved as well as highly variable sequences and encode outer dense fiber proteins of the sperm tail. *Molecular reproduction and development*, *51*, 167-175.

Huang, P., Senga, T., & Hamaguchi, M. (2007). A novel role of phospho-β-catenin in microtubule regrowth at centrosome. *Oncogene*, *26*(30), 4357-4371.

Hüber, D., & Hoyer-Fender, S. (2007). Alternative splicing of exon 3b gives rise to ODF2 and Cenexin. *Cytogenetic and genome research*, *119*(1-2), 68-73.

Imajo, M., Miyatake, K., Iimura, A., Miyamoto, A., & Nishida, E. (2012). A molecular mechanism that links Hippo signalling to the inhibition of Wnt/β‐catenin signalling. *The EMBO journal*, *31*(5), 1109-1122.

Irons, M. J., & Clermont, Y. (1982). Formation of the outer dense fibers during spermiogenesis in the rat. *The Anatomical Record*, *202*(4), 463-471.

Irons, M. J., & Clermont, Y. (1982). Kinetics of fibrous sheath formation in the rat spermatid. *American Journal of Anatomy*, *165*(2), 121-130.

Ishikawa, H., Kubo, A., Tsukita, S., & Tsukita, S. (2005). Odf2-deficient mother centrioles lack distal/subdistal appendages and the ability to generate primary cilia. *Nature cell biology, 7*(5), 517-524.

Jho, E. H., Lomvardas, S., & Costantini, F. (1999). A GSK3β phosphorylation site in axin modulates interaction with β-catenin and Tcf-mediated gene expression. *Biochemical and biophysical research communications*, *266*(1), 28-35.

Jones, R. C. (1999). To store or mature spermatozoa? The primary role of the epididymis. *International journal of andrology*, *22*(2), 57-66.

Joyner, A. L. (1993). Gene targeting: a practical approach. p 230. IRL Press, Oxford, United Kingdom.

Jürgens, G., Wieschaus, E., Nüsslein-Volhard, C., & Kluding, H. (1984). Mutations affecting the pattern of the larval cuticle inDrosophila melanogaster. *Wilhelm Roux's archives of developmental biology*, *193*(5), 283-295.

Kamal, A., Mansour, R., Fahmy, I., Serour, G., Rhodes, C., & Aboulghar, M. (1999). Easily decapitated spermatozoa defect: a possible cause of unexplained infertility. *Human Reproduction*, *14*(11), 2791-2795.

Kamitani, T., Kito, K., Nguyen, H. P., & Yeh, E. T. (1997). Characterization of NEDD8, a developmentally down-regulated ubiquitin-like protein. *Journal of Biological Chemistry*, *272*(45), 28557-28562.

Kaplan, D. D., Meigs, T. E., Kelly, P., & Casey, P. J. (2004). Identification of a role for β-catenin in the establishment of a bipolar mitotic spindle. *Journal of biological chemistry*, *279*(12), 10829-10832.

Kemler, R. (1993). From cadherins to catenins: cytoplasmic protein interactions and regulation of cell adhesion. *Trends in Genetics*, *9*(9), 317-321.

Kerr, J. B., & De Kretser, D. M. (1974). The role of the Sertoli cell in phagocytosis of the residual bodies of spermatids. *Journal of reproduction and fertility*, *36*(2), 439-440.

Kierszenbaum, A. L., & Tres, L. L. (2002). Bypassing natural sperm selection during fertilization: the *azh* mutant offspring experience and the alternative of

spermiogenesis in vitro. *Molecular and cellular endocrinology*, *187*(1), 133-138.

Kikuchi, A. (1999). Roles of Axin in the Wnt signalling pathway. *Cellular signalling*, *11*(11), 777-788.

Kim, S. M., Choi, E. J., Song, K. J., Kim, S., Seo, E., Jho, E. H., & Kee, S. H. (2009). Axin localizes to mitotic spindles and centrosomes in mitotic cells. *Experimental cell research*, *315*(6), 943-954.

King, S. M. (2000). The dynein microtubule motor. *Biochimica et Biophysica Acta (BBA)-Molecular Cell Research*, *1496*(1), 60-75.

Kishimoto, N., Cao, Y., Park, A., & Sun, Z. (2008). Cystic Kidney Gene *seahorse* Regulates Cilia-Mediated Processes and Wnt Pathways.*Developmental cell*, *14*(6), 954-961.

Klein, P. S., & Melton, D. A. (1996). A molecular mechanism for the effect of lithium on development. *Proceedings of the National Academy of Sciences*,*93*(16), 8455-8459.

Kobayashi, T., & Dynlacht, B. D. (2011). Regulating the transition from centriole to basal body. *The Journal of cell biology*, *193*(3), 435-444.

Kohn, A. D., & Moon, R. T. (2005). Wnt and calcium signaling: β-catenin-independent pathways. *Cell calcium*, *38*(3), 439-446.

Kracklauer, M. P., Wiora, H. M., Deery, W. J., Chen, X., Bolival, B., Romanowicz, D., Simonette, R. A., Fuller, M. T., Fischer, J. A., & Beckingham, K. M. (2010). The Drosophila SUN protein Spag4 cooperates with the coiled-coil protein Yuri Gagarin to maintain association of the basal body and spermatid nucleus. *Journal of cell science*,*123*(16), 2763-2772.

Lanneau, D., Brunet, M., Frisan, E., Solary, E., Fontenay, M., & Garrido, C. (2008). Heat shock proteins: essential proteins for apoptosis regulation.*Journal of cellular and molecular medicine*, *12*(3), 743-761.

Lapenta, V., Chiurazzi, P., van der Spek, P., Pizzuti, A., Hanaoka, F., & Brahe, C. (1997). *SMT3A*, a Human Homologue of the *S. cerevisiae SMT3* Gene,

Maps to Chromosome 21qter and Defines a Novel Gene Family. *Genomics*, *40*(2), 362-366.

Lawrence, P. A., Struhl, G., & Casal, J. (2007). Planar cell polarity: one or two pathways? *Nature Reviews Genetics*, *8*(7), 555-563.

Lim, C. C., Lewis, S. E. M., Kennedy, M., Donnelly, E. T., & Thompson, W. (1998). Human sperm morphology and in vitro fertilization: sperm tail defects are prognostic for fertilization failure. *Andrologia*, *30*(1), 43-47.

Lindemann, C. B. (1996). Functional significance of the outer dense fibers of mammalian sperm examined by computer simulations with the geometric clutch model. *Cell motility and the cytoskeleton*, *34*(4), 258-270.

Liu, C. Y., Zha, Z. Y., Zhou, X., Zhang, H., Huang, W., Zhao, D., Xiong, Y., Lei, Q. Y., & Guan, K. L. (2010). The hippo tumor pathway promotes TAZ degradation by phosphorylating a phosphodegron and recruiting the SCFβ-TrCP E3 ligase.*Journal of biological chemistry*, *285*(48), 37159-37169.

Louie, R. K., Bahmanyar, S., Siemers, K. A., Votin, V., Chang, P., Stearns, T., Nelson, W. J., & Barth, A. I. (2004). Adenomatous polyposis coli and EB1 localize in close proximity of the mother centriole and EB1 is a functional component of centrosomes. *Journal of cell science*, *117*(7), 1117-1128.

Lupas, A., Van Dyke, M., & Stock, J. (1991). Predicting coiled coils from protein sequences. *Science*, *252*(5009), 1162-1164.

MacDonald, B. T., Tamai, K., & He, X. (2009). Wnt/β-catenin signaling: components, mechanisms, and diseases. *Developmental cell*, *17*(1), 9-26.

Mahajan, R., Delphin, C., Guan, T., Gerace, L., & Melchior, F. (1997). A small ubiquitin-related polypeptide involved in targeting RanGAP1 to nuclear pore complex protein RanBP2. *Cell*, *88*(1), 97-107.

Mandelkow, E., & Mandelkow, E. M. (1995). Microtubules and microtubule-associated proteins. *Current opinion in cell biology*, *7*(1), 72-81.

Marmor, D., & Grob-Menendez, F. (1991). Male infertility due to asthenozoospermia and flagellar anomaly: detection in routine semen analysis. *International journal of andrology*, *14*(2), 108-116.

Mardin, B. R., Lange, C., Baxter, J. E., Hardy, T., Scholz, S. R., Fry, A. M., & Schiebel, E. (2010). Components of the Hippo pathway cooperate with Nek2 kinase to regulate centrosome disjunction. *Nature cell biology*, *12*(12), 1166-1176.

Matunis, M. J., Coutavas, E., & Blobel, G. (1996). A novel ubiquitin-like modification modulates the partitioning of the Ran-GTPase-activating protein RanGAP1 between the cytosol and the nuclear pore complex. *The Journal of cell biology*, *135*(6), 1457-1470.

Matzuk, M. M., & Lamb, D. J. (2008). The biology of infertility: research advances and clinical challenges. *Nature medicine*, *14*(11), 1197-1213.

Miki, K., Qu, W., Goulding, E. H., Willis, W. D., Bunch, D. O., Strader, L. F., Perreault, S. D., Eddy E. M., & O'Brien, D. A. (2004). Glyceraldehyde 3-phosphate dehydrogenase-S, a sperm-specific glycolytic enzyme, is required for sperm motility and male fertility. *Proceedings of the National Academy of Sciences of the United States of America*, *101*(47), 16501-16506.

Morales, C. R., Oko, R., & Clermont, Y. (1994). Molecular cloning and developmental expression of an mRNA encoding the 27 kDa outer dense fiber protein of rat spermatozoa. *Molecular reproduction and development*, *37*(2), 229-240.

Mortimer, S. T. (1997). A critical review of the physiological importance and analysis of sperm movement in mammals. *Human Reproduction Update*, *3*(5), 403-439.

McCREA, P. D., Turck, C. W., & Gumbiner, B. (1991). A homolog of the armadillo protein in Drosophila (plakoglobin) associated with E-cadherin. *Science, 254*(5036), 1359-1361.

Murakami, M., Nakagawa, M., Olson, E. N., & Nakagawa, O. (2005). A WW domain protein TAZ is a critical coactivator for TBX5, a transcription factor implicated in Holt–Oram syndrome. *Proceedings of the National Academy of Sciences of the United States of America*, *102*(50), 18034-18039.

Nebel, B. R., Amarose, A. P., & Hackett, E. M. (1961). Calendar of gametogenic development in the prepuberal male mouse. *Science,134*(3482), 832-833.

Nishida, T., Tanaka, H., & Yasuda, H. (2000). A novel mammalian Smt3‐specific isopeptidase 1 (SMT3IP1) localized in the nucleolus at interphase. *European Journal of Biochemistry*, *267*(21), 6423-6427.

Oko, R. (1988). Comparative analysis of proteins from the fibrous sheath and outer dense fibers of rat spermatozoa. *Biology of reproduction*, *39*(1), 169-182.

Otani, H., Tanaka, O., Kasai, K. I., & Yoshioka, T. (1988). Development of mitochondrial helical sheath in the middle piece of the mouse spermatid tail: regular dispositions and synchronized changes. *The Anatomical Record,222*(1), 26-33.

Oulad-Abdelghani, M., Bouillet, P., Décimo, D., Gansmuller, A., Heyberger, S., Dollé, P., Bronner, S., Lutz, Y., & Chambon, P. (1996). Characterization of a premeiotic germ cell-specific cytoplasmic protein encoded by Stra8, a novel retinoic acid-responsive gene. *The Journal of cell biology*, *135*(2), 469-477.

Ozawa, M., Baribault, H., & Kemler, R. (1989). The cytoplasmic domain of the cell adhesion molecule uvomorulin associates with three independent proteins structurally related in different species. *The EMBO Journal*, *8*(6), 1711.

Panda, D., Goode, B. L., Feinstein, S. C., & Wilson, L. (1995). Kinetic stabilization of microtubule dynamics at steady state by tau and microtubule-binding domains of tau. *Biochemistry*, *34*(35), 11117-11127.

Park, T. J., Mitchell, B. J., Abitua, P. B., Kintner, C., & Wallingford, J. B. (2008). Dishevelled controls apical docking and planar polarization of basal bodies in ciliated epithelial cells. *Nature genetics*, *40*(7), 871-879.

Pedersen, H. (1972). The postacrosomal region of the spermatozoa of man and *Macaca arctoides*. *Journal of ultrastructure research*, *40*(3), 366-377.

Peifer, M., Berg, S., & Reynolds, A. B. (1994). A repeating amino acid motif shared by proteins with diverse cellular roles. *Cell*, *76*(5), 789-791.

Petersen, C., Füzesi, L., & Hoyer-Fender, S. (1999). Outer dense fibre proteins from human sperm tail: molecular cloning and expression analyses of two

cDNA transcripts encoding proteins of~ 70 kDa. *Molecular human reproduction*, *5*(7), 627-635.

Porter, M. E., & Sale, W. S. (2000). The 9+ 2 axoneme anchors multiple inner arm dyneins and a network of kinases and phosphatases that control motility. *The Journal of cell biology*, *151*(5), F37-F42.

Ramos, A., & Camargo, F. D. (2012). The Hippo signaling pathway and stem cell biology. *Trends in cell biology*, *22*(7), 339-346.

Kierszenbaum, A. L., Rivkin, E., & Tres, L. L. (2008). Expression of Fer testis (FerT) tyrosine kinase transcript variants and distribution sites of FerT during the development of the acrosome-acroplaxome-manchette complex in rat spermatids. *Developmental Dynamics*, *237*(12), 3882-3891.

Rosales, J. L., Sarker, K., Ho, N., Broniewska, M., Wong, P., Cheng, M., van der Hoorn, F. A. & Lee, K. Y. (2008). ODF1 phosphorylation by Cdk5/p35 enhances ODF1-OIP1 interaction. *Cellular Physiology and Biochemistry*, *20*(5), 311-318.

Russell, L., & Clermont, Y. (1976). Anchoring device between Sertoli cells and late spermatids in rat seminiferous tubules. *The Anatomical Record*, *185*(3), 259-277.

Russell, L. D., Ettlin, R. A., Hikim, A. P. S., & Clegg, E. D. (1993). Histological and histopathological evaluation of the testis. *International journal of andrology*, *16*(1), 83-83.

Russell, L. D., & Malone, J. P. (1980). A study of Sertoli-spermatid tubulobulbar complexes in selected mammals. *Tissue and Cell*, *12*(2), 263-285.

Russell, R. R. (1979). Glucan-binding Proteins of Streptococcus mutatis Serotype c. *Journal of general microbiology*, *112*(1), 197-201.

Russell, S. D. (1984). Ultrastructure of the sperm of Plumbago zeylanica. *Planta*, *162*(5), 385-391.

Salahshor, S., & Woodgett, J. R. (2005). The links between axin and carcinogenesis. *Journal of clinical pathology*, *58*(3), 225-236.

Schalles, U., Shao, X., van der Hoorn, F. A., & Oko, R. (1998). Developmental expression of the 84-kDa ODF sperm protein: localization to both the cortex and medulla of outer dense fibers and to the connecting piece. *Developmental biology*, *199*(2), 250-260.

Schwarz-Romond, T., Metcalfe, C., & Bienz, M. (2007). Dynamic recruitment of axin by Dishevelled protein assemblies. *Journal of cell science*, *120*(14), 2402-2412.

Seifert, J. R., & Mlodzik, M. (2007). Frizzled/PCP signalling: a conserved mechanism regulating cell polarity and directed motility. *Nature Reviews Genetics*, *8*(2), 126-138.

Shao, X., Tarnasky, H. A., Lee, J. P., Oko, R., & van der Hoorn, F. A. (1999). Spag4, a novel sperm protein, binds outer dense-fiber protein Odf1 and localizes to microtubules of manchette and axoneme. Developmental biology, 211(1), 109-123.

Shao, X., Tarnasky, H. A., Schalles, U., Oko, R., & van der Hoorn, F. A. (1997). Interactional Cloning of the 84-kDa Major Outer Dense Fiber Protein Odf84 leucine zippers mediate associations of Odf84 and Odf27. Journal of Biological Chemistry, 272(10), 6105-6113.

Shao, X., & van der Hoorn, F. A. (1996). Self-interaction of the major 27-kilodalton outer dense fiber protein is in part mediated by a leucine zipper domain in the rat. Biology of reproduction, 55(6), 1343-1350.

Shen, Z., Pardington-Purtymun, P. E., Comeaux, J. C., Moyzis, R. K., & Chen, D. J. (1996). UBL1, a human ubiquitin-like protein associating with human RAD51/RAD52 proteins. *Genomics*, *36*(2), 271-279.

Simons, M., Gloy, J., Ganner, A., Bullerkotte, A., Bashkurov, M., Krönig, C., Schermer, B., Benzing, T., Cabello, O. A., Jenny, A., Mlodzik, M., Polok, B., Driever, W., Obara, T., & Walz, G. (2005). Inversin, the gene product mutated in nephronophthisis type II, functions as a molecular switch between Wnt signaling pathways. *Nature genetics*, *37*(5), 537-543.

Slusarski, D. C., & Pelegri, F. (2007). Calcium signaling in vertebrate embryonic patterning and morphogenesis. *Developmental biology*, *307*(1), 1-13.

Smith, W. C., & Harland, R. M. (1992). Expression cloning of noggin, a new dorsalizing factor localized to the Spemann organizer in Xenopus embryos. *Cell*, *70*(5), 829-840.

Sokol, S., Christian, J. L., Moon, R. T., & Melton, D. A. (1991). Injected Wnt RNA induces a complete body axis in Xenopus embryos. *Cell*, *67*(4), 741-752.

Song, D. H., Dominguez, I., Mizuno, J., Kaut, M., Mohr, S. C., & Seldin, D. C. (2003). CK2 phosphorylation of the armadillo repeat region of β-catenin potentiates Wnt signaling. *Journal of Biological Chemistry*, *278*(26), 24018-24025.

Soung, N. K., Kang, Y. H., Kim, K., Kamijo, K., Yoon, H., Seong, Y. S., Kuo, Y. L., Miki, T., Kim, S. R., Kuriyama, R., Giam, C. Z., Ahn, C. H., & Lee, K. S. (2006). Requirement of hCenexin for proper mitotic functions of polo-like kinase 1 at the centrosomes. *Molecular and cellular biology*, *26*(22), 8316-8335.

Southern, E. M. (1975). Detection of specific sequences among DNA fragments separated by gel electrophoresis. *Journal of molecular biology*, *98*(3), 503-517.

Sprando, R. L., & Russell, L. D. (1987). A comparative study of Sertoli cell ectoplasmic specializations in selected non-mammalian vertebrates. *Tissue and Cell*, *19*(4), 479-493.

Stackpole, C. W., & Devorkin, D. (1974). Membrane organization in mouse spermatozoa revealed by freeze-etching. *Journal of ultrastructure research*, *49*(2), 167-187.

Sun, Y., & MacRae, T. H. (2005). Small heat shock proteins: molecular structure and chaperone function. *Cellular and Molecular Life Sciences CMLS*, *62*(21), 2460-2476.

Sun, Y., & MacRae, T. H. (2005). The small heat shock proteins and their role in human disease. *Febs Journal*, *272*(11), 2613-2627.

Suzuki-Toyota, F., Ito, C., Toyama, Y., Maekawa, M., Yao, R., Noda, T., Iida, H., & Toshimori, K. (2007). Factors maintaining normal sperm tail structure during epididymal maturation studied in Gopc$^{-/-}$ mice. *Biology of reproduction*, *77*(1), 71-82.

Takeichi, M. (1995). Morphogenetic roles of classic cadherins. *Current opinion in cell biology*, *7*(5), 619-627.

Tanaka, H., Iguchi, N., Isotani, A., Kitamura, K., Toyama, Y., Matsuoka, Y., Onishi, M., Masai, K., Maekawa, M., Toshimori, K., Okabe, M., & Nishimune, Y. (2005). HANP1/H1T2, a novel histone H1-like protein involved in nuclear formation and sperm fertility. *Molecular and cellular biology*, *25*(16), 7107-7119.

Tang, X. M., Lalli, M. F., & Clermont, Y. (1982). A cytochemical study of the Golgi apparatus of the spermatid during spermiogenesis in the rat. *American Journal of Anatomy*, *163*(4), 283-294.

Thaler, C. D., & Cardullo, R. A. (1995). Biochemical characterization of a glycosylphosphatidylinositol-linked hyaluronidase on mouse sperm.*Biochemistry*, *34*(24), 7788-7795.

Tolwinski, N. S., & Wieschaus, E. (2004). Rethinking WNT signaling.*TRENDS in Genetics*, *20*(4), 177-181.

Toshimori, K. (1998). Maturation of mammalian spermatozoa: modifications of the acrosome and plasma membrane leading to fertilization. *Cell and tissue research*, *293*(2), 177-187.

Turner, K. J., Sharpe, R. M., Gaughan, J., Millar, M. R., Foster, P. M., & Saunders, P. T. (1997). Expression cloning of a rat testicular transcript abundant in germ cells, which contains two leucine zipper motifs. *Biology of reproduction*, *57*(5), 1223-1232.

Tybulewicz, V. L., Crawford, C. E., Jackson, P. K., Bronson, R. T., & Mulligan, R. C. (1991). Neonatal lethality and lymphopenia in mice with a homozygous disruption of the c-*abl* proto-oncogene. *Cell*, *65*(7), 1153-1163.

Van der Hoorn, F. A., Tarnasky, H. A., & Nordeen, S. K. (1990). A new rat gene RT7 is specifically expressed during spermatogenesis. *Developmental biology*, *142*(1), 147-154.

Vera, J. C., Brito, M., Zuvic, T., & Burzio, L. O. (1984). Polypeptide composition of rat sperm outer dense fibers. A simple procedure to isolate the fibrillar complex. *Journal of Biological Chemistry*,*259*(9), 5970-5977.

Wantae, K., Minseong, K., & Eek-hoon, J. (2013). Wnt/beta-catenin signalling: from plasma membrane to nucleus. *Biochemical Journal*, *450*(1), 9-21.

Wijnhoven, B. P. L., Dinjens, W. N. M., & Pignatelli, M. (2000). E-cadherin-catenin cell-cell adhesion complex and human cancer. *British Journal of Surgery*, *87*(8), 992-1005.

Wolosewick, J. J., & Bryan, J. H. (1977). Ultrastructural characterization of the manchette microtubules in the seminiferous epithelium of the mouse.*American Journal of Anatomy*, *150*(2), 301-331.

Yamamoto, H., Kishida, S., Kishida, M., Ikeda, S., Takada, S., & Kikuchi, A. (1999). Phosphorylation of axin, a Wnt signal negative regulator, by glycogen synthase kinase-3β regulates its stability. *Journal of Biological Chemistry*, *274*(16), 10681-10684.

Yang, K., Meinhardt, A., Zhang, B., Grzmil, P., Adham, I. M., & Hoyer-Fender, S. (2012). The small heat shock protein ODF1/HSPB10 is essential for tight linkage of sperm head to tail and male fertility in mice. *Molecular and cellular biology*, *32*(1), 216-225.

Zamboni, L., & Stefanini, M. (1971). The fine structure of the neck of mammalian spermatozoa. *The Anatomical Record*, *169*(2), 155-172.

Zarsky, H. A., Cheng, M., & van der Hoorn, F. A. (2003). Novel RING finger protein OIP1 binds to conserved amino acid repeats in sperm tail protein ODF1. *Biology of reproduction*, *68*(2), 543-552.

Zeng, L., Fagotto, F., Zhang, T., Hsu, W., Vasicek, T. J., Perry Iii, W. L., Lee, J. J., Tilghman, S. M., Gumbiner, B. M & Costantini, F. (1997). The Mouse

Fused Locus Encodes Axin, an Inhibitor of the Wnt Signaling Pathway That Regulates Embryonic Axis Formation. *Cell*, *90*(1), 181-192.

Zhao, B., Li, L., Tumaneng, K., Wang, C. Y., & Guan, K. L. (2010). A coordinated phosphorylation by Lats and CK1 regulates YAP stability through SCFβ-TRCP. *Genes & development*, *24*(1), 72-85.

7. Abbreviations

aa	Amino acid(s)
Ab (Abs)	Antibody (antibodies)
ALH	Amplitude of the lateral head displacement
ANC-1	Anchorage 1 protein
APC	Adenomatous polyposis coli
APMBT	Phenyl-benzothiazole
APS	Ammonium persulfate
ATP	Adenosine triphosphate
BCF	Beat cross frequency
bp	base pair(s)
BSA	Bovine serum albumin
Cdk5	Cyclin-dependent kinase 5
cDNA	complementary DNA
CK1	Casein kinase 1
CK II	Casein kinase II
Co-IP	Co-immunoprecipitation
C-terminal	Carboxyl-terminal
C-X-P	Cysteine-X-proline
DAPI	4`,6`-diamidino-2-phenylindole
dATP	Deoxyadenosine triphosphate
deg. oocytes	degenerated oocytes
DMEM	Dulbecco's Modified Eagle's Medium
DMSO	Dimethyl sulfoxide
DNA	Deoxyribonucleic acid
Dnase	Deoxyribonuclease
dpp	days *post partum*
DTT	Dithiothreitol
Dvl	Dishevelled
ECFP	enhanced cyan fluorescent protein
ECL	enhanced chemiluminescence
E. coli	*Escherichia coli*
EDTA	Ethylenediaminetetraacetic acid
EM	Electron micrographs
ER	Endoplasmic reticulum
ES	Embryonic stem
et al.	et alii (and others)
FBS	Fetal bovine serum
Fig	Figure
fl	full length
FS	Fibrous sheath

Fz	Frizzled
g	gram(s)
x g (or RCF)	relative centrifugal force
G418	Geneticin
GAPDH	Glyceraldehyde-3-Phosphate Dehydrogenase
GFP	Green fluorescent protein
Gopc	Golgi-associated PDZ- and coiled-coil motif-containing protein
GSK3β	Glycogen synthase kinase 3β
h	hour(s)
HA	Human influenza hemagglutinin
HANP1/H1T2	Human Testis-specific H1 histone
HCG	Human chorionic gonadotrophin
HEK293	Human embryonic kidney cell line
HEPES	Hydroxyethyl piperazineethanesulfonic acid
Hh	Hedgehog
HPRT	Hypoxanthine phosphoribosyltransferase
HRP	Horseradish peroxidase
hSav1	Salvador
HSPB10	Heat shock protein B10
HTCA	Head-to-tail coupling apparatus
Hz	Hertz
IFT	Intraflagellar transport
IgG	Immunoglobulin G
Inc.	Incorporated
INM	Inner nuclear membrane
IVF	*in vitro* fertilization
K	Kinase
KASH	Klarsicht/ANC-1/Syne-1 homology
kb	kilobase
kDa	kilodalton
KLC3	Kinesin light chain 3
ko	*Knock out*
l	liter(s)
LB	Lysogeny broth
LEF	lymphoid enhancer factor
LiAc	Lithium acetate
LINC	Linker of nucleoskeleton and cytoskeleton
LRP6	Low density lipoprotein receptor-related protein 6
LSM	Confocal laser scanning microscopy
M	molar
mAb	mouse antibody
MBP	maltose binding protein
MBS	Modified Barth's Saline

MCF7	Michigan Cancer Foundation-7
mg	Milligram(s)
min	Minute(s)
MIS	Müllerian inhibiting substance
ml	Millimeter(s)
mM	Millimolar(s)
MSP-300	Muscle-specific protein 300
Mst2	Mammalian sterile 20-like kinase 2
MTOC	Microtubule-organizing center
NEAA	Nonessential amino acids
Nek2A	Never in mitosis A-related kinase 2
ng	nanogram(s)
nM	nanomolar
nm	nanometer(s)
N-terminal	Amino-terminal
ODF	Outer dense fiber
OF	Fopflash
OIP1	ODF1-interacting protein
ONM	Outer nuclear membrane
OT	Topflash
p-	phospho-
p35	35kDa protein
PBS	Phosphate-buffered saline
PCM	Pericentriolar material
PCP pathway	Planar cell polarity pathway
PCR	Polymerase chain reaction
PDGF	Platelet-derived growth factor
PFA	Paraformaldehyde
pg	picogram(s)
pH	Potentium hydrogenii
PK	Protein kinase
PKC	Protein kinase C
PL-FITC	fluorescein isothiocyanate-labeled peanut lectin
pmol	picomol(s)
PMSF	Phenylmethanesulfonyl fluoride
PMSG	Pregnant mare serum gonadotrophin
rpm	revolutions per minute
RPMI	Roswell Park Memorial Institute
RT-PCR	reverse transcription-PCR
SD	Standard Deviation
SDS-PAGE	Sodium dodecyl sulfate polyacrylamide gel electrophoresis
sec	second(s)
SFRP	Secreted Fz-related protein

sh	small hairpin or short hairpin
SH3	SRC homology 3 domain
sHSPs	small heat shock proteins
siRNA	small interfering RNA
SPAG4	Sperm associated antigen 4
SPAG4L	Sperm associated antigen 4-like
SSC	mouse spermatogonial stem cells
STR	straightness
Stra8	Stimulated by retinoic acid gene 8
SUN	Sad1p, UNC-84 domains
SYCP3	Synaptonemal complex protein 3
SYNE-1	Synaptic nuclear envelope protein 1
Tab.	Table
TAE	Tris-acetate-EDTA
TAZ	Tafazzin
TBST	Tris-buffered saline with Tween 20
TCF	T-cell factor
Tcf4	Transcription factor 4
TEMED	Tetramethylethylenediamine
Thr	Threonine
β-TrCP	β-transducin repeat-containing protein
U	Unit
UNC	UNCoordinated
UV	Ultraviolet
μF	microfarad
μl	microliter(s)
μM	micromolar
μm	micrometer(s)
μg	microgram(s)
V	volt
VAP	average path velocity
VCL	curvilinear velocity
VSL	straight line velocity
Wnt	int/Wingless
wt	wild-type
w/v	weight/volume
YFP	Yellow fluorescent protein

8. Supplemental data of reporter gene assays

8.1 The influence of over-expressed ODF2 on β-catenin activity using reporter gene assays in NIH3T3 and HEK293 cells

NIH3T3							
	No DNA	*phRL, OF*	*phRL, OT*	*phRL, OT, β-catenin*	*phRL, OT, β-catenin, 138NCGFP*	*phRL, OT, β-catenin, LiAc*	*phRL, OT, β-catenin, 138NCGFP, LiAc*
firefly reader	1378	7374	3351	7731	2866	23049	14646
	-	5052	3223	7944	2892	27829	10768
	-	-	2900	6141	2467	27565	11363
renilla reader	28441	57509562	40843648	25475516	21544719	12824167	9482575
	-	45787517	40352438	30597611	21652981	14101061	8083070
	-	-	37308972	28038856	18109621	14439908	9175368

HEK293							
	No DNA	*phRL, OF*	*phRL, OT*	*phRL, OT, β-catenin*	*phRL, OT, β-catenin, 138NCGFP*	*phRL, OT, β-catenin, LiAc*	*phRL, OT, β-catenin, 138NCGFP, LiAc*
firefly reader	961	20753	16270	211473	89203	1009959	228679
	-	19154	17980	248284	86838	1160628	169968
	-	-	11780	143457	84167	808708	190763
renilla reader	18779	29108351	20304142	12056326	12741802	19926587	11099048
	-	27400430	22385849	13308495	13984956	22309634	9381381
	-	-	15517483	10491709	12734080	16499128	8250112

8.2 Canonical Wnt reporter gene assay using Odf2 constructs

	no DNA	phRL, OF	phRL, OT	phRL, OT, β-catenin	phRL, OT, β-catenin, 13.8 NC-GFP	phRL, OT, β-catenin, human ODF2	phRL, OT, β-catenin, cenexin	phRL, OT, β-catenin, 13.8	phRL, OT, β-catenin, N-terminal	phRL, OT, β-catenin, cenexin insertion	phRL, OT, β-catenin, ODF2NC	phRL, OT, β-catenin, ODF2N2C	phRL, OT, β-catenin, ODF2NC1	phRL, OT, β-catenin, ODF2NC2
firefly reader	1556	727203	357278	3706065	1770570	2443493	513833	653735	2379942	1218055	617988	1479930	1059918	1000305
	1352	566166	379842	3601263	2029647	2961604	828840	858302	2141210	1491183	598273	1402661	1111664	1291889
	1225	584894	428492	3154732	1847670	3057815	932986	782598	2401239	1287619	639719	1091387	1013088	1571251
renilla reader	7893	12720777	8268050	5908044	6380253	5508231	2882880	3770576	4828445	4263478	6099054	7277764	5840538	4684783
	6506	11674570	8782529	4036168	5272017	5100628	11701633	4134301	3674833	4529053	5347415	5709796	6678989	5796507
	6634	15732937	10695043	5747074	6689655	7278079	6012836	5733381	6307252	6400197	5153624	5450932	5685871	7168344

8.3 The influence of centrosomal and cytoskeletal proteins on canonical Wnt reporter

	No DNA	*phRL, OT*	*phRL, OF*	*phRL, OT, β-catenin*	*phRL, OT, β-catenin, ninein*	*phRL, OT, β-catenin, centrin*	*phRL, OT, β-Catenin, α-tubulin*	*phRL, OT, β-Catenin, γ-tubulin*	*phRL, OT, β-Catenin, ε-tubulin*
firefly reader	1727	2053181	2616769	11325074	5002019	5768227	269360	578413	4324384
	1480	1897068	2724786	11259601	4789159	7442195	308977	613497	5371153
	1293	1801418	2507826	12265290	4474195	6988264	322815	557159	5356482
renilla reader	11380	19722658	22747805	6617463	8806157	9087101	2079207	4790265	7399142
	13328	18306177	26293198	7371483	8603418	11337738	2394214	5258110	8214671
	13778	19948063	25515116	8149283	8478043	11268234	2786499	5060458	8931643

8.4 The influence of centrosomal and cytoskeletal proteins on canonical Wnt reporter with or without nocodazole and taxol

	no DNA	phRL, OT	phRL, OF	phRL, OT, β-catenin	phRL, OT, β-catenin, nocodazole	phRL, OT, β-catenin, taxol	phRL, OT, β-catenin, centrin	phRL, OT, β-catenin, centrin, nocodazole	phRL, OT, β-catenin, centrin, taxol	phRL, OT, β-catenin, α-tubulin	phRL, OT, β-catenin, α-tubulin, nocodazole	phRL, OT, β-catenin, α-tubulin, taxol	phRL, OT, β-catenin, γ-tubulin	phRL, OT, β-catenin, γ-tubulin, nocodazole	phRL, OT, β-catenin, γ-tubulin, taxol
firefly reader	1922	2343863	1865420	30870594	27434451	27855739	4126153	4622874	6016341	255148	187021	324754	706663	514207	613523
	1744	2072318	1500930	28118226	21216248	28061931	4995649	3888025	5082827	252443	217163	334952	626348	544673	795007
	1667	2326734	1649516	35785426	14986673	27232861	6082622	4269483	5671293	228713	292817	375300	694543	801020	737758
renilla reader	6472	1.2E+07	9620606	5703392	3585699	3341999	4230393	1770936	2449634	478749	356827	575657	2115175	1122236	1190226
	6438	1.1E+07	8070933	5244613	3323177	3251070	4295177	2078628	2137638	773710	443351	613472	2027657	1400594	1382980
	5945	1.2E+07	8549691	5542448	2075873	3314698	4702423	2153993	2163663	706000	522976	686293	2135341	1932101	1377596

Curriculum Vitae

Name: **Kefei Yang**

Last Degree: Dipl

Mailing Address: Department of Developmental Biology,

Johann-Friedrich-Blumenbach-Institute of Zoology and

Anthropology, Georg-August-University of Göttingen,

Justus-von-Liebig-weg 11

37077 Göttingen

E-mail Address: kyang@gwdg.de

Academic Education:

2009 - present: Doctoral study at Department of Developmental Biology,

Johann-Friedrich-Blumenbach-Institute of Zoology and

Anthropology, Göttingen Centre for Molecular Biosciences

(GZMB), Erst-Caspari-Haus, Georg-August-University

Göttingen, Germany

Research thesis supervised by Prof. Dr. Sigrid Hoyer-Fender.

Title of Thesis:

Functional Analysis of Two Major Sperm Tail Proteins

Identifies ODF1 as Being Essential for the Tight Linkage of the

Sperm Head to the Tail via SPAG4 and ODF2 as A Component

of the β-catenin Destruction Complex

2008 - 2009:	Diploma thesis at Department of Developmental Biology, Johann-Friedrich-Blumenbach-Institute of Zoology and Anthropology, Göttingen Centre for Molecular Biosciences (GZMB), Erst-Caspari-Haus, Georg-August-University Göttingen, Germany
	Research thesis supervised by Prof. Dr. Sigrid Hoyer-Fender.
	Title of Thesis:
	Expression Centrosomaler Proteine in Tumorzelllinien

2001 - 2008:	Biology study, Georg-August-University Göttingen, Germany

1999 - 2001:	Learning German at AStA and Language Centre German as a Foreign Language, Georg-August-University Göttingen, Germany

1995 - 1999:	Medicine study, Shenyang Medical School Shenyang, Liaoning, P. R. China

Publications

Yang, K., Meinhardt, A., Zhang, B., Grzmil, P., Adham, I. M., & Hoyer-Fender, S. (2012). The small heat shock protein ODF1/HSPB10 is essential for tight linkage of sperm head to tail and male fertility in mice. *Molecular and cellular biology*, *32*(1), 216-225.

Pletz, N., Medack, A., Rieß, E. M., **Yang, K.**, Kazerouni, Z. B., Hüber, D., & Hoyer-Fender, S. (2013). Transcriptional activation of Odf2/Cenexin by cell cycle arrest and the stress activated signaling pathway (JNK pathway).*Biochimica et Biophysica Acta (BBA)-Molecular Cell Research*, *1833*(6), 1338-1346.

Zitaterklärung

Die folgenden Kapitel meiner Dissertation, inklusive der Abbildungen und Tabellen, 1.1.4, 2.2.2.1, 2.2.2.2, 2.2.2.3, 2.2.2.4, 2.2.2.5, 2.2.2.6, 2.2.2.7, 2.2.2.8, 2.2.2.9, 2.2.2.11, 3.1.1.1, 3.1.1.2, 3.1.1.3, 3.1.1.4, 3.1.1.5, 4.1 sind im Wesentlichen aus meiner eigenen Publikation „Yang, K., Meinhardt, A., Zhang, B., Grzmil, P., Adham, I. M., & Hoyer-Fender, S. (2012). The small heat shock protein ODF1/HSPB10 is essential for tight linkage of sperm head to tail and male fertility in mice. *Molecular and Cellular Biology*, 32(1), 216-225" übernommen worden.